DISSERTATION

A TALE OF TWO VIRUSES: THE ABILITY OF NEW WORLD MAMMALS TO HOST OLD WORLD VIRUSES

Submitted by

Juliette Lewis

Department of Microbiology, Immunology, and Pathology

In partial fulfillment of the requirements

For the Degree of Doctor of Philosophy

Colorado State University

Fort Collins, Colorado

Fall 2022

Doctoral Committee:

Advisor: Tony Schountz

Rebekah Kading
Allison Vilander
Kathryn Stoner

ABSTRACT

A TALE OF TWO VIRUSES: THE ABILITY OF NEW WORLD MAMMALS TO HOST OLD WORLD VIRUSES

The majority of human pandemics throughout history have zoonotic origins. The etiological agent of the bubonic plague, which devastated the human population as it emerged and re-emerged, was a result of spillover from rodents to humans via an arthropod vector. In more recent years, novel emerging pathogens are often viruses. From the vector-borne flaviviruses such as West Nile virus, dengue virus, and Zika virus, to the notorious coronaviruses, ever-reassorting influenza viruses, and high consequence paramyxoviruses, animal reservoirs are a source of endless spillover potential. What is the common thread woven among these spillovers? They are the products of anthropogenic change; the domestication of animals, such as livestock, birds, and pets, the encroachment of humans into and destruction of natural habitats, and the construction of urban habitats create new interfaces between animals that may have not interacted otherwise and provide the opportunity for viruses to transmit and adapt to new hosts, including humans.

Like ancient history, much of human pandemic history has been centered in the Old World. As a result, surveillance efforts have primarily focused on areas where important spillover events have historically occurred, such as China, southeast Asia, and Africa. Consistent surveillance in these regions will help us prepare for another spillover event from those same geographic origins. However, surveillance tunnel vision on the Old World leaves us vulnerable and unsuspecting in the western hemisphere, where those same anthropogenic factors are at play in creating interfaces for spillover events. Several viruses have already shown us that pathways

from animals to humans are in place for viruses in the New World, and that Old World viruses are capable of establishing transmission cycles in new animal species. For example, the first documented case of West Nile virus in humans was in Uganda in 1937. Over the course of the 20th century, its range expanded to include all of the Old World. In 1999, West Nile virus made its debut in New York City, and quickly became endemic to most of North America, spreading through its reservoir host, birds. This is not a new story: Zika virus, dengue virus, rabies virus, and SARS-CoV-2 were all imported to the New World where they gained entry to wildlife and domestic animal populations.

In this work, the primary goal was to assess the ability of New World mammals to host high-consequence Old World viruses. First, henipaviruses are examined, which are members of the viral family *Paramyxoviridae* and includes Nipah virus (NiV) and Hendra virus (HeV), two species that cause high fatality in humans. Henipaviruses exist primarily in their reservoir hosts, which include bats, rodents, and shrews in the Old World, and very recently, opossums in the New World. To provide context and summarize what is known about the circulation of paramyxoviruses in New World bats, chapter 2 of this dissertation reports on surveillance efforts, gaps, and findings.

The third chapter herein investigates the susceptibility of a New World bat species, the Jamaican fruit bat (*Artibeus jamaicensis*), to henipaviruses using *in vitro* and *in vivo* methods. The immune response of Jamaican fruit bat cells to infection by these viruses was characterized, as well as how a model henipavirus, Cedar virus (CedV), adapts to Jamaican fruit bat cells. Our data indicate that Jamaican fruit bat cells are susceptible to NiV, HeV, and CedV. NiV and HeV were able to effectively shut down the antiviral response in the bat cells while CedV induced high antiviral gene expression. Serial passaging of CedV on Jamaican fruit bat cells resulted in several mutations to the viral genome and an improved ability to replicate

and cause cytopathic effect in the cells. Lastly, intranasal challenge of three Jamaican fruit bats with CedV resulted in a transient infection with oral and rectal shedding, viremia in one bat, and seroconversion. These results indicate that a widespread species of New World bat is susceptible to experimental henipavirus infection, and that they could potentially be a reservoir should henipavirus spillback occur in the Americas.

While our investigation into Jamaican fruit bats as potential hosts of henipaviruses was underway, news of the “novel coronavirus-19” broke. In response, we shifted the focus of our work to the new virus threatening public health: SARS-CoV-2. To contribute to the understanding of SARS-CoV-2 and explore potential spillback hosts, we pivoted to determining the susceptibility of a subspecies of North american deer mouse (*Peromyscus maniculatus nebrascensis*) to the virus. Initial susceptibility testing revealed that SARS-CoV-2 causes a subclinical infection in deer mice, though pathology was evident in the upper and lower respiratory tracts. Immune gene assessment via qPCR arrays indicate that deer mice mount a pro-inflammatory type I inflammatory response to control infection. In a subsequent experiment, the ability of deer mice to transmit SARS-CoV-2 conspecifically was determined up to two passages. This experiment established that deer mice are capable of sustained intraspecific transmission, an important characteristic of a potential reservoir.

Given the wide geographic distribution and numerous species of deer mice, we conducted susceptibility testing of two additional deer mouse species (*P. polionotus, P.* californicus) and two additional subspecies of North American deer mouse (*P. m. sonoriensis, P. m. bairdii*). Virus isolation from oral swabs and lung samples and seroconversion indicate that all tested species and subspecies of deer mice are susceptible and suggest broad susceptibility of mice in the genus *Peromyscus* to SARS-CoV-2. Interestingly, two California deer mice (*P. californicus*) developed clinical signs and one was euthanized for humane reasons. Given that SARS-CoV-2

has already been transmitted from humans to a number of animals, including American mink (*Neogale vison*) and white-tailed deer (*Odocoileus virginianus*), it is not unreasonable that deer mice, a geographically ubiquitous peridomestic animal, could be naturally exposed to the virus.

The work presented herein demonstrates that there are viable wildlife hosts for important pathogenic human viruses in the New World. Surveillance, although sparse, has shown that viruses related to human pathogens circulate in rodents and bats in the Americas, and therefore it is critical to be prepared for a spillover event in this geographic region by increasing surveillance efforts and characterizing potential animal hosts from which viruses may emerge. As deforestation, urbanization, and climate change progress, new opportunities for virus-sharing between wildlife, domestic animals, and humans are created and will, undoubtedly, result in the next pandemic.

TABLE OF CONTENTS

Chapter 1: Introduction to Paramyxoviruses and bats

1.1 Introduction to paramyxoviruses

1.1.1 Paramyxovirus introduction

Paramyxoviridae is a family within the viral order Mononegavirales with negative-stranded RNA genomes. Paramyxoviruses (PMVs) are hosted by vertebrates and include many viruses of medical and veterinary importance. These include Nipah virus (NiV), Hendra virus (HeV), sosuga virus, measles virus, mumps virus, human parainfluenza viruses (HPIV), and respiratory syncytial virus (RSV) in humans and canine distemper virus (CDV), Newcastle disease virus (birds), and rinderpest virus (cattle). NiV and HeV cause disease in pigs and horses, respectively, and severe disease in humans. Although NiV, HeV, and sosuga virus are the only pathogenic PMVs for which bats are confirmed reservoirs, there is evidence that mumps virus, RSV, HPIV, and CDV may have evolved from viruses that originated in bats (Drexler et al., 2012; Hause et al., 2021).

1.1.2 Paramyxovirus replication

The cellular entry receptors used by PMVs vary by genus. Rubulaviruses and respiroviruses use sialic acid-containing molecules, whereas henipaviruses and morbilliviruses use protein receptors. When a PMV binds to its cellular receptor, it initiates fusion of the viral envelope with the cell membrane and releases the virion into the cell. Once uncoating occurs, the viral RNA-dependent RNA-polymerase (RdRp), which is a functional component of the L protein, transcribes the negative sense RNA genome sequentially from 3’ to 5’ (Figure 1.1). Transcription is terminated between each gene at a gene-end signal, where polyadenylation occurs. The RdRp then initiates transcription of the next gene. Resulting mRNAs have 5’-caps and 3’-polyadenylated tails. Gene expression is regulated by the RdRp sometimes reading

through the gene termination sequences, which results in a polycistronic mRNA, and only the first gene gets translated. Additionally, the RdRp will sometimes dissociate from the genome between genes. These two mechanisms create a gradient with genes closer to the 3' end expressed more frequently. In most PMVs, polymerase stuttering and resultant frameshifting within the P gene results in the addition of one or two guanines, leading to the generation of additional mRNAs that encode accessory proteins V and W that are important in modulating the host innate immune response. The RdRp switches into replicase mode to generate new viral genomes when the encapsidation process begins and triggers the RdRp to ignore all gene-end signals and generate a full antigenome which can then be used as a template to make genome copies. Virion assembly is coordinated primarily by the viral matrix protein near the plasma membrane of the cell and culminates in the budding of the virus progeny.

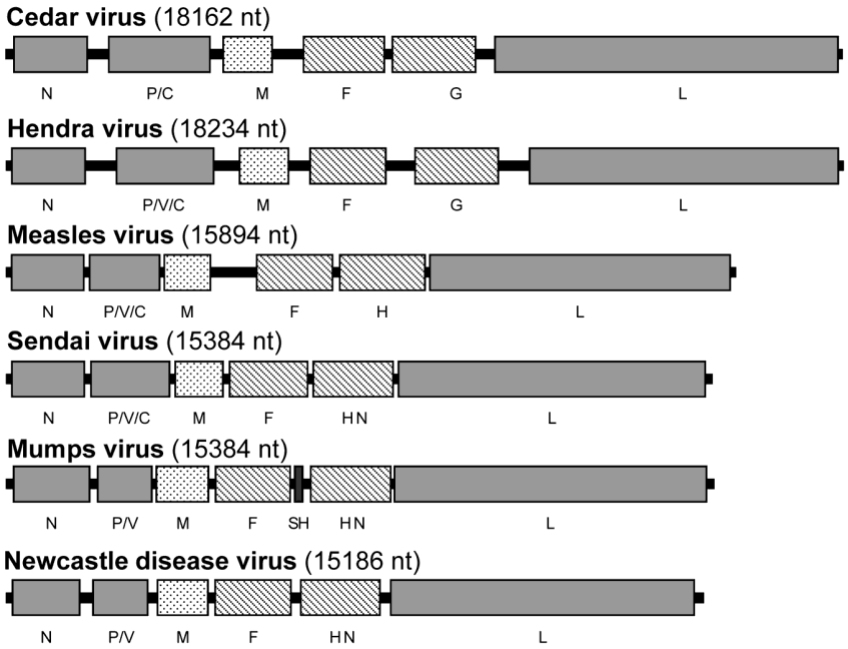

Figure 1.1 Genome organization of representative PMVs. PMV genomes are 15-19kb in length and include 6-10 genes. There are transcription start/stop signals within each gene. The P gene of some species contains an additional ORF and/or an RNA editing site which enables the transcription of additional mRNAs.
Marsh GA, de Jong C, Barr JA, Tachedjian M, Smith C, et al. (2012) Cedar Virus: A Novel Henipavirus Isolated from Australian Bats. PLOS Pathogens 8(8): e1002836.
https://doi.org/10.1371/journal.ppat.1002836

1.1.3 Immunomodulation by Paramyxoviruses

1.1.3.1 Interferon response introduction

The type I interferon (IFN) response is the first line of defense against viral infection in cells. When pattern recognition receptors (PRRs) such as retinoic acid-inducible gene-I (RIG-I), melanoma differentiation associated-5 (MDA-5), Toll like receptors -3, -7, and-9 (TLRs), and others bind their virus-associated activating ligand, a signaling cascade leads to the production of type I interferons, including IFNα, IFNβ and IFNω. Interferons have both paracrine and autocrine effects. When they bind to the type I interferon receptor of a cell, signaling through JAK1 leads to STAT1 phosphorylation which promotes STAT1 homodimerization or heterodimerization with STAT2. STAT1 homodimers or STAT1/STAT2 heterodimers with IRF9 translocate to the nucleus where they are transcription factors for interferon stimulated genes (ISGs), and interferon response factors (IRFs) that induce an antiviral state in the cell. Because this system is so essential for the induction of an antiviral state, many virus genomes encode proteins that interrupt the signaling cascade.

1.1.3.2 V and W protein mechanisms

PMVs use various mechanisms to disrupt interferon signaling to promote viral infection longevity and productivity. All pathogenic henipavirus P gene products target the interferon signaling pathway by binding STAT1 and inhibiting phosphorylation through a shared N-terminal domain. P and V bind STAT1 in the cytoplasm to prevent phosphorylation and nuclear translocation, whereas the W protein binds to STAT1 in the nucleus and inhibits signaling there (Shaw et al., 2004b). Specifically, the NiV V protein binds to STAT1 and prevents IFN-induced tyrosine phosphorylation by sequestering STAT1 in high molecular-weight complexes in the cytoplasm of human 2FTGH cells (Rodriguez et al., 2002). The V protein accomplishes this cytoplasmic accumulation through the presence of a nuclear export signal that prevents entry of the V-

STAT1 complex to the nucleus (Rodriguez et al., 2004). V protein mechanisms of interferon antagonism utilized by other PMVs are listed in Table 1.1.

Table 1.1. V protein activity of different Paramyxoviruses. The V protein of PMVs often has interferon antagonizing properties, which it typically achieves through inhibition or destruction of STAT1 or STAT2.

Virus	Genus	Target protein	Mechanism of action	Reference
Newcastle disease virus	*Orthoavulavirus*	p-STAT1	Targets P-STAT1 for ubiquitin-mediated proteolytic degradation	(Qiu et al., 2016)
Measles virus	*Morbillivirus*	STAT1 and STAT2	Inhibits STAT protein phosphorylation and translocation to the nucleus	(Palosaari et al., 2003; Takeuchi et al., 2003)
Mumps virus	*Rubulavirus*	RACK1, STAT1	Inhibits STAT1 interaction with the interferon receptor, prevents STAT1 phosphorylation, and promotes ubiquitin-mediated degradation of STAT1	(Kubota et al., 2002; Kubota et al., 2005; Yokosawa et al., 2002)
Parainfluenza virus 5	*Rubulavirus*	STAT1	Promotes formation of a ubiquitin ligase complex that ubiquitinates STAT1, targeting it for degradation	(Young et al., 2000)
Human parainfluenza virus 2	*Rubulavirus*	STAT2	Induces proteolytic degradation of STAT2	(Parisien et al., 2001)

1.2 Henipaviruses

There are currently 5 species of *Henipavirus* recognized by the International Committee for the Taxonomy of Viruses, including NiV, HeV, Cedar virus (CedV), Mojiang virus (MoV), and Ghana virus (GhV), as well as 10 putative henipaviruses that have been detected by sequencing or isolated but not yet formally classified.

1.2.1 Overview of henipavirus species

1.2.1.1 Hendra virus

Hendra virus was the first henipavirus that was discovered. It was detected during an encephalitis outbreak in Hendra, Australia in 1994 involving two human cases with one fatality and the deaths of 20 horses (Murray et al., 1995). Since then, there have been sporadic outbreaks resulting in 7 human cases, 4 of which were fatal (Field, 2016). Hendra virus presentation in humans usually begins with flu-like symptoms and can progress to a more severe illness involving encephalitis and neurological signs. In one case, a patient had a fatal relapse 13 months following the initial onset of and apparent recovery from illness (Field, 2016). HeV uses ephrins B2 and B3 as receptors, which allow entry to endothelial cells and the nervous system, respectively (Bonaparte et al., 2005; Negrete et al., 2006). In all 7 human cases, the infected people had direct contact with an infected horse and human-to-human transmission has not been documented.

1.2.1.2 Nipah virus

Nipah virus was discovered in 1998 during an outbreak of viral encephalitis among pig farmers in Malaysia (Chua et al., 1999). Patients presented with fever, headache, dizziness, and vomiting with about half of cases progressing to involve encephalitis and neurological symptoms (Goh et al., 2000). Like HeV, NiV uses ephrins B2 and B3 as cell entry receptors. Cases were primarily among people who had direct contact with pigs, and of the 257 cases, there were 100 deaths (fatality rate 39%)(CDC, 1999). Later, neutralizing antibodies against NiV were identified in 5 species of bats native to Malaysia, suggesting that the initial spillover had been from local bats to pigs, and subsequently to humans (Chua et al., 2002). Soon after the outbreak of NiV in Malaysia, NiV infections were confirmed in Singapore in abattoir workers who handled pigs imported from Malaysia (CDC, 1999). The Singapore outbreak was limited to 11 cases and

controlled by the culling of pigs imported from Malaysia and only one case resulted in death. Beginning in 2001, outbreaks of NiV have been reported in Bangladesh almost annually. Unlike in Malaysia, Bangladesh outbreaks have mostly originated from the human consumption of date palm sap contaminated by urine and/or feces of infected Indian flying foxes (*Pteropus medius*) (Luby et al., 2006). In addition, NiV outbreaks are sustained in Bangladesh by more efficient person-to-person transmission than in the Malaysia outbreak (Nikolay et al., 2019). The Bangladesh outbreaks have also resulted in higher mortality rates, with the average case fatality rate for 2008-2012 of 85% (Ambat et al., 2019). Genetic analysis of virus isolates from Malaysia and Bangladesh led to the classification of the etiologic agents of these outbreaks as two different strains of NiV, NiV-Bangladesh and NiV-Malaysia (Harcourt et al., 2005).

1.2.1.3 Cedar virus

Cedar virus was isolated from urine pool samples taken from under a flying fox colony in Cedar Grove, Southeast Queensland, Australia as a part of Hendra virus surveillance efforts (Marsh et al., 2012a). The colony consisted of both black flying foxes and grey-headed flying foxes. Genetic characterization of CedV revealed that it lacks the highly conserved RNA editing site in the P gene which codes for the accessory proteins V and W, and probably lost it long ago. It was noted that, in comparison to NiV and HeV, CedV induced high levels of IFNβ expression in HeLa cells, probably because of the missing V and W proteins that suppress the interferon response. Infection of henipavirus animal models including ferrets, guinea pigs, and mice, resulted in a limited infections without clinical signs that resulted in viral clearance and a neutralizing antibody response (Marsh et al., 2012b). Similar results were later reported in Syrian hamsters (*Mesocricetus auratus*), another henipavirus animal model in which NiV infection is invariably fatal (Schountz et al., 2019). Notably, CedV was shown to be unable to use ephrin B3 as a cell-entry receptor, which could pose a supplementary explanation to the lack of pathogenicity in tested animal models in addition to the inability to modulate host

immunity to the scale of NiV and HeV (Laing et al., 2019). There have been no documented cases of CedV infection in humans.

1.2.1.4 Ghana virus

Ghana virus was detected by sequencing in feces collected beneath a colony of straw-colored fruit bats (*Eidolon helvum*) in Kumasi, Ghana (Drexler et al., 2012). Although there have been no known human cases of GhV infection, serological studies in the area indicated henipavirus exposure in human populations, especially among individuals who handle bats in the bushmeat trade (Pernet et al., 2014). *In vitro* studies have indicated that GhV is able to infect and cause syncytia formation in human, bat, and simian cells (Lawrence et al., 2014). GhV has not been isolated nor generated by reverse genetics, limiting the ability to study its virology.

1.2.1.5 Mojiang virus

In 2012, three miners who had been working in the Mojiang mine in the Yunnan province of China fell ill with severe pneumonia and died. Subsequent efforts to find the etiological agent led to the discovery of MoV in rats (*Rattus flavipectus*) that were living in the mine. The full-length genome was obtained from these samples, but no infectious virus could be recovered (Wu et al., 2014). While phylogenetics revealed that MoV is a henipavirus, it is phylogenetically distinct from NiV, HeV, CedV, and GhV. MoV has not been isolated nor a reverse genetics system created. It was determined that MoV was not the etiological agent of the miners' disease, and there have been no documented human infections.

1.2.2.1 Gamak virus and Daryeong virus (putative)

Gamak virus and Daryeong virus were sequenced and GAKV was isolated from kidney tissues collected from shrews (*Crocidura asiurus and C. shantungensis*) in the Republic of Korea in

2017-2018 (Lee et al., 2021b). The sequences were highly similar to other henipaviruses and includes the RNA editing site to produce V and W proteins. Phylogenetic analysis revealed that GAKV and DARV specifically clustered with MojV. *In vitro* assays indicate that GAKV is capable of infecting human cells, and upon infection elicits an antiviral immune response. There have been no documented human infections by these viruses. These viruses have not been formally accepted by the ICTV at the time of this writing.

1.2.2.2 Langya virus (putative)

Langya virus (LayV) was detected in shrews following cases of febrile illness in the Shandong and Henan provinces of China in 2018 (Zhang et al., 2022). Patients, mostly farmers, presented with fever, cough, anorexia, fatigue, and other flu-like symptoms. A survey of domestic and wild animals in the area revealed a 27% prevalence of the virus in shrews and low prevalence seropositivity in goats and dogs. Human-to-human transmission is not currently suspected.

1.2.2.3 Other henipavirus detections (putative)

Henipaviruses are being continually and increasingly detected around the world. Melian and Denwin viruses were detected in shrews in Guinea and Belgium, respectively (Vanmechelen et al., 2022). Four genomes have also been published on GenBank representing new henipaviruses sequenced from shrews in China as well (GenBank accession numbers OM030314-OM030317). A new henipavirus, Peixe-Boi virus, has been detected in a wooly mouse opossum (*Marmosa demerarae*) in Brazil, expanding both the geographical and host range of henipaviruses (Hernández et al., 2022). These viruses have not been formally accepted by the ICTV at the time of this writing.

1.2.3 Animal models of henipavirus disease

1.2.3.1 Syrian hamsters

Syrian hamsters are a well-developed laboratory animal and exhibit similar NiV and HeV disease to that seen in humans (Guillaume et al., 2009; Rockx et al., 2011; Wong et al., 2003). Infected Syrian hamsters display systemic vascular disease, multi-organ involvement, syncytia formation, pneumonia, neurological signs, and virus shedding through urine (Geisbert et al., 2012). Hamsters have been used as models for development of vaccines and anti-virals (Geisbert et al., 2012) .

1.2.3.2 Ferrets

Ferrets (*Mustela furo*) are an important animal model of henipavirus infection (Bossart et al., 2009; Pallister et al., 2009; Pallister et al., 2011). Upon infection with NiV or HeV, ferrets have systemic vascular disease, infection of multiple organs, fever, cough, nasal discharge, respiratory distress, neurological signs, syncytia formation, and virus shedding via the oral and rectal route. Ferrets have been used for vaccine and anti-viral studies as well as studies of pathogenesis and immune response (Geisbert et al., 2012).

1.2.3.3 African green monkeys

African green monkeys (AGMs; *Chlorocebus sabaeus*) most consistently recapitulate the pathology of henipavirus infection of humans (Geisbert et al., 2010; Rockx et al., 2010). Virus and associated pathology were detectable in almost all organ systems. AGMs exhibited neurological disease associate with infections, with severe brain congestion, hemorrhage, and edema. Pulmonary involvement is also consistent, with an acute respiratory distress-like syndrome including severe lung congestion and hemorrhage. As the most phylogenetically

similar to humans out of the described animal models, AGMs are an important for preclinical testing of vaccines and antivirals (Geisbert et al., 2012).

1.2.3.3 Other animals

Cats and guinea pigs also develop fatal clinical disease upon infection with HeV and NiV and have pathological lesions of pneumonia similar to those seen in horses; however, these models do not recapitulate the neurological involvement that occurs in human infection. Rats, rabbits, mice, dogs, and chickens were challenged with HeV but did not become infected, although rats, rabbits, and dogs seroconverted. Horses and pigs are also utilized to study HeV and NiV in the relevant intermediate hosts (Hooper et al., 1997; Li et al., 2010; Middleton et al., 2002).

1.2.4 NiV P gene products are pathological determinants in animal models

Satterfield *et al.* created NiV mutants with either V or W knocked out (V_{KO}NiV and W_{KO}NiV) via reverse genetics and characterized these mutants in primary human endothelial cells and in ferrets (Satterfield et al., 2015). The authors found that V_{KO}NiV had attenuated growth in primary human brain and microvascular endothelial cells, and cytokine detection assays showed higher cytokine expression for both the W_{KO}NiV and V_{KO}NiV. Specifically, cytokines with a role in lymphocyte recruitment were found to be upregulated in W_{KO}NiV infected primary human endothelial cells. In experimentally infected ferrets, the authors described survival of all V_{KO}NiV-infected ferrets, whereas all W_{KO}NiV and wildtype virus infected ferrets succumbed to disease. A follow-up study demonstrated that C knockout NiV (C_{KO}NiV) caused mortality in 100% of infected ferrets (Satterfield et al., 2016). In the same study, a C and W knockout NiV was attenuated, with 60% fatality and chronic neurological deficits in surviving animals.

Similar experiments were described in Syrian golden hamsters by Yoneda *et al* (Yoneda et al., 2010). When the 50% lethal dose (LD_{50}) was calculated for W_{KO}NiV, it was very similar to that of the wildtype virus. However, when the LD_{50} assay was performed for V_{KO}NiV or a C knockout NiV (C_{KO}NiV), all hamsters survived the challenge at the highest dose of 10^5 PFUs. This C_{KO}NiV infection outcome is notably different than that observed by Satterfield *et al* in ferrets.

1.2.5 Henipavirus studies in bats

HeV infection studies have been carried out in the black flying fox (*Pteropus alecto*) and grey-headed flying fox (*Pteropus poliocephalus*) (Halpin et al., 2011; Williamson et al., 1998; Williamson et al., 2000; Woon et al., 2020). Findings were similar in all studies; bats had no clinical signs or gross pathology and rare and sporadic virus presence in various tissues by RT-PCR, virus isolation, and immunostaining. Transplacental transmission was demonstrated by immunostaining in the placenta and virus isolation from a fetus (Williamson et al., 2000). The most recent study examined the immune response at early timepoints of HeV infection in black flying foxes compared to ferrets (Woon et al., 2020). No differences were identified that may explain the difference in infection outcome.

Experimental infections of bats with NiV are even more limited. The grey-headed flying fox, large flying fox (*Pteropus vampyrus*) , and Egyptian fruit bat have been experimentally challenged with NiV (Halpin et al., 2011; Middleton et al., 2007; Seifert et al., 2020). Egyptian fruit bats were found to not support NiV replication (Seifert et al., 2020). Grey-headed flying foxes shed virus in urine, had detectable virus in some tissues, and seroconverted (Middleton et al., 2007). Limited, inconsistent pathology was seen without associated viral immunostaining. Studies in the large flying fox indicated that NiV infection was not well-supported (Halpin et al., 2011). Virus was only detected in swabs from 1/8 bats, and no viral RNA was detected in any tissues. Low antibody titers were reported.

1.2.6 Summary and future directions

Surveillance efforts in the last decade have revealed a much greater host and geographic range than previously recognized for henipaviruses. The emergence of shrews as henipavirus reservoirs opens a new front on which to study this viral genus. Additionally, the detection of henipaviruses in South America expands the geographical range significantly, and the presence of a henipavirus in an opossum brings up the question: where else are they hiding?

The ability of henipaviruses to infect humans is historically and experimentally well established. NiV, HeV, and LayV have caused human outbreaks with disease ranging from flu-like to severe with high mortality. The periodic spillover events also give evidence that humans have, and will likely continue to have, regular contact with henipavirus reservoirs; thus, it is essential that surveillance and characterization efforts for henipaviruses continue and increase, especially in the Americas where they are less well-characterized.

The literature also reveals that little is known about the relationship between henipaviruses and their natural reservoirs, pteropid bats. Experimental infections of flying foxes have provided inconsistent data about tissue tropism, shedding, and immune response to NiV and HeV. The challenges of working with bats, particularly large species such as flying foxes, contributes greatly to the paucity of knowledge about this virus-host system.

1.3 Introduction to Chiroptera

Comprising over 20% of mammalian species, the order Chiroptera boasts incredible bat diversity, geographic range, and trophism diversity. This order is also fascinating for the ability of some members to use echolocation and as the only mammals capable of true sustained

flight. Equally impressive is the wide range of viruses for which bats act as hosts, reservoirs, and vectors.

1.3.1 Bats provide many ecosystem services

Bats provide numerous ecosystem services that are essential for maintaining sustainable ecosystems. The majority of bat species are obligate or facultative insectivores, and as such spend the nights hunting for their arthropod prey. Bats may hunt insects by collecting them above fields, forests, and bodies of water, or glean them from thick foliage in dense forests. The high metabolism of bats requires that they consume a large quantity of insects, often to the benefit of humans. Around the world, bats protect crops from insect pests, saving the farming economy billions of dollars on insecticides and lost crops (Kunz et al., 2011).

Similarly, frugivorous and nectivorous bats provide essential services for the ecosystem which provide great benefits to humans. Frugivorous bats are seed dispersers for 549 species of plant in the neotropics alone (Lobova, 2009). Nectivorous bats as well as some frugivorous bats serve as pollinators for many species of plants as well, including the economically important agave plant. Because bats are central to the health of the ecosystems and as such contribute significantly to the furtherance of human interest, an appropriate balance must be found between the methods used to study bats and conserving their lives and habitats.

1.3.2 Bats are viral reservoirs and vectors of pathogenic human viruses

Along with the fascinating and beneficial traits of bats, there is the less desirable role that they play as reservoirs and vectors of human pathogens. Evidence has been found supporting a link between bats and over 20 viral families, many of which cause significant human disease, animal disease, or economic impact (Chen et al., 2014). Among the viruses hosted by bats are many that have not yet spilled over into humans but have the potential, such as new strains of

Influenza A viruses, PMVs, and numerous SARS-like coronaviruses (Breed, 2008; Kandeil et al., 2019; Li et al., 2005). Besides those mentioned here, surveillance has revealed the presence of many viruses in bats with unknown pathogenic potential.

1.3.2.1 Coronaviruses

The viral family *Coronaviridae* consists of enveloped, spherical, positive-sense RNA viruses. The subfamily *Orthocoronavirinae* contains the genera *Alphacoronavirus, Betacoronavirus, Gammacoronavirus,* and *Deltacoronavirus.* Alpha- and betacoronaviruses infect mammals, with six species that are known to cause human disease ranging in severity from the common cold (HCoV-229E, HCoV-NL63, HCoV-OC43, HCoV-HKU1) to potentially fatal respiratory disease (SARS-CoV, MERS-CoV, SARS-CoV-2). Bats are the likely reservoirs of the ancestral SARS-CoV, MERS-CoV, and SARS-CoV-2 due to detection of hundreds of closely related viruses in bats near the geographical location of the outbreaks and elsewhere (Corman et al., 2018). One likely reason that these viruses have not been directly isolated or sequenced from bats is because coronavirus spillover into humans seems to require an intermediate host which allows adaptations to the spike protein (viral entry-facilitating protein) which enables the virus to infect humans.

1.3.2.2 Filoviridae

Viruses in the family *Filoviridae* have been causing hemorrhagic disease with high case fatality rates (80-90%) since Marburg virus (MARV) emerged in Germany and Yugoslavia in 1967 from imported infected African green monkeys. Filoviruses have a negative sense genome within the filamentous capsid, which is all enclosed in an envelope. Filovirus infection in humans causes severe disease that starts with a flu-like presentation and can progress to involve multiple organ systems an severe systemic hemorrhage. Sudan ebolavirus emerged in Nzara, South Sudan in

1976. Since then, intermittent spillover events have caused epidemics. In 2007, it was reported that MARV RNA was detected in an Egyptian fruit bat (*Rousettus aegyptiacus*) (Towner et al., 2007). Since then numerous reports have described molecular and serological evidence of Marburgviruses in Egyptian fruit bats, and many outbreaks can be traced to human exposure to bats (Schuh et al., 2017b). The status of bats as the reservoir for ebolaviruses is less concrete, with patchy detection of anti-ebolavirus antibodies, even in the geographic locations of outbreaks. New evidence supports bats as the reservoir as a novel ebolavirus of unknown pathogenic potential, Bombali virus, was sequenced from bats living in human dwellings in Sierra Leone (Goldstein et al., 2018). Further research and surveillance will be necessary to determine the role of bats in ebolavirus ecology.

1.3.2.3 Flaviviridae

Flaviviruses are medically important vector-borne viruses, causing significant morbidity and mortality globally each year (Pierson and Diamond, 2020). They are enveloped, spherical, positive-sense RNA viruses, and cause a variety of clinical manifestations typically beginning with flu-like symptoms and having the potential to progress to neurological involvement. There is significant evidence from surveillance (serological and molecular) and experimental infections that indicate bats are competent hosts of flaviviruses including Zika virus, dengue virus, West Nile virus, and others (Calderón et al., 2021; Fagre et al., 2021b; Kading and Schountz, 2016; Torres-Castro et al., 2021b). However, it is yet unknown how significant a role bats play in maintaining and spreading these viruses.

1.3.2.4 Lyssaviridae

The viral genus *Lyssavirus* contains 14 species, one of which is the etiological agent of rabies, rabies virus (RABV). Lyssaviruses are enveloped, negative-sense RNA viruses with a bullet-

shaped virion structure. Rabies disease manifests as severe neurological symptoms and causes tens of thousands of deaths annually, as human infection is almost always fatal (WHO, 2021). Circulation of RABV in bats is limited to New World species. In particular, the common vampire bat (*Desmodus rotundus*) is responsible for the transmission of rabies to livestock via their feeding habits (Johnson et al., 2014). The status of bats as the reservoir for RABV is debated, as the typical definition of a reservoir species indicates that it maintains the virus without significant pathology. Bats do succumb to rabies; however, the fatality rate is closer to 30% than the 100% seen in other mammals (Turmelle et al., 2010).

1.3.2.5 Paramyxoviridae

Bats are the reservoir for several viruses in the family *Paramyxoviridae*, most notoriously henipaviruses. Pteropid bats are the reservoir for NiV and HeV, with transmission to humans occurring directly in NiV or through intermediate host pigs and horses (NiV and HeV, respectively). Porcine orthorubulavirus, the etiologic agent of blue-eye disease in pigs in Mexico, has been identified in several species of Mexican bats. Other PMVs with unknown pathogenic potential identified in bats are CedV, GhV, myotis bat morbillivirus, and Angavokely virus (Drexler et al., 2009; Lee et al., 2021a; Madera et al., 2022; Marsh et al., 2012b). Bats are also host to a variety of unidentified PMVs (see chapter 2).

1.3.3 Characteristics of bat immunity

Given the propensity of bats to host high-consequence human and veterinary pathogens with little or no pathology, it has been proposed that unique immunological characteristics may be responsible for controlling infection in a way that minimizes damage inflicted by the viruses themselves or by the immune response. Several of the pathogens hosted by bats cause severe

pathology in humans via over-activation of the immune system such as filoviruses and coronaviruses.

1.3.3.2 The bat interferon response

In the black flying fox (*Pteropus alecto*), constitutive *Ifnα* expression but minimal up-regulation upon stimulation by poly(I:C) was described in various tissues from wild-caught bats (Zhou et al., 2016). Similar lack of upregulation upon poly(I:C) treatment was reported for interferons in *in vitro* studies of the big brown bat (Banerjee et al., 2017). This is in sharp contrast to humans, who typically maintain undetectable levels of IFNα in an uninfected state, but then experience a quick and drastic upregulation upon infection (Rodero et al., 2017). This difference could indicate that some bats have developed mechanisms to be more tolerant to infection and prevent excessive immune activation. It could also mean that IFNα is under tight translational regulation in an uninfected state, but the continual presence of mRNA allows a faster response to challenge. This phenomenon will need to be further examined in other bat species, as experiments in Egyptian fruit bat cells do not indicate constitutive interferon expression (Pavlovich et al., 2018). Many human pathogens with bat reservoir roots have non-structural proteins that inhibit the interferon response (Frieman et al., 2007; Kopecky-Bromberg et al., 2007; Shaw et al., 2004a; Valmas et al., 2010; Zhang et al., 2012). It is possible that the bat interferon response drove the evolution of these interferon-inhibiting capabilities.

The repertoire of interferon genes varies greatly between bat species. For example, the black flying fox has an apparently contracted type I interferon locus with only three IFNα genes (Zhou et al., 2016). Studies of the genomes of *M. lucifugus, P. vampyrus,* and *R. aegyptiacus* revealed the apparent expansion of type I interferons in these bats and particularly of IFNω (Kepler et al.,

2010; Pavlovich et al., 2018). Comparison of the interferon locus of additional species will be necessary to elucidate any evolutionary patterns that may be present.

1.3.3.3 Bats may have more inhibitory mechanisms that prevent immune overactivation

Further examples of distinctive immune system features of bats include the apparent presence of additional regulatory mechanisms in the inflammatory pathway. Banerjee et al (2017) identified a binding site for c-Rel, a transcriptional regulator, in the promoter of TNF in the big brown bat (*Eptesicus fuscus*) genome. Cellular assays then revealed that TNF was not highly upregulated upon stimulation with poly(I:C) except for when c-Rel RNA was knocked down with specific siRNA. TNF plays a role in inflammation, and is often implicated in cytokine storm and sepsis, which is the cause of severe disease in humans infected with several bat-associated viruses (Fajgenbaum and June, 2020).

The complete loss of the PYHIN family of genes was observed in a genomic study of ten bat species (*Pteropus alecto, Eidolon helvum, Rhinolophus ferrumequinum, Megaderma iyra, Myotis lucifugus, Myotis davidii, Myotis brandtii, Eptesicus fuscus, Pteronotus parnellii)* (Ahn et al., 2016). The PYHIN gene products are a family of immune sensors that detect intracellular DNA, which can be associated with infection or oxidative damage to self-DNA. Activation of the inflammasome and interferon pathway follows. This adaptation is hypothesized to protect bats from DNA damage associated with their high metabolic rate during flight.

Pavlovich *et al* (2018) generated a high-coverage genome for the Egyptian fruit bat (*Rousettus aegyptiacus*) and described the unusual presence of inhibitory motifs in nine of ten natural killer (NK) cell receptor genes. NK cells are important in the antiviral response, and interaction with an infected cell presenting non-self-peptides on MHC-I leads to the NK cells delivering a kill signal to the infected cell. Since bat NK cells have additional inhibitory motifs compared to those

other mammals, perhaps an excessive apoptotic response is prevented, and there is less overall tissue damage. Along the same lines, analysis of the NK cells receptor genes indicated a potential preference for signaling through DAP10, which is less associated with cytokine production and induction of inflammation than DAP12. These characteristics suggest bats may have evolved mechanisms to increase immunotolerance, preventing the immunopathology seen in humans.

1.3.3.4 Bat adaptive immunity

Bat adaptive immunity is poorly understood, with only a few studies comprising the current working knowledge. Generally, bats appear to have the 5 canonical classes of immunoglobulin (Ig) constant chains: IgA, IgD, IgE, IgG, and IgM (Butler et al., 2011). Antibody specificity in animals is influenced to varying degrees by genetic recombination, somatic hypermutation (SHM), and somatic gene conversion of Ig variable heavy (V_H) genes that encode a portion of the antibody that binds the antigen. The number of V_H genes in bat genomes appears to vary by species, but studies of the genomes of the little brown bat (*Myotis lucifugus*), flying foxes, and the Egyptian fruit bat suggest that bats have a larger repertoire of V, D, and J genes in the immunoglobulin heavy chain locus that may provide more specificity in their naïve antibody response through combinatorial diversity (Baker et al., 2010; Bratsch et al., 2011; Larson et al., 2021). Whether or not somatic hypermutation plays a role in affinity maturation is not yet certain, though there was little evidence of somatic hypermutation in the little brown bat (Bratsch et al., 2011). In support of a combinatorial diversity hypothesis, the bat antibody response to infection is often inconsistent and non-neutralizing or minimally neutralizing (Halpin et al., 2011; Schuh et al., 2019; Schuh et al., 2017a; Subudhi et al., 2018).

1.3.3.5 Challenges, gaps, and future directions in bat immunology

The majority of what we know about the bat immune system has been determined in pteropid bats. While studying pteropid bats is essential, they represent only a small portion of bat diversity and, given the evolutionary distance between bat families, may not be representative of phylogenetically distant families. It is difficult to study bats in a controlled manner due to the rarity of captive colonies kept for the purpose of infectious disease and immunology research. In the absence of captive colonies, wild-caught bats have been utilized for some studies. However, wild-caught bats come with a long list of uncontrolled variables, a few of which include pathogen exposure status, infection status, age, diet, and environmental factors.

There are several reasons that it is difficult to maintain captive colonies of bats. First is the need for free-flight space. For some species of bats, such as flying foxes which have large wingspans, a very large enclosure would be required to allow free flight. Second is the dietary needs of bats. Specifically, over half of bat species rely on insectivory for sustenance and replicating natural hunting conditions for insectivorous bats would be extremely challenging. Thus, adapting bats to a fortified mealworm diet is the most effective solution, but this is not well-tolerated by every species or by every individual bat.

Previous research has provided some description of the bat immune system, but most of the findings come from genomic and transcriptomic methods or *in vitro* experiments. While the data gleaned from such studies can be used to formulate hypotheses, only rigorously designed *in vivo* experiments informed by *in silico* and *in vitro* studies can fill in with certainty the knowledge gaps surrounding bat immunology.

Chapter 2: A review of paramyxovirus surveillance in bats

2.1 Introduction

With over 1,400 species, bats (order *Chiroptera*) make up a large proportion of mammalian biodiversity. Bats also boast incredible diversity in habitat, inhabiting six of seven continents, and in the diets consumed by different species, including frugivores, insectivores, nectarivores, omnivores, carnivores, and sanguivores (Kunz and Fenton, 2005). As a result of the dietary and habitat diversity of bats, they provide many ecosystem services such as seed dispersal, pollination, and arthropod suppression. Additionally, they are central in the ecology of many human and veterinary pathogens. The ubiquitous distribution of bats and humans across the world also creates numerous interfaces for the potential exchange of pathogens from bats to humans and vice versa. There have been several notable such exchanges in the last 20 years, including severe acute respiratory syndrome coronavirus (SARS-CoV), Nipah virus (NiV), Hendra virus (HeV), Middle Eastern respiratory syndrome coronavirus (MERS-CoV), and potentially SARS-CoV-2. (Chua et al., 2002; Halpin et al., 2000; Towner et al., 2009; Zhou et al., 2020a). These are only a few examples in infectious disease history that give cause to invest resources in better understanding the role and potential of bats to serve as infectious disease reservoirs.

Paramyxoviridae, a family of negative-stranded RNA viruses, includes many pathogens of medical and veterinary importance. A few of these include NiV, HeV, measles virus (MeV), mumps virus, human parainfluenza viruses (HPIV), and canine distemper virus (CDV). Bats are the reservoir for NiV and HeV and many paramyxoviruses (PMVs) of unknown pathogenic potential including Cedar virus, Ghana virus, and myotis bat morbillivirus and there is evidence that bats are the reservoir of the ancestors of MeV, HPIV, and CDV (Chua et al., 2002; Drexler

et al., 2012; Halpin et al., 2000; Hause et al., 2021; Lee et al., 2021a; Marsh et al., 2012b). There have been significant surveillance efforts in regions where zoonotic PMVs are known to circulate in bats such as Southeast Asia, Australia, and Africa. While these efforts are essential to tracking known pathogens, it is of equal importance to sample in regions where there is unknown spillover potential. North and South America are underrepresented in bat sampling and viral discovery efforts, despite this region having the greatest bat species diversity in the world (Alves et al., 2018). It is also established that South American bats do host PMVs. Mapuera virus (MAPV) was discovered in a little yellow-shouldered bat (*Sturnira lilium*) in Brazil in 1979 (Zeller et al., 1989). There have not been any known cross-species transmissions of MAPV but it is able to infect and inhibit the interferon response in a wide variety of mammalian cells (Hagmaier et al., 2007). The porcine orthorubulavirus La Piedad Michoacan virus (LPMV) has also been detected in several species of bats in Mexico. LPMV causes blue eye disease in swine, which involves neurological and respiratory disease and mortality, mainly in piglets. It can also cause reproductive failure in adult swine (Stephan et al., 1988). Blue eye disease represented a significant threat to the swine industry in Mexico, and fortunately has been mostly controlled through preventative measures. While it is unconfirmed that bats are a reservoir for LPMV, phylogenetic analysis of the LPMV genome suggest close relation to other PMVs identified in bats, and LPMV has been isolated from tissues in free-ranging bats (Cuevas-Romero et al., 2021).

Modelling of the impact of climate change on bat species richness across the globe in the context of potential spillover risk predicted high spillover risk in several historic spillover locations such as the Chinese Yunnan province and other parts of southeast Asia as well as many parts of South and Central America (Beyer et al., 2021). These high risk areas overlap with deforestation fronts (Pacheco, 2021). In areas of rapid habitat loss, bats are forced to retreat to find suitable habitats and may end up sharing space with new species of bats and

other animals (Williams-Guillén and Perfecto, 2010). Not only does this increase the population density in that area but it also provides the opportunity for new interactions between bat individuals and species, and the sharing of viromes that comes with it.

In the interest of furthering the understanding of PMV circulation in New World bats, we have compiled the available reports of PMV detections in bats from the literature and various databases. Examining that data has revealed several patterns as well as many sampling gaps and methodology/reporting inconsistencies across studies. Herein is a discussion of the data and recommendations for future sampling efforts.

2.2 Methods

2.2.1 Literature search

PubMed was queried with the following search: (bats OR chiroptera) AND (North America OR South America OR Americas OR Latin America OR Central America OR New World) AND (PMV OR PMVs OR Paramyxoviridae OR virome). 66 results matched the search input and were manually sorted for relevance to the topic of this review. 18 of the 66 results were determined to be relevant. Of these studies, 13 included definitive, individual-level data which could be used in the quantitative analysis. Three studies were pooled-sample studies which are summarized but not quantitatively assessed. Three studies were serological studies (1 of which also included molecular-based individual-level detection and is included in quantitative assessment) The results from these studies were manually extracted and compiled.

2.2.2 Database search

To identify host-virus associations between New World bat species and PMVs, all bat species associated with at least one PMV were extracted from the VIRION database (Carlson et al

2021) on June 26, 2022. Bat genera present in the Western hemisphere (referred to as New World) were extracted, and species in the genera *Myotis, Pipistrellus*, and *Eptesicus* from the Eastern hemisphere (referred to as Old World) were manually removed. Records were deduplicated and compared to the unique host-virus associations obtained from Virus Pathogen Database and Analysis Resource (ViPR), the database of bat-associated viruses (DBatVir) (accessed 6/17/2022) (Chen et al., 2014), and those identified in the peer-reviewed literature.

2.2.3 Data synthesis

Two datasets were compiled to report findings thoroughly and accurately. The surveillance dataset includes studies that report positive and negative results, allowing for calculation of prevalence. Inclusion criteria for the surveillance table are: bats must have been tested for evidence of PMV infection, location must be in the western hemisphere, detection method must be definitive (RT-PCR, deep sequencing, virus isolation) and performed on an individual level (each bat was sampled and assayed for detection), available experimental design data must include total number of sampled bats, number of positive individuals, and individual animal descriptions that at least include genus. Serology and deep sequencing of pooled samples from multiple animals are not included.

The second data set, PMV detections, collects PMV detections on an individual level, i.e. each entry indicates a single bat in which one or more PMV was detected. Inclusion criteria for this table are: a PMV must have been detected, location must be in the western hemisphere, detection method must be definitive (RT-PCR, virus isolation, deep sequencing) and performed on an individual level (each bat was sampled and assayed for detection), available information must include taxonomic identification down to at least the genus level. Serology and deep sequencing of pooled samples from multiple animals are not included.

Additional information included in both data sets if available is bat sex and age, date, country, specific location of sampling, type of sample, and GenBank accession number(s).

2.2.4 Statistics

Prevalence values were compared in R using the prop.test function to compute the chi square value and associated p-values. 95% confidence interval was calculated for prevalence values in R using the exactci function from the PropCI package in R.

2.3 Results

2.3.1 Data granularity of the included studies

Seventeen studies were included in the quantitative portion of this review, 13 of which are published and 4 of which were unpublished had sequences deposited in GenBank. Of these, 11 published papers provided negative data. The majority of studies included in this review provided at least a range of years in which samples were collected (16/17 studies) but only 7/17 gave a more specific date that included at least the month of sampling. While all 17/17 studies indicated the country in which sampling occurred, 13/17 provided location at the level of either city/province or latitude/longitude. Sample type tested was indicated in 13/17 studies. Age and sex of sampled animals were reported in 1/17 and 3/17 studies, respectively.

2.3.2 PMV RNA has been detected in 23 species of bats in 6 countries

The literature and database search resulted in the identification of 207 PMV detections from 23 bats species in the New World (Table 2.1). The surveillance data indicate that 103 total species have been tested for PMVs. While the exact number of bat species in the New World is likely undetermined, there are currently 405 bat species recognized in the Americas (IUCN, 2022).

Using this value, 25.4% (103/405) of bat species in the New World have been tested for PMV RNA and 5.7% (23/405) have had a positive PMV detection.

Surveillance for PMVs has been conducted in 9/35 countries in the New World with over 75% of bats sampled in Brazil, Mexico, and the United States of America (USA). PMVs have been detected in 6 countries: Bolivia, Brazil, Costa Rica, French Guiana, Mexico, and the USA (Table 2.1). However, given the ability of bats to travel long distances, it is necessary to consider the full geographic range of the species which have been shown to host PMVs. Figure 2.1 shows the overlap of the ranges of the species listed in Table 2.1, with deforestation fronts superimposed. The density of PMV+ species appears to with proximity to the equator. The major deforestation fronts also overlap with the areas of greatest species diversity.

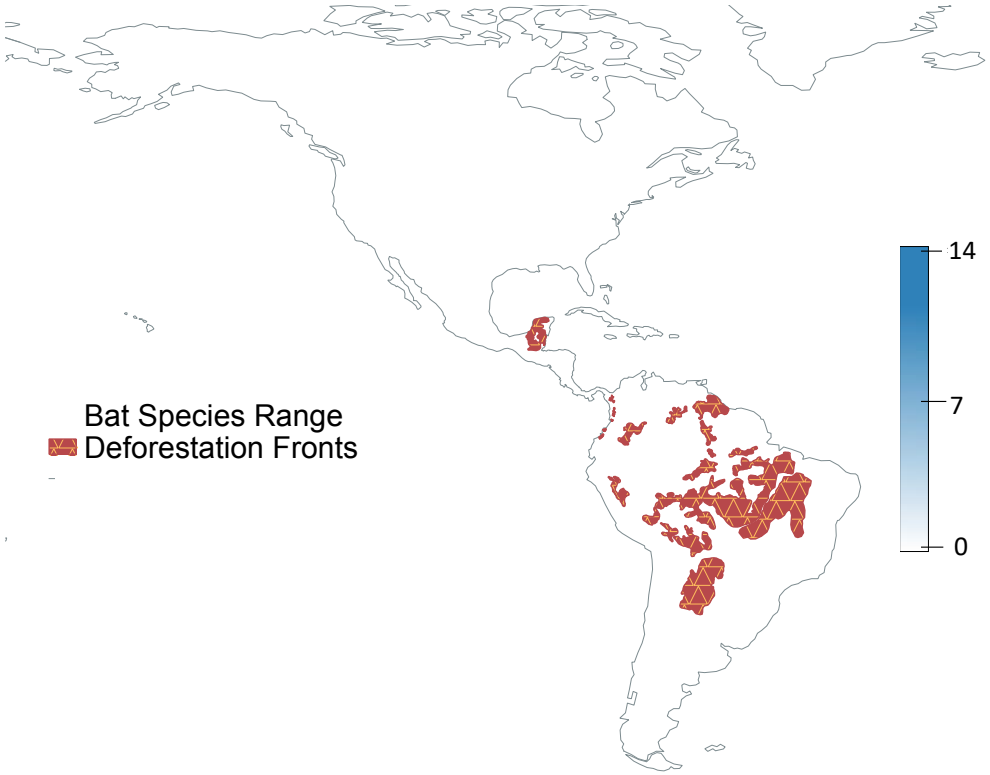

Figure 2.1. Range of PMV+ bat species in the Americas. Species range .SHP files were accessed through the IUCN Red List website (https://www.iucnredlist.org/) and loaded into QGIS (https://qgis.org/en/site/index.html). The deforestation .SHP file was accessed through the World Wildlife Fund (https://globil.panda.org/datasets/46b29ddaf2a54730844000ce8c431f83/about) The gradient represents the number of overlapping species ranges.

Table 2.1 Number of PMV detections by bat species and sampling country. Table generated with PMV detections data.

Genus	Species	Bolivia	Brazil	Costa Rica	French Guiana	Mexico	USA	Grand Total
Antrozous	pallidus						4	4
Artibeus	jamaicensis					7		7
	literatus					1		1
	phaeotis					1		1
	planirostris		1					1
	spp.					3		3
Carollia	brevicauda		4					4
	perspicillata		9	1	6			17
Desmodus	rotundus		11		29	4		44
Diaemus	youngi		2					2
Eptesicus	fuscus						1	1
Glossophaga	soricina		1					1
Macrotus	californicus						1	1
Myotis	californicus/ ciliolabrum						5	5
	keaysi	4						4
	riparius		2					2
	velifer						2	2
Nyctinomops	femorosaccus						4	4
Phyllostomus	elongatus		2					2
	hastatus	1	2					3
Pteronotus	alitonus				1			1
	parnellii		3	77		4		84
Sturnira	lilium		1			1		2
Tadarida	brasiliensis		4				7	11
Grand Total		5	42	78	36	21	24	207

2.3.3 PMVs are significantly more prevalent in haematophagous bats than bats with other diet types.

Using the surveillance table, data were grouped by diet type (Figure 2.2) and prevalence was calculated. Chi-square tests were run for all diet type pairings, and p-values are summarized in supplementary table 2.2. Haematophagus bats had the highest prevalence of PMV RNA (21.9%) followed by insectivorous bats (3.2%), frugivorous bats (1.2%), and nectarivorous bats (0.7%) (Figure 2.3). PMV RNA was not detected in any carnivorous bats in the literature examined here. Our search effort identified 196 records of hematophagous bats being tested for PMV RNA including the two species *D. rotundus* (n=191) and *D. youngi.* (n=5). Of the 43

hematophagous bats that were positive, 41 were *D. rotundus* (prevalence=21.5%) and 2 were *D. youngi* (prevalence=40%).

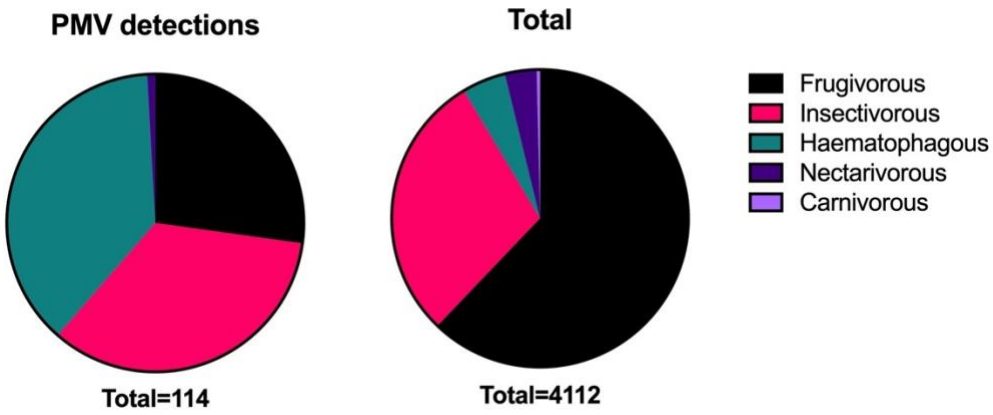

Figure 2.2. Proportions of total sampled bats and PMV positive bats by diet type. 5 diet types were represented in the surveillance data, with PMVs detected in 4.

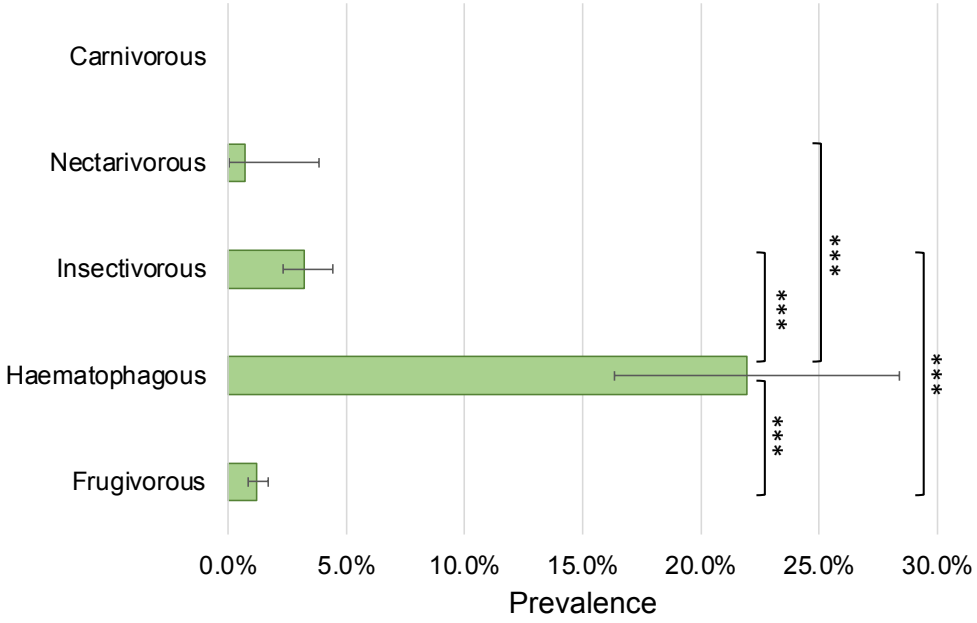

Figure 2.3. Prevalence of PMV RNA in bats by diet type. Prevalence values were calculated by dividing the number of PMV detections by the total number of bats sampled for each diet category. The prop.test function in R was used to compare the prevalence between diet groups and calculate chi square values and p-values (listed in Supplementary Table 2.2) 95% confidence intervals for the prevalence values were calculated using the exactci function from the PropCI package in R.

3.3.4 PMV prevalence is linked to bat family

The surveillance data was grouped by bat family (Figure 2.4) and prevalence was calculated. Mormoopid bats have the highest prevalence of PMV detection (6.3%) followed by mollosids (5.0%), vespertillionids (2.6%), and phyllostomids (2.5%). No PMVs were detected in emballonurids, natalids, or the one noctilionid bat tested. Chi square tests were used to compare bat families and revealed that mormoopid bats have a significantly higher prevalence of PMVs than phyllostomids (p=0.00439) and vespertillionids (p=0.0469), and molossids have significantly higher prevalence than phyllostomids (p=0.00375) (Figure 2.5, Supplementary Table 2.3).

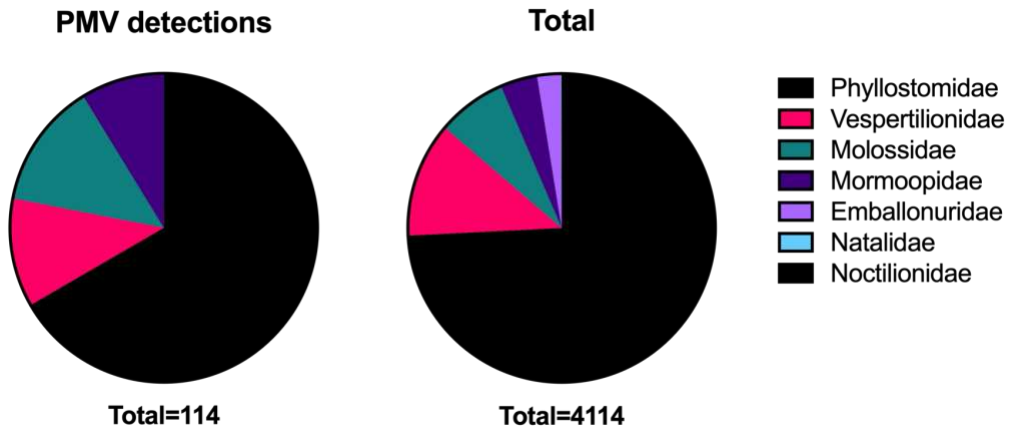

Figure 2.4. Proportions of total sampled bats and PMV detections by bat family. 7/9 New World bat families were sampled (unsampled include Thyropteridae and Furipteridae) and PMVs were detected in 4.

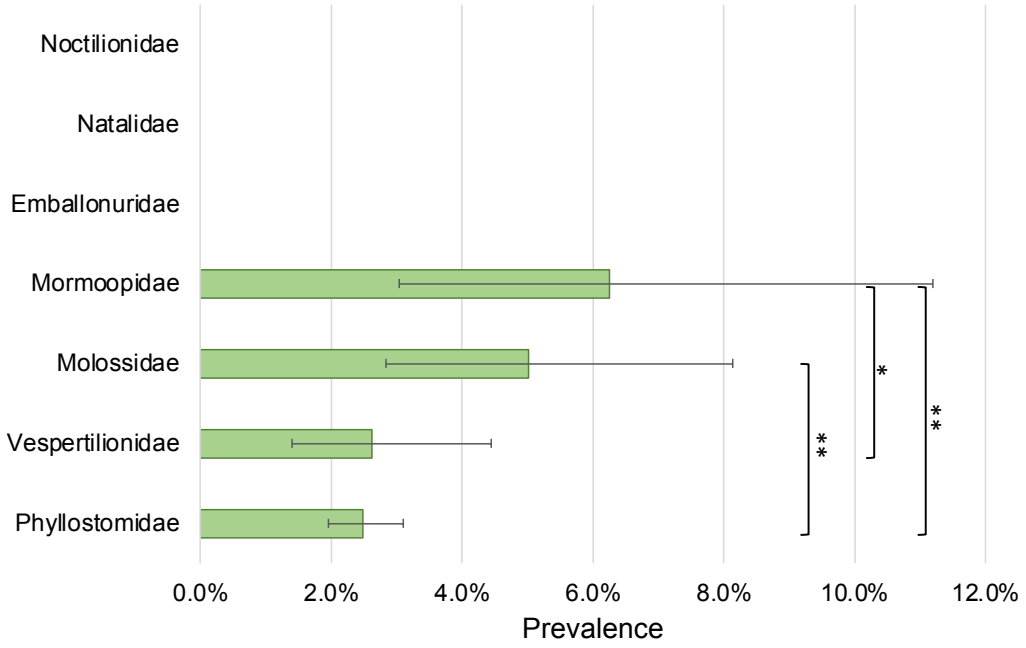

Figure 2.5. Prevalence of PMVs in bats by family. P values and 95% CIs were calculated with the same methods used for diet type prevalence.

2.3.5 Paramyxoviruses detected by high-throughput sequencing

The literature search returned 8 studies that used deep sequencing of pooled samples to detect viruses or examine the bat virome, 3 of which reported detection of PMV-related sequences. While these data were not granular enough to include in our quantitative analysis, they still provide valuable information about PMVs in New World bats.

Bolatti and colleagues collected oral and rectal swabs from 49 non-pregnant female bats from a maternity roost of Brazilian free-tailed bats (*Tadarida brasiliensis*) in Rosario, Argentina. The samples were screened for papillomaviruses using pan-PMV primers, and 5 papillomavirus-positive samples (4 rectal, 1 oral) were pooled and deep sequenced. One read correlated to the family Paramyxoviridae (Bolatti et al., 2020).

Pierle et al collected pooled feces from three roosts of (*Myotis chiloensis*) roosts and one roost of Brazilian free tailed bats. RNA from fecal samples was screened using pan-PMV primers and samples from 2018 and 2021 from one Chilean myotis bat roost were identified as positive for PMV RNA (number of positive samples not reported). Viral enrichment and deep sequencing were performed but revealed no contigs related to PMV sequences (Aguilar Pierlé et al., 2022).

De Witt et al pooled tissue (liver, kidney, heart, lung, intestine) RNA from 6 white-winged vampire bat (*Diaemus youngi*) bats. Deep sequencing returned 3 sequences related to PMVs, but RT-PCR attempts failed to amplify the sequences from individual tissues.

2.3.6 Serological surveys suggest circulation of PMVs in Latin American bats

Schultz *et al* screened 84 bats from Trinidad using ELISA for NiV G and F proteins and a multiplex Luminex serological assay for NiV, HeV, CedV, and GhV G proteins. Three out of 84 bats were positive for henipavirus cross-reactive antibodies by the Luminex assay, while 28 were positive by ELISA for NiV F or G or both (Schulz et al., 2020b). Tissues from 78 of the bats, including lung, liver, kidney, spleen, and brain were screened by RT-PCR using respire-morbilli-henipavirus primers and none were detected. These data at included in our surveillance data collection. Another serological survey by de Araujo *et al* screened 76 bats from 11 species for anti-NiV N protein antibodies by ELISA and IFA. 9 serum samples were positive by ELISA and 13 were positive by IFA (de Araujo et al., 2017). Salas-Rojas *et al* (2004) surveyed 108 bats in the state of Colima, Mexico for porcine orthorubulavirus (PorPV) reactive antibodies, and one male little yellow bat (*Rhogeessa parvula major*) was found to be seropositive.

These studies further support the presence of circulating PMVs in South America, and specifically henipa-like viruses. Serological surveillance in conjunction with molecular testing of

urine, feces, and oral and rectal swabs may provide more information about the circulation of and exposure to PMVs within bat communities.

2.4 Discussion

2.4.1 Data granularity

One of the purposes of this study was to examine the granularity of data reported in surveillance studies for PMVs. Data fields that were almost ubiquitously reported were the species sampled, the year (or range of years), the country of sampling, and the sample type. Also common was date including at least month and location. The format of the location varied from providing city, state/province, or latitude/longitude. To provide maximum specificity, latitude/longitude of sampling sites and exact date should be collected and reported. Information regarding age/reproductive status and sex of the bats sampled was rarely reported. Data granularity is important for many reasons. First, it is often free and easy to collect and report. This type of information can be used to look for trends in what demographic of bats is testing positive (or negative) for viruses, and, if there are trends present, they can lend insight to what host factors may be important in virus-host interactions. Prior studies have identified the reproductive cycle, age, and season as factors associated with viral prevalence for several virus families (Amman et al., 2012; Cappelle et al., 2021; Edson et al., 2019; Hayman, 2015; Montecino-Latorre et al., 2020; Mortlock et al., 2019; Plowright et al., 2008). Also problematic is not reporting negative sampling; only about half (114/207) of PMV detections had the correlating negative surveillance data available, limiting the ability to analyze PMV prevalence.

To summarize, collection and reporting of maximum information including exact date, latitude/longitude of sampling location, and bat species, age, sex, and reproductive status for all sampled animals is recommended. By standardizing the collection and open sharing of this data

from field surveillance, a database could be created that includes granular data about bat demographics, their infection status, spatial, and temporal information and allow for predictive and risk assessment modelling to promote more targeted surveillance and spillover preparedness in the future.

2.4.2 Sampling and detection methods

Going into the future of PMV surveillance, there are several recommended methodology considerations. First is to prioritize using RT-PCR on samples from individual bats to provide the most data granularity and most accurate prevalence. RT-PCR primers should be standardized in surveillance efforts to facilitate phylogenetic analysis of detected PMVs even in the absence of a whole genome sequence. Several surveillance studies used the PAR (pan-paramyxovirus) and RMH (respiro-, morbilli-, henipaviruses) primers designed by Tong and colleagues, and these or updated primer sets targeting the same region may be good candidates (Tong et al., 2008).

While serology may seem an attractive method to detect prior infections, and should not be altogether dismissed, bat serology is often inconsistent and even experimentally infected bats do not necessarily seroconvert (Halpin et al., 2011; Schuh et al., 2019; Schuh et al., 2017a; Subudhi et al., 2018). Additionally, serology provides little certainty about what viruses bats have been exposed to, as all that can be concluded is cross-reactivity to the antigen tested. Therefore, serology likely provides an underestimate of viral exposure and does not provide identification of circulating viruses unless paired with molecular detection methods.

Similarly, high-throughput sequencing of pooled samples is not an ideal detection method. First, it precludes the identification of positive individuals (unless samples are also individually screened) and the calculation of prevalence. Second, the methods of sample collection and

handling are highly variable (number of sheets/arrangement of sheets under roosts, pool size, etc). These factors can and should be computationally optimized for virus detection as a part of experimental design (Giles et al., 2021b). This method is also less sensitive than performing RT-PCR on individual samples. The majority of studies that used high-throughput sequencing were not specifically searching for PMV sequences but rather characterizing the virome of bat colonies. Efforts to coordinate with groups that perform virome analysis could result in availability of additional samples that could be tested for PMVs.

2.4.3 Hematophagous bats should be prioritized in PMV surveillance efforts

There are three species of vampire bat; the common vampire bat, the white-winged vampire bat, and the hairy-legged vampire bat (*Diphylla ecaudata*). The common vampire bat is ubiquitous throughout Central and South America, living in diverse environments that include sea level to the high Andes mountains, coastal deserts, tropical rainforests, and anthropogenic habitats (Van de Vuurst et al., 2022). The common vampire bat traditionally feeds on medium to large wild mammals, but urbanization has resulted in the removal of their prey's natural habitat, and therefore their natural prey, from some areas of their geographic range. This prey has been readily replaced by the livestock farming industry, which provide a very reliable food source. Areas of livestock farming often represent areas of deforestation or landscape that has been anthropogenically altered otherwise. In this review, we identify hematophagous bats as having significantly higher prevalence of PMV RNA than bats of any other diet type (Figure 2.5). The hematophagous bats included in our dataset are primarily the common vampire bat (n=191) and a few white-winged vampire bat (n=5) The surprisingly high prevalence of PMVs in the vampire bats sampled (21.9%), along with the tendency of these bats to congregate in regions of livestock farming and live near human dwellings make them a key species to watch for potential zoonotic PMVs. Whether the greater prevalence of PMVs in vampire bats is attributable to their diet or to another phylogenetic characteristic cannot be concluded in this review, however the

result either way is the same; the common vampire bat and white-winged vampire bat should be targeted during PMV surveillance in the western hemisphere. As one of the major reservoir species for rabies virus, these bats are frequently tested for rabies virus so these samples could be leveraged for PMV surveillance.

In analyzing difference in prevalence between bat families, it was found that mormoopid bats have significantly higher prevalence than phyllostomid and vespertilionid bats and molossid bats have a significantly higher prevalence than phyllostomid bats. It is difficult to ascertain why this difference is observed with the present analyses, so the next step will be to perform phylofactorization to determine what factors may be influencing the prevalence of PMVs in these bat families. Another limiting factor in this analysis was the lack of information about 72 PMV detections in Parnell's mustached bat that are available as sequences on GenBank (Rasche, unpublished). The work remains unpublished, but this data would likely change the calculated prevalence for Mormoopidae.

2.4.4 Summary

This review provides a comprehensive report of PMV surveillance in New World bats to date. The compiled data reveal that PMVs are present in many New World bat species, and at a high prevalence in some, especially vampire bats. Consistency of data collection and methodology will greatly improve the ability to model and predict potential PMV spillover events from bats to humans and enhance preparedness for when it occurs.

Chapter 3: The Jamaican fruit bat as a potential model for *Henipaviruses*

3.1 Introduction

Henipavirus is a genus within the negative-stranded RNA virus family *Paramyxoviridae*. It contains 6 species including the highly pathogenic Nipah and Hendra viruses, and Cedar virus (CedV), Ghana virus (GhV), and Mojiang virus (MoV) which have with unknown pathogenic potential. The most recently discovered pathogenic henipavirus is Langya virus (LayV), which has caused 35 cases of febrile illness in China without mortality (Zhang et al., 2022). Thus far, all henipavirus spillovers have occurred in the Old World; Australia (HeV), China (LayV), and NiV (Southeast Asia) (Selvey et al., 1995; Zhang et al., 2022). However, henipaviruses and henipavirus exposures have been detected in bats across the world, including the Americas (Schulz et al., 2020a; Zhang et al., 2022; Zieger et al., 2017).

CedV was isolated from a urine pool collected beneath a flying fox colony near Cedar Grove, Queensland, Australia (Marsh et al., 2012a). It lacks V and W genes, which encode interferon antagonist proteins found in other pathogenic PMVs, including NiV and HeV. Experimental CedV infection of ferrets, guinea pigs, mice, and Syrian hamsters revealed no apparent pathogenicity; all animals cleared the infection and survived (Marsh et al., 2012b; Schountz et al., 2019). CedV was selected for use in the majority of this study for its classification as a BSL2 virus.

The Jamaican fruit bat (*Artibeus jamaicensis*) is an excellent candidate model for studying henipavirus potential in New World bats because its geographic range and diet create an

interface with humans, and serological evidence indicates it may be naturally exposed to henipaviruses (Schulz et al., 2020a). Jamaican fruit bats are native to Mexico, through Central America to northwestern South America, as well as the Greater and many of the Lesser Antilles. In Central and South America it often lives near commercial fruit plantations and consumes the crops. They also can roost in urban areas and often live in close proximity to livestock. Bats of the genus *Artibeus* have also been identified as susceptible to a number of viruses of interest, including porcine orthorubulavirus (KC906170.1), an unclassified PMV (MN907425.1), flaviviruses, rabies virus, Tacaribe virus, and bat influenza A virus (subtype H18N11)(Barrantes Murillo et al., 2022; Campos et al., 2019; Downs et al., 1963; Machain-Williams et al., 2013; Seetahal et al., 2020; Tong et al., 2013; Torres-Castro et al., 2021a; Zieger et al., 2017). There is also serological evidence that Jamaican fruit bats in Trinidad have been exposed to henipaviruses (Schulz et al., 2020a). Because of the pathogenic potential of henipaviruses, it is important to study potential New World bat hosts to be prepared for future spillover events. In this chapter, I report *in vitro* and *in vivo* characterization of the Jamaican fruit bat as a potential henipavirus host using CedV as a model virus.

3.2 Materials and Methods

3.2.1 Cells and viruses

Jamaican fruit bat kidney (AJK) cells are primary cells isolated from bats in our closed breeding colony. Briefly, whole kidneys were minced with scissors, trypsinized and grown in DMEM supplemented with 10% FBS. During cell passage, cells that detached first during trypsinization were discarded to remove fibroblasts. Fresh medium was added to the flask and every 2 days the trypsin process was repeated for a total of 10 days. This effectively removes all fibroblasts. Primary AJK cells were generated from 7 bats and designated AJK1-AJK7. Of these, AJK1, AJK2, AJK3, and AJK7 were from male bats and AJK4, AJK5, and AJK6 were are from female

bats. Vero E6 cell line was obtained from ATCC and maintained in DMEM supplemented with 10% FBS. NiV-Bangladesh, HeV, and CedPV were work was conducted at Rocky Mountain Laboratories under BSL-4. The BSL2 infectious clone CedV was supplied by Eric Laing at Uniformed Services University.

3.2.2 Infection of AJK1 cells with NiV, HeV, and CedPV

AJK1 cells were seeded at 1 x 10^5 cells/well in a 12-well plate. They were then infected at an MOI of 0.1 with CedPV, NiV, HeV, or mock infected with media for 30 minutes at 37°C. Inocula were then removed, cells were washed once with medium, and 2 mL of 2% FBS in DMEM was added. At 1, 24, 48, and 72 hours post inoculation, supernatant RNA and cellular RNA were extracted using the QIAmp Viral RNA Mini Kit (Qiagen, #52904) and RNeasy Mini Kit (Qiagen Cat #74106), respectively. After extraction, RNA was stored at -80°C until analysis.

3.2.3 Reverse transcriptase quantitative PCR (RT-qPCR)

RNA from infections was utilized with the Real-Time Ready RNA Virus Master kit (Roche Diagnostics product #05619416001) according to manufacturer's instructions using primers and probes listed in supplementary Table 3.1 on a Lightcycler 96 instrument (Roche Cat# 05815916001). RNA extracted from known concentrations of CedV was used as controls to calculate viral RNA concentrations. NiV and HeV controls were unavailable, so the CedV controls were used for all three viruses.

3.2.4 qPCR arrays

The Primer-BLAST tool (https://www.ncbi.nlm.nih.gov/tools/primer-blast/) was used along with the Jamaican fruit bat genome (GCA_004027435.1) to design specific primers (Integrated DNA Technologies) for innate immune genes as well as a housekeeping gene, GAPDH

(Supplementary Table 1). cDNA was generated from RNA using the QuantiNova Reverse Transcription Kit (Qiagen, Cat# 205410). The resulting cDNA was used in the qPCR arrays with the QuantiNova SYBR Green PCR Kit (Qiagen, Cat# 208056) which was cycled with the following parameters on a LightCycler 96 Instrument (Roche Cat# 05815916001): Preincubation at 95°C for 120 seconds, 50 cycles of 95°C for 5 seconds, 60°C for 10 seconds. The fold change in gene expression was calculated using the $\Delta\Delta C_T$ method (Livak and Schmittgen, 2001).

3.2.5 Infection of AJK2-7 cells with CedV.

Infection and RNA extractions were performed as described in 3.2.2 with collection of 200 µL of supernatant for use in virus quantification by $TCID_{50}$. Supernatant was stored at -80ºC until $TCID_{50}$ was performed.

3.2.6 Tissue culture infectious dose 50% assay ($TCID_{50}$)

Supernatant samples were serially diluted 1:10 starting with undiluted sample down to a 10^{-7} dilution. 30 µL of each dilution was inoculated onto Vero E6 cells in 5 replicates on a 96-well plate. 150 µL of DMEM supplemented with 2% FBS was then added to each well. Cells were incubated at 37ºC for 72 hours before being scored for cytopathic effect. Each well was scored either positive or negative for cytopathic effect and the Reed-Muench method was used to calculate titer in $TCID_{50}$/mL (Reed and Muench, 1938).

3.2.7 Passaging CedV on AJK cells

Virus was passaged on AJK4 cells by infecting cells at an MOI of 0.1 (except for in generation of P3 and P10, for which this MOI wasn't possible because of no detectable titer of the prior passage; in these instances, 1 mL of prior passage was used). Infected cells were kept in

DMEM containing 2% FBS at 37°C and 8% CO_2. Supernatant was collected 72 hours post infection, supplemented with FBS to achieve 10%, centrifuged to remove cell debris, aliquoted, and stored at -80°C. The titers of each passage were determined by $TCID_{50}$ on Vero cells.

3.2.8 Infection of AJK4 cells with P0, P6, and P10 CedV

Infection, RNA collection, and supernatant collection were performed as described in 3.2.5.

3.2.9 Whole genome sequencing of serially passaged CedV

Samples were prepared for sequencing using a multiplexed PCR method designed for generating coding-sequence-complete genomes for sequencing on Illumina instruments. cDNA was generated with a SuperScript™ IV Reverse Transcriptase kit (Invitrogen Cat# 18090010) using vendor recommended volumes (Invitrogen) at the following conditions: 23°C for 10min, 50°C for 10 min, 55°C for 10 min, 80°C 10 min, 4°C hold. Primers for multiplexed PCR were designed with reference NC_025351.1 Cedar virus isolate CG1a using the online Primal Scheme primer designer software (http://primal.zibraproject.org) and default settings. Two 100 uM primer pools (pools A and B) were generated as previously described (Quick et al., 2017). Briefly, primers with adjacent regions were added to alternate pools to prevent overlapping reactions within pools. Primer pools were diluted to 10 uM prior to use. Each cDNA sample was amplified in concurrent reactions with primers from pool A and pool B using Q5 2x Master Mix (NEB Cat# M0492S) at ½ vendor recommended volumes at the following cycling conditions: 98°C for 30s, 30 cycles of 98°C for 15 s and 65°C for 5 min, 4°C hold. A and B reactions were combined by volume following amplification. Samples were purified post-PCR using a 1X concentration of AMPure XP beads (Beckman Cat# A63881) following manufacturer recommended instructions. End tailing was performed with a KAPA Hyperprep kit (Roche Cat # 07962347001) using ¼ vendor recommended volumes and the following conditions: 20°C for 30

min, 65°C for 30 min, 4°C hold. KAPA UDI barcodes were ligated with KAPA Hyperprep kit using ¼ vendor recommended volumes and the following conditions: 20°C for 15 min. Samples were purified post-adaptor ligation using a 0.8X concentration of AMPure XP beads (Beckman). Final library amplification was done with KAPA Library Amp Primer Mix (Roche Cat# 7958994001) using vendor recommended volumes and the following conditions: 98°C for 45s, 10 cycles of 98°C for 15 s, 60°C for 60 s, and 72°C for 30 s. Samples were purified post-library amplification using a 0.8X concentration of AMPure XP beads (Beckman). Samples were quantified with Qubit dsDNA Broad Range kit (Thermo Fisher Cat#Q32850) and pooled by mass at 10ng each. The final pool was normalized to 1 ng/μL and analyzed for size and quality with a TapeStation D1000 Screen Tape assay (Agilent Cat# 5067-5582). Library QC was performed using the KAPA Library Quantification Kit (Roche Cat# KR0405) using ¼ vendor recommended volumes. Library was denatured, and a 10% PhiX control (Illumina Cat# FC-110-3001) was spiked in. Library was loaded at a concentration of 8pM and sequenced with a MiSeq V2 Nano 500 cycle kit (Illumina Cat# MS-102-2003). Reads aligning to the host genome (WHU_Ajam_v2, GCA_014825515.1) were filtered out prior to calling and identifying viral variants with custom bash and R scripts (https://github.com/stenglein-lab/viral_variant_caller).

3.2.10 Experimental inoculations of Jamaican fruit bats

Three bats (2M, 1F) were swabbed orally and rectally as well as bled, and were subsequently anesthetized with 3% isoflurane to effect with an oxygen flow rate of 1.75 L/min. The bats were inoculated intranasally with 5 x 10^4 pfus of CedV which had been passaged on Vero E6 cells 4 times. While anesthetized, bats were distinguished by painting their toenails with different colors of nail polish. Bats recovered on a heating pad until they were mobile and alert.

3.2.11 Non-terminal bat sampling procedures

On days 3, 6, 10, 14, 21 and 28 post-inoculation, all bats were swabbed orally and rectally to monitor potential routes of transmission. Swabs were placed in 500 μL of viral transfer media (VTM) and stored at -80°C. Urine was collected opportunistically by pipetting or catching it in a microcentrifuge tube and adding equal volume VTM. Bats were bled by puncturing the cephalic vein using a 23-gage needle and pipetting the blood into BD microtainer tubes containing K_2EDTA to be used in qRT-PCR. Amount of blood collected was limited to ≤50 μL. After collection, pressure was applied to the vein until bleeding stopped, and bat was returned to its cage.

3.2.12 Euthanasia and Necropsy

On day 28 post challenge, the three bats were euthanized. To euthanize, bats were heavily anesthetized using 3% isoflurane with an oxygen flow rate of 1.75 L/min until there were no signs of deep pain as tested by firmly pinching the foot. A thoracotomy was then performed using standard sterilized scissors to puncture the skin, muscle, and diaphragm caudal to the sternum. The chest cavity was then cut caudally to cranially to prevent negative pressure from building in the thorax. Terminal bleeds were performed by inserting a 21-gauge needle into the apex of the heart and yielded a maximum volume between 1 and 1.5 mL per bat. 50 μL of blood was reserved in a BD microtainer tube with K_2EDTA and the rest was transferred to a BD microtainer serum separation tube (SST) and allowed to clot before centrifugation at 20,000 rcf for 90 seconds. Serum was collected and stored at -80ºC until analysis. Euthanasia was immediately followed by necropsy. Bats were assessed for gross pathology and then samples of lung, liver, spleen, and kidney were collected and flash frozen in LN_2 then stored at -80ºC until analysis. Processing of tissue samples included homogenization on a TissueLyser (Qiagen) at 50 hz for 5 minutes followed by centrifugation at 10,000 rcf to pellet any debris. Resulting

supernatant was used RNA extraction for viral RNA quantification. RNA was extracted from blood and tissues using the RNeasy Mini Kit (Qiagen Cat #74106). RT-qPCR was performed as described in section 3.2.3.

3.2.13 Serology

A 96-well plate of Vero E6 cells was infected with CedV at an MOI of 0.1 and incubated for 72 hours and then fixed with 85% acetone for 20 minutes at -20ºC then stored at 4ºC for use as substrate in an ELISA due to lack of available CedV antigen. Serum from bats 28 days post-challenge was serially diluted 2-fold starting at a 1:100 dilution. Plates were washed 0.05% Tween 20-PBS and blocked with SuperBlock T20 Blocking Buffer (ThermoFisher Cat#37536) for 1 hour at room temperature. Plate was washed with PBS-tween and PBS. Sera from experimentally infected bats and negative control serum from an uninfected bat were incubated on fixed infected cells for 1 hour at room temperature. Plate was washed and then 150 µL protein A/G-HRP (ThermoFisher) was added to the wells at a concentration of 2 µg/mL and incubated at room temperature for 30 minutes. Plates were washed and 100 µL of KPL ABTS one component peroxidase substrate (SeraCare Cat# 5120-0046) was added and incubated at room temperature for 30 minutes. 100 µL of ABTS Stop Solution was then added and plates were read at 405 nm on an EMax Plus Microplate Reader (Molecular Devices). The limit of detection was set at three standard deviations above the average OD of the negative control serum.

3.3 Results

3.3.1 Primary Jamaican fruit bat kidney cells are susceptible to henipavirus infection.

AJK1 cells were infected with NiV, HeV, or CedV at an MOI of 0.1 and photomicrographs were taken every 24 hours. At 72 hpi, NiV and CedV infected cells displayed classical syncytia formation that is associated with henipavirus infection (Figure 3.1B and E). Syncytia formation was observed in HeV infected cells at 48 hpi (Figure 3.1C), but HeV infected cells experienced extensive cell death by 72 hpi such that no syncytia were visible (Figure 3.1D). RT-qPCR showed that viral RNA copies increased over the course of study, indicating active viral replication (Figure 3.2). The growth curve is similar in shape between the three viruses; however, NiV viral RNA concentrations remained about 1-2 $\log_{10}(TCID_{50}$ equivalents/mL) lower than those of HeV and CedV including at 1 hpi. qPCR arrays using innate immune gene primers revealed that NiV and HeV are able to modulate the interferon response while CedV is not (Figure 3.3). At 48 and 72 hpi, HeV-infected cells had high upregulation of CASP1. IL-15Rα was also highly upregulated in HeV-infected cells at 48 and 72 hpi.

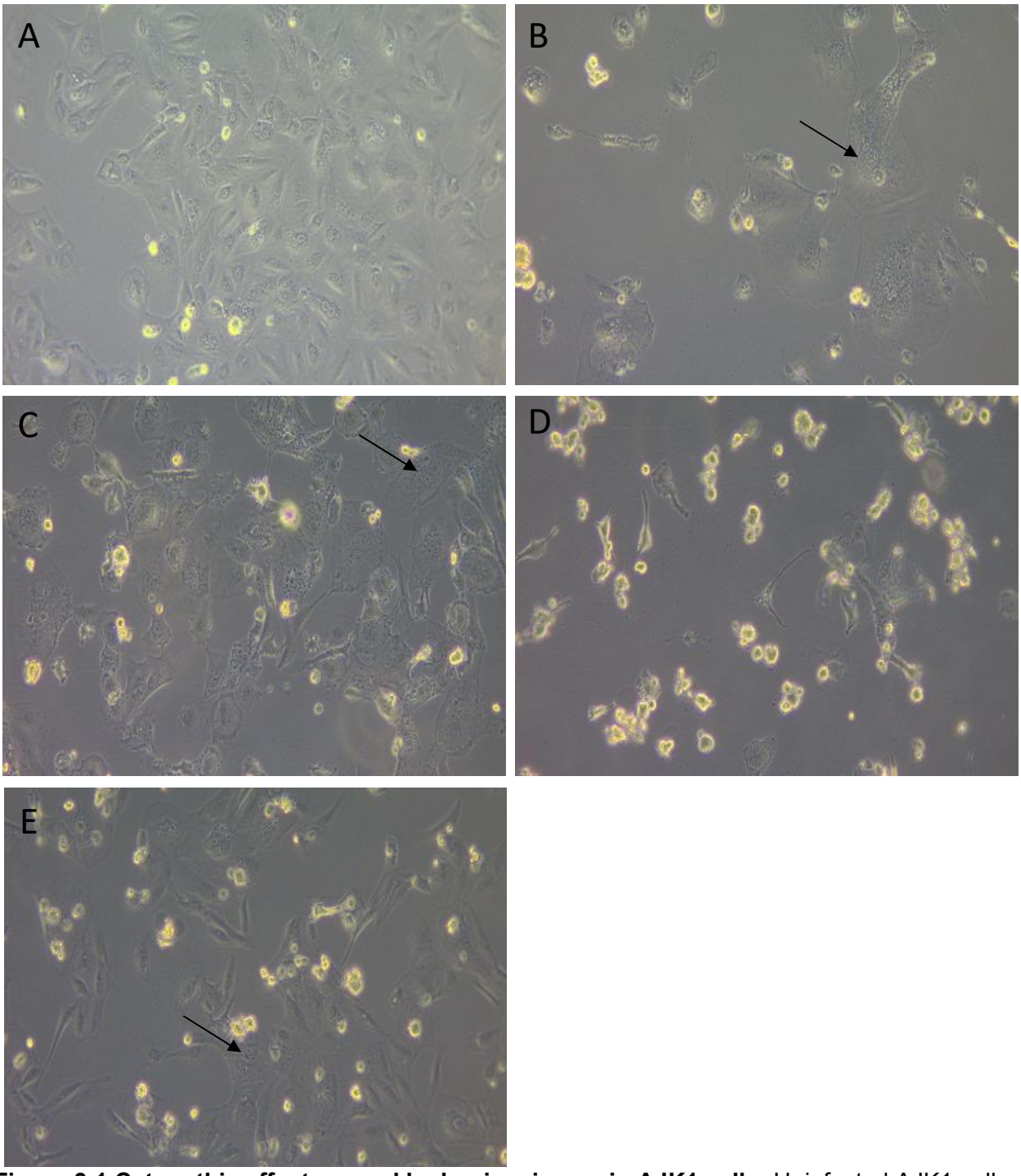

Figure 3.1 Cytopathic effect caused by henipaviruses in AJK1 cells. Uninfected AJK1 cells (A), NiV (B), HeV (D), and CedV (E) infected AJK cells after 72 hours, and HeV infected cells at 48 hpi (C). Arrows indicate syncytia formation.

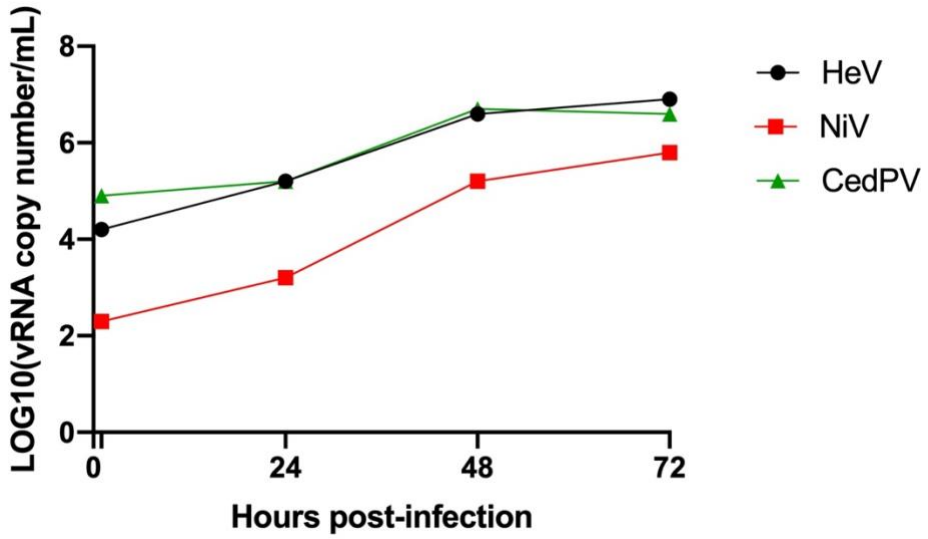

Figure 3.2 Comparison of growth kinetics of NiV, HeV, and CedPV in AJK1 cells. Cells were infected at an MOI of 0.1 with NiV, HeV, or CedPV, or mock-infected with media. Supernatant RNA was extracted at 1, 24, 48 and 72 hours and analyzed by qRT-PCR to determine the concentration of viral RNA using CedV standards.

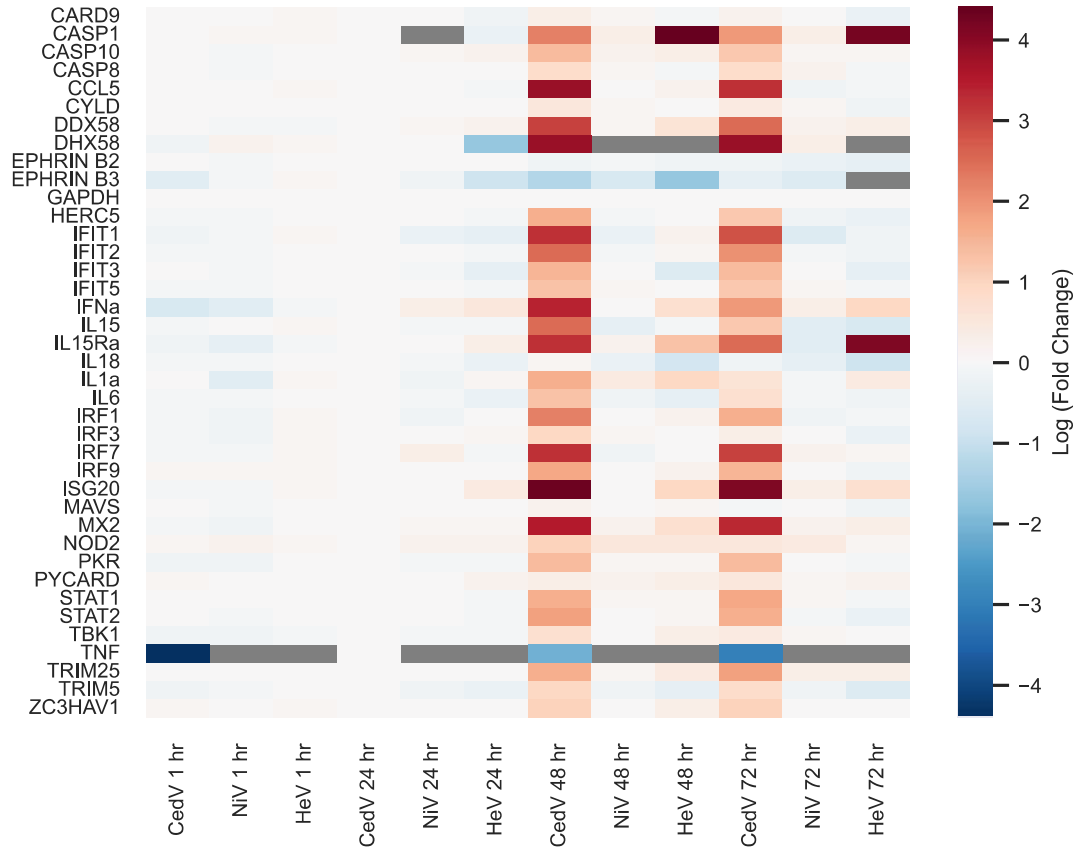

Figure 3.3 Change in gene expression at 72 hours post infection with CedV, NiV, or HeV. Values calculated using $\Delta\Delta C_T$ method with GAPDH used as normalization gene. Not shown are

undetectable genes (CXCL10, IL1B, TLR7) and genes with negligible changes in expression (CYLD, Ephrin B2, Ephrin B3, IRF3, MAVS, TBK1).

3.3.2 Seven biological replicates of AJK cells are susceptible to CedV infection and generate a similar innate immune response.

After confirming that AJK1 cells are susceptible to NiV, HeV, and CedPV, AJK2-7 were tested for susceptibility using an infectious clone CedV at BSL-2. The infections were performed and analyzed using the same methods as the infection performed at BSL-4. Growth kinetics of CedV in cell lines AJK2-7 were similar to replication in AJK1 cells as evidenced by infectious virus titers and viral RNA concentration (Figure 3.4A and B). Cellular RNA from each infection timepoint was used in qPCR arrays to examine transcription upregulation of 42 innate immune genes as well as one housekeeping gene (GAPDH) and Ephrin B2 and Ephrin B3 (cell entry receptors for CedV). Notably, some cytokines were undetectable in uninfected cells, precluding the calculation of fold change. IFN-β, IFN-λ, IL-1β, and TNF were undetectable in uninfected controls but present in most 24, 48, and 72 hpi cellular RNA from infected AJK cells. IL-15, IL-18, IL-1α, and IL-6 overall did not show large increases in expression. The chemoattractant CCL5 was highly upregulated in all cells, but particularly in AJK4 in which it was upregulated 1.3 x 10^5-fold at 48 hpi. IFN-α gene transcription was upregulated at 48 and 72 hpi in all 7 cell lines. Transcription of genes associated with the induction and maintenance of an antiviral intracellular state (all four IFIT genes, CASP1, CASP8, and CASP10, HERC5, PKR, PYCARD) were highly upregulated at 48 and 72 hpi in all cell lines. Similarly, genes associated with proteins with direct antiviral activity (TRIM5, TRIM 25, MX2) and viral detection and antiviral signaling (MAVS, Nod2, PKR, DDX58 (RIG-I), DHX58, IL-15rα, IRFs, STAT1 and 2) were upregulated in all 7 cell lines at 48 and 72 hpi.

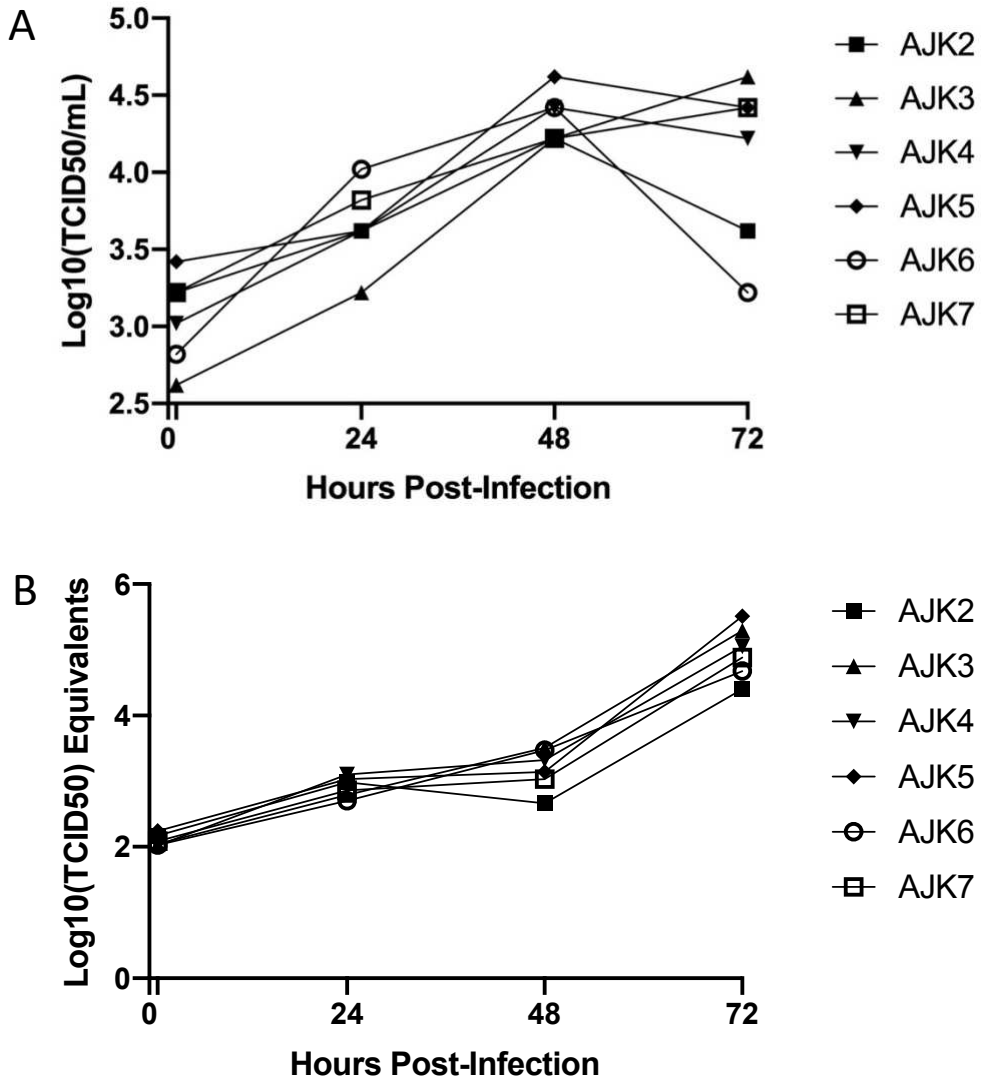

Figure 3.4 Comparison of growth kinetics of CedV in six biological replicates of primary Jamaican fruit bat kidney cells. AJK2-7 were infected at an MOI of 0.1 and supernatant was collected at 1, 24, 48, and 72 hours post-infection. Virus titer was determined by TCID50 assay (A) and supernatant RNA was used in RT-qPCR to quantify viral RNA (B).

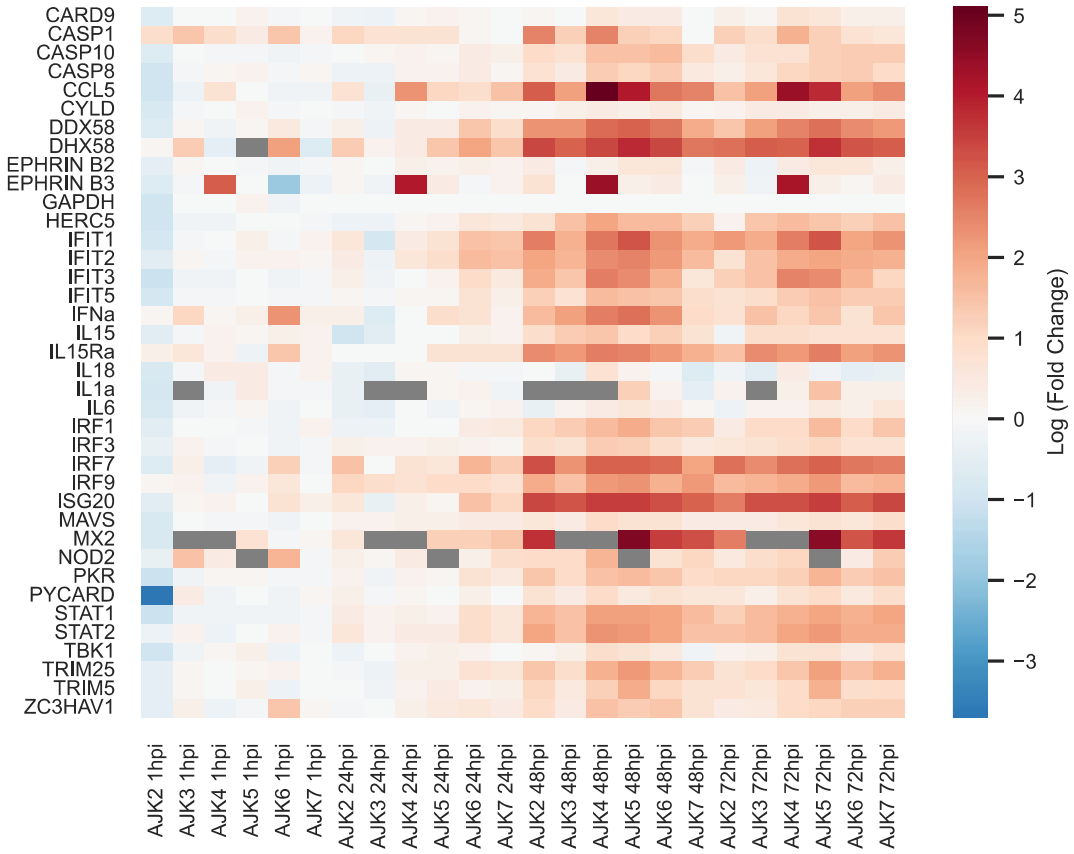

Figure 3.5 Innate immune gene expression of AJK2-7 infected with CedV. AJK cells were infected with CedV at an MOI of 0.1 and cellular RNA was extracted at 1, 24, 48, and 72 hpi. Values calculated using ΔΔCT method with GAPDH used as normalization gene.

3.3.3 Passaging CedV on AJK4 cells results in changes to the viral genome and increased ability to cause cytopathic effect.

CedV was passaged on AJK4 cells 10 times to observe how host factors may influence viral adaptation. The resultant passage 10 (P10) virus was sequenced to reveal mutations that occurred (Table 3.1). P6 was further investigated in addition to P10 because it had the highest titer of the 10 passages, and thus may represent a point at which CedV acquired adaptations to the AJK4 cells (Figure 3.6). Cytopathic effect (CPE) was compared between P0, P6, and P10 CedV on AJK4 cells over 72 hours following infection at 0.1 MOI and increased CPE was observed in the cells infected with P6 and P10 CedV (Figure 3.7). Notable genome changes

included two mutations to the polymerase gene (N858I and D303G), one mutation in the fusion protein gene (K548E), and one mutation in the nucleocapsid gene (S445G).

Table 3.1. Mutations detected in CedV genome after 10 passages on AJK4 cells. Values indicated proportion of reads that contained the mutation.

Mutation	Gene	Amino acid change	Functionality change	P0	P10
N858I	polymerase	asparagine to isoleucine	polar to hydrophobic	0	0.52
K548E	fusion	lysine to glutamate	pos to neg charge	0.68	1
S445G	nucleocapsid	serine to glycine	not too different	0.67	1
D303G	polymerase	aspartate to glycine	acid to non-acid	0	0.22

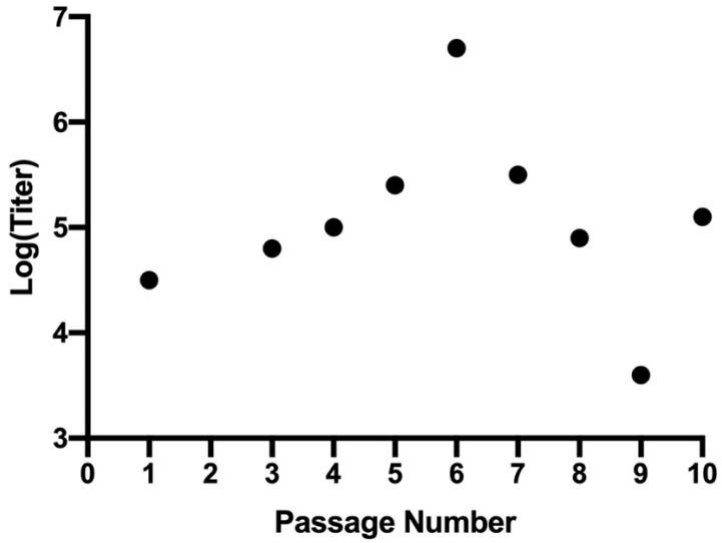

Figure 3.6 Titers of each CedV passage. Titers were determined by $TCID_{50}$ assay. Passage 2 titer was below the limit of detection.

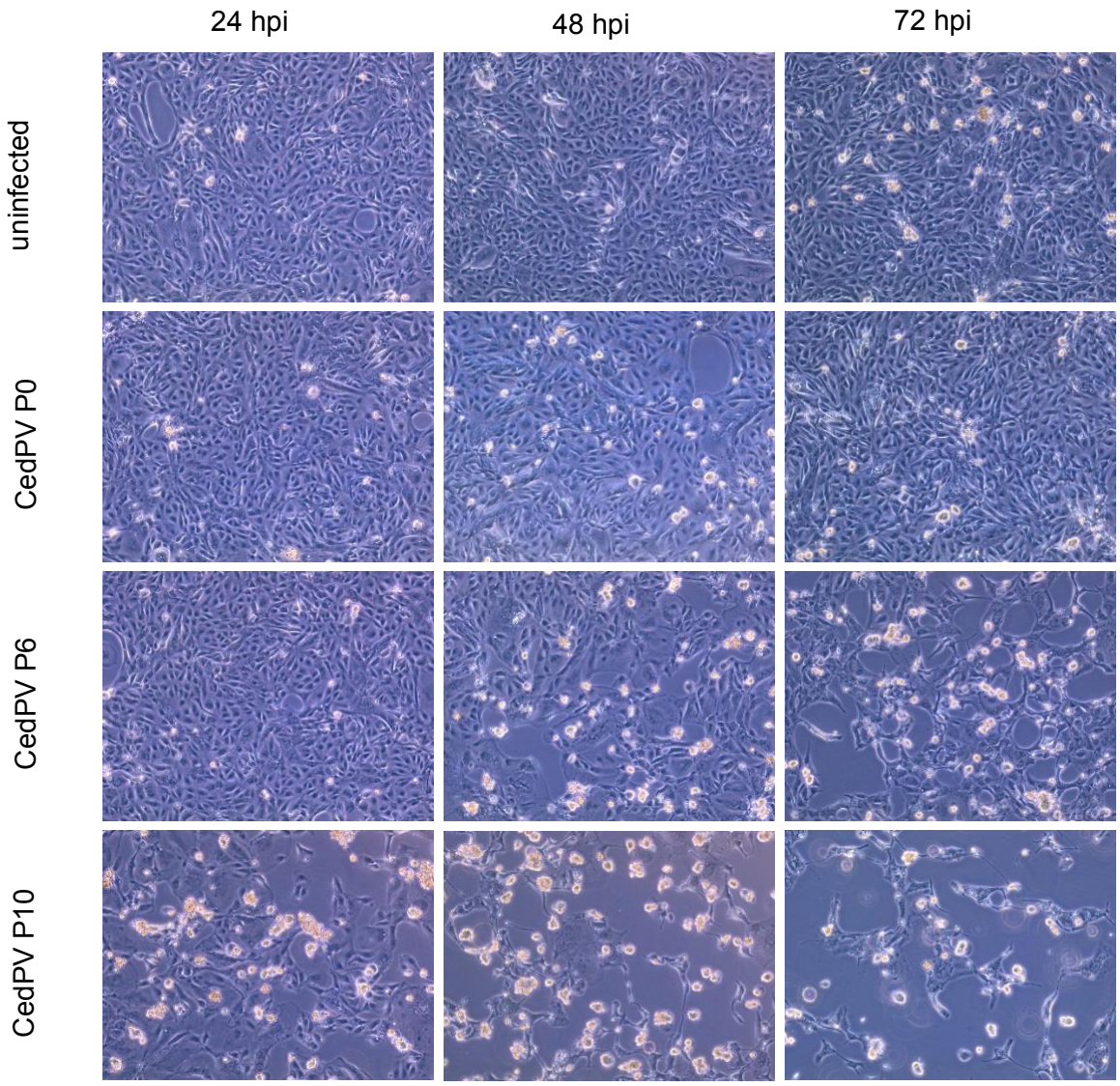

Figure 3.7. Cytopathic effect caused by different passaged of CedV. Photomicrographs were taken every 24 hours over the course of AJK4 cell infection with P0, P6, or P10 CedV alongside an uninfected control. 100X magnification.

3.3.4 Jamaican fruit bats exhibit transient shedding and viremia and develop antibody response when challenged with CedV.

Three bats (2M, 1F) were intranasally challenged with 1 x 10^5 PFU of CedV. Oral swabs, rectal swabs, and blood were collected on days 3, 6, and 10 post-challenge. Euthanasia and full necropsy were performed 28 days post-challenge. Viral RNA was detected in day 3 and 6 oral and rectal swabs, and in the female's blood sample from day 10. At the time of necropsy, it was

found that the female was pregnant. ELISA was performed using serum collected at the time of necropsy and two bats (1M, 1F) had anti-CedV antibody titers of 400, and the third (M) had a titer of 200. No neutralizing antibodies were detected by serum neutralization assay.

3.4. Discussion

Old World pteropid bats are reservoirs of henipaviruses including NiV, HeV, GhV, and CedV (Chua et al., 2002; Drexler et al., 2009; Halpin et al., 2000; Marsh et al., 2012a). NiV and HeV have maintained a pattern of intermittent spillover since their initial emergence causing hundreds of human cases and deaths. While pteropid and other Old World bats have been investigated for their role as reservoirs for PMVs since the emergence of NiV and HeV, New World bats have been neglected despite the known presence of PMVs in bats in the Americas. In this work we showed that seven biological replicates of primary Jamaican fruit bat cells (AJK1-7) are susceptible to CedV infection, and that AJK1 cells are also susceptible to NiV and HeV infection. During infection, NiV and HeV suppressed the innate immune response of the AJK1 cells. This suggests that the V and W proteins bind the STAT1 protein of New World bats and inhibit phosphorylation, which is the main mechanism of interferon antagonism by the V and W proteins. CedV was unable to antagonize the immune response to the extent of NiV and HeV, further suggesting that V and W are the pathogenic determinants of henipavirus infection. NiV, HeV, and CedV caused hallmark syncytia formation and cell death, with HeV causing the most extensive cell death over the study course. HeV-infected cells had highly upregulated CASP1 mRNA in contrast to NiV, and CASP1 plays a role in initiating cell pyroptosis, which could be the mechanism behind the more dramatic cell death observed in the HeV-infected cells (Miao et al., 2011). More targeted qPCR arrays would need to be designed in order to clarify the pathway of cell death.

Serological evidence of New World bat exposure to henipa-like viruses has been found in Trinidad and Brazil, and molecular evidence of henipaviruses has been identified in a bat in Costa Rica and opossums in Brazil (de Araujo et al., 2017; Hernández, 2022; Schulz et al., 2020b). It is important to consider that habitat loss and changing resource landscapes create new opportunities for zoonotic spillover events and have contributed to impactful spillover events in the past (Kessler et al., 2018). Therefore our *in vivo* study provides important evidence that the Jamaican fruit bat, a populous and widespread bat species in Central America, are potential henipavirus hosts in the New World. Identification of viral RNA in oral and rectal swabs highlights these as potential routes of transmission, and also an important non-terminal sampling method. At the time of necropsy, it was found that the female in our study was pregnant. Because only the female had detectable viral RNA in a blood sample, it is possible that the immunosuppression involved with pregnancy inhibited her ability to control the infection as efficiently as the two males in the study. It has been previously found that pregnancy is a risk factor for HeV infection in little red flying foxes, and therefore maternity roosts may also be an important target to increase non-terminal sampling efficiency (Plowright et al., 2008).

A theory in bat immunology is that the bat interferon response is “always on” and this can keep viral infections at bay. This was suggested after unusually high levels of constitutive IFNα mRNA were reported in black flying fox (*Pteropus alecto*) kidney cells and tissues (Zhou et al., 2016). In addition it was reported that there was minimal upregulation of IFNα following incubation with polyI:C. A similar experiment in Leschenault’s rousette bat showed minimal IFNα upregulation upon poly I:C treatment as well (Omatsu et al., 2008). Our data supports a classic interferon response in Jamaican fruit bats in which there is extremely low or undetectable levels of interferon mRNA in uninfected cells, with rapid and dramatic increase in interferon expression upon viral challenge. This effect was observable for INFα, IFNβ, and IFNλ in uninfected cells compared to CedV infected cells. Interferon was not upregulated in NiV or HeV infected cells,

presumably due to the interferon antagonist properties of proteins V and W. But in CedV infected cells there was greater than 10^4-fold increase of IFNα, IFNβ, and IFNλ mRNA at 48 and 72 hours post infection with CedV. It is possible that interferon expression patterns may be different between New and Old World bats; however, this will require a comparison using similar cells/tissues and the same stimulant (virus or polyI:C) to confirm.

To address the question of how a henipavirus may adapt to a New World bat host, CedV was passaged 10 times on AJK4 cells. There was no clear trend in the titer over the course of 10 passages, but passage 10 did replicate to a higher titer than P0. When a comparative growth curve study was performed on P0, P6 (highest titer passage), and P10, there was an increase in ability to cause CPE from P0 to P6 and from P6 to P10. Interestingly, when innate immune gene expression was compared between P0 and P10 CedV-infected cells, it was found that P10 may be more effective at activating the innate immune response. This could explain the increase in CPE over the passages as well, suggesting that apoptosis may be responsible for the CPE. This is consistent with the discrepant CPE induction by NiV and HeV in AJK1 cells; HeV was activating the innate response more than NiV and seemingly resultant was increased CPE. Deep sequencing of P0, P6, and P10 CedV also revealed some potential explanations for the increased CPE. One of the mutations that became fixed was a lysine-to-glutamate substitution at position 548 of the fusion protein. Position 548 is in between two functionally important di-tyrosine motifs (positions 533 and 553) of the fusion protein cytoplasmic tail. Mutation of the di-tyrosine motif at position 553 has been shown to increase cell surface expression and fusogenicity of the F protein (Fischer et al., 2020). It is possible that the mutation of a nearby residue impacted this site and lead to a similar outcome. This is a potential cause of the increased CPE because the fusion protein drives the ability of the virus to cause an infected cell to fuse to adjacent cells, thus forming syncytia. To clarify which mutations are responsible for

the changes in ability to cause CPE, site directed mutagenesis could be used to create four infectious clones, each containing one of the mutations listed in Table 3.1.

Serological and molecular evidence show that there are henipaviruses circulating in bats and other mammals in the New World. It is important, for this reason, to intensify research efforts to characterize henipaviruses and potential New World hosts as well as ramp up surveillance efforts in areas that are most high risk for spillover events, such as sites of deforestation.

Chapter 4: Introduction to Coronaviruses and Deer Mice

4.1 Introduction to SARS-CoV-2

4.1.1. Overview of *Coronaviridae*

The viral family *Coronaviridae* is comprised of helical, enveloped, positive sense RNA viruses that are further classified into two subfamilies including *Coronavirinae* and *Torovirinae*. *Coronavirinae* contains all medically relevant coronaviruses, and consists of four genera: *Alphacoronavirus, Betacoronavirus, Gammacoronavirus,* and *Deltacoronavirus* (Figure 4.1). Viruses within these genera have a broad host range, including humans, a variety of other mammals, and birds. Coronaviruses have the largest genome sizes of all RNA viruses, with up to 32 kb. This work focuses on the coronavirus severe acute respiratory syndrome coronavirus-2 (SARS-CoV-2) within the genus *Betacoronavirus.*

4.1.2 Overview of betacoronaviruses

Betacoronaviruses are divided into five subgenera; *Embecovirus*, *Sarbecovirus, Merbecovirus, Nobecovirus,* and the most recently added *Hibecovirus. Embecovirus* contains coronavirus species that are hosted by rodents and the species *Betacoronavirus 1*, which infects cattle and humans and a subspecies of which (human coronavirus OC43) causes the common cold. *Merbecovirus* contains the emerging human pathogen Middle Eastern respiratory syndrome coronavirus (MERS-CoV) that first spilled over from dromedary camels to humans in Saudi Arabia in 2012 (Ferguson and Van Kerkhove, 2014; Zaki et al., 2012). MERS-CoV has caused over 800 human cases and has a case fatality rate of about 35% (WHO). Merbecoviruses, nobecoviruses, and hibecoviruses have been identified primarily in bats. The only sarbecovirus species is the severe acute respiratory syndrome-related coronavirus. Subspecies include

SARS-CoV, SARS-CoV-2, and several SARS-like CoVs identified in bats and pangolins. Sarbecoviruses, specifically SARS-CoV-2, will be the focus of this work.

4.1.3 Sarbecovirus replication

Infection of a host cell is initiated when the viral spike (S) protein domain S1 binds the host cell receptor angiotensin-converting enzyme-2 (ACE2) and the S protein domain S2 mediates conformational changes which culminate in the fusion of the viral envelope with the host cell membrane (if TMPRSS2 is present) or clathrin-mediated endocytosis (if TMPRSS2 is absent/insufficient) (Jackson et al., 2022). Proteolytic cleavage of the S2 domain to expose the fusion peptide is required to facilitate cell entry. The most common protease that performs this cleavage during sarbecovirus infection is TMPRSS2, which co-localizes with ACE2 in pneumocytes (Shulla et al., 2011). Once in the cytoplasm, the first two-thirds of the viral genome serves as a mRNA and the replication-transcription complex (RTC) is translated. The RTC is encoded by the genomic RNA in ORF1a and ORF1b, which have a small overlapping section (Figure 4.1). For the entire RTC to be translated, ribosomal frameshifting must occur at the overlap, backtracking to the start of ORF1b. Once assembled, the RTC can generate the negative-sense antigenomes and subgenomic RNA (sgRNA). The antigenome and -sgRNA are used as templates from which the positive-sense genome and subgenomic mRNA can be copied. When the -sgRNAs are transcribed, the same 5' leader sequence is joined to a body RNA encoded by a sequence at the 3' end of the genome via template switching. Both the genome and sgRNAs have 5' caps and 3' poly-adenylated tails. Viral assembly occurs in the endoplasmic reticulum-Golgi intermediate compartment (ERGIC) where genome-nucleocapsid complexes then bud through the ERGIC to receive their envelope containing the membrane protein, envelope protein, and S protein. Assembled virions are then exported in vesicles and released from the host cell via exocytosis.

4.1.3.1 Coronavirus recombination

An important feature of coronavirus molecular biology is the ability to undergo homologous and non-homologous recombination. This process is facilitated by the same mechanism that results in sgRNA transcription- template switching. Recombination results in significant changes to the genome, which may either provide an evolutionary advantage or disadvantage. It is hypothesized that a recombination event led to the emergence of SARS-CoV-2, and evidence indicated that it has facilitated the continual emergence of variants with increased transmissibility, virulence, and the ability to escape immunity to other variants (Focosi and Maggi, 2022).

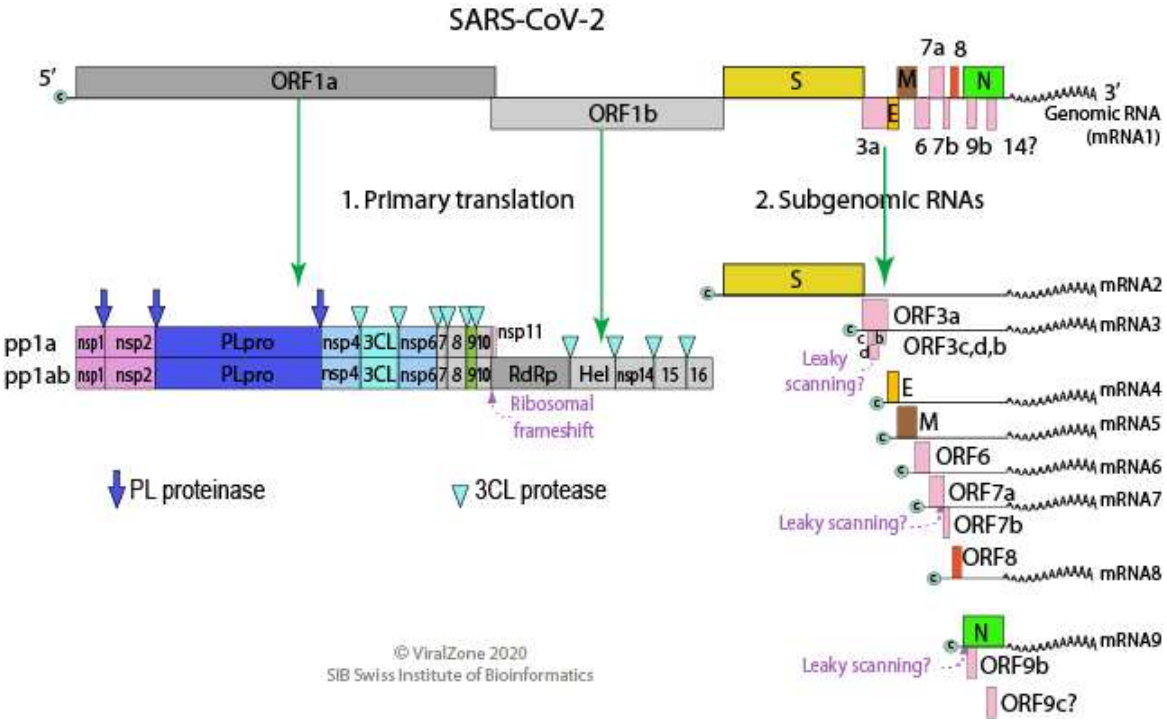

Figure 4.1 Diagram of SARS-CoV-2 genome. ORF1a and ORF1b act as both genome and mRNA and encode the replication-transcription complex. Subgenomic mRNAs are generated by template switching that combines the 5' leader sequence with a gene towards the 3' end, creating a 3' nested set.
Source: https://viralzone.expasy.org/resources/nCoV_genome_bis.png

4.1.4 Pathogenesis of SARS-CoV-2 infection in humans

The clinical disease caused by SARS-CoV-2, COVID-19, ranges from asymptomatic to respiratory failure and death. The most common symptoms are fever, cough, myalgia, and fatigue. Pathological findings in patients with severe COVID-19 include diffuse alveolar damage, hyaline membrane formation, desquamation of pneumocytes, and fibrin deposits (Martines et al., 2020). Severe disease is associated with the induction of a cytokine storm, which is caused when SARS-CoV-2 enters type-II alveolar pneumocytes and induces production of inflammatory cytokines such as TNF, IL-6, and IL-1 (He et al., 2006). The downstream effects of this cytokine storm can include acute respiratory distress syndrome (ARDS), multi-organ failure, sepsis, and septic shock.

4.1.5 Animal models of COVID-19

A number of animal models displaying varying degrees of susceptibility, clinical signs, and pathology have been explored for COVID19, including Syrian hamsters (*Mesocricetus auratus*), the Roborovski dwarf hamster (*Phodopus roborovskii*), the Chinese hamster (*Cricetulus griseus*), wildtype and human ACE2 (hACE2) transgenic mice (*Mus musculus*), ferrets (*Mustela putorius furo*), Chinese tree shrew (*Tupaia belangeri chinensis*), mink (*Neogale vison*), and several non-human primates including rhesus macaques (*Macaca mulatta*), cynomolgus macaques (*Macaca fascicularis*), the African green monkey (*Chlorocebus aethiops*), and the common marmoset (*Callithrix jacchus*). The Chinese tree shrew, marmoset, and wild-type mouse are ineffective models due to limited susceptibility. Old World monkey models recapitulate human lung pathology most closely, and their phylogenetic proximity to humans makes them important pre-clinical animal models for treatment and vaccine candidates. The most commonly used animal models due to similarity to humans in disease course, similarity to humans in immune response, or ease of use, are listed in Table 4.1, along with the clinical signs, pathology, lethality, and advantages and disadvantages of that model.

Table 4.1 Description of most used COVID-19 animal models. Description of the observed pathology, lethality, advantages, and disadvantages of the most used animal models of COVID.

Animal	Clinical signs	Pathology	Lethal?	Advantages	Disadvantages	Reference
Syrian hamsters	Rapid breathing, lethargy, ruffled fur, weight loss	Diffuse alveolar damage, hyaline membrane formation, mononuclear cell infiltration, hemorrhage	No	Natural susceptibility, similar lung pathology to humans, conspecific transmission	No ARDS, short infection course	(Chan et al., 2020a)
hACE2 transgenic mice	Weight loss	Interstitial pneumonia	Yes	Lung pathology observed	High cost, inefficient viral replication	(Bao et al., 2020a)
Ferret	Fever, lethargy, cough, rhinorrhea	Lymphoplasmacytic perivasculitis, vasculitis, mild peribronchitis	No	Cough and fever present, conspecific transmission	Virus primarily replicates in upper respiratory tract	(Shi et al., 2020a)
Rhesus macaque	Reduced appetite, weight loss, lethargy	Interstitial pneumonia	No	Phylogenetically close to humans, disease severity dependent on age, similar symptoms to humans	Non-lethal, high cost	(Munster et al., 2020)

4.1.6 Transmission of SARS-CoV-2 from humans to animals

4.1.6.1 American mink

The most notable human-to-animal spillover of SARS-CoV-2 to date was on mink farms across the world. These farms almost exclusively use American mink (*Neogale vison*). The first spillover was reported in the Netherlands in 2020, where SARS-CoV-2 was transmitted to mink by mink farm workers and then back to humans, resulting in community spread of a mink-adapted SARS-CoV-2 variant (Hammer et al., 2021; Larsen et al., 2021). This mink-adapted variant acquired 5 spike protein mutations which allowed it to partially evade immunity induced by prior infection (Hoffmann et al., 2021). Since the initial spillover in Denmark, SARS-CoV-2 in mink has been reported in Canada, France, Greece, Italy, Latvia, Lithuania, the Netherlands, Poland, Spain, Sweden, and the United States on mink farms and in wild mink (WOAH, 2022). The repeated spillover led to the culling of millions of minks across the world. Notably, American mink were sold in Wuhan wet markets where SARS-CoV-2 is hypothesized to have originally spilled over (Xiao et al., 2021).

4.1.6.2 Cats

The susceptibility of cats to SARS-CoV-2 was determined early in the COVID-19 pandemic, with reports of infection in pet cats and captive big cats from zoos all over the world. Big cat species with confirmed SARS-CoV-2 infection include tigers (*Panthera tigris*), lions (*Panthera leo*), lynx, snow leopards (*Panthera uncia*), fishing cats (*Prionailurus viverrinus*), and pumas (*Puma concolor*) (WOAH, 2022). Cats were not often observed to have clinical signs of disease, with only occasional mild respiratory symptoms associated with infection. Human-to-cat transmission was the most often reported event involving cats, with only one report of cat-to-cat transmission and no cat-to-human transmissions documented (Bao et al., 2021; Doliff and Martens, 2022).

4.1.5.3 Deer

White-tailed deer (*Odocoileus virginianus*) have been identified as susceptible and able to transmit SARS-CoV-2 conspecifically, with one study identifying SARS-CoV-2 RNA at a prevalence of up to 82.5% in farmed and free-ranging deer in the United States (Chandler et al., 2021; Kuchipudi et al., 2022). Experimental infection revealed that SARS-CoV-2 infection in deer is subclinical (Cool et al., 2022). While surveillance continues to indicate SARS-CoV-2 circulation in free-ranging and captive white-tailed deer population in the United States, there have not been any documented cases of deer-to-human transmission (Willgert et al., 2022).

4.1.5.4 Other animals

SARS-CoV-2 infection has been reported in a variety of other animals. Alongside cats, dogs were a concern early in the pandemic, however testing of dogs in homes with infected owners and experimental infections reveal low susceptibility (Bosco-Lauth et al., 2020; Shi et al., 2020b). Pet Syrian hamsters have been reported become infected with SARS-CoV-2 following contact with an infected person. In one case, about 50% of Syrian hamsters in a pet store were infected with SARS-CoV-2, delta variant, which was then transmitted back into humans who visited the pet store and had contact with the hamsters (Yen et al., 2022). Other animals with isolated reports of SARS-CoV-2 infection include hippopotamus (*Hippopotamus amphibius*), gorillas (*Gorilla gorilla*), otters (*Aonyx cinereus*), spotted hyenas (*Crocuta crocuta*), a coatimundi (*Nasua nasua*), and binturong (*Arctictis binturong*) (WOAH, 2022).

4.1.6 The coronavirus spike protein is a determinant of host range and immunity

The spike protein is comprised of two domains; S1, which is more variable among species of coronavirus and contains the receptor-binding domain (RBD), and S2, which is more conserved and initiates a conformational change upon receptor binding which facilitates the fusion of the

virion with the host cell membrane. The spike protein is also the primary target for neutralizing immunity resulting from infection or immunization (in the case of SARS-CoV-2) (Premkumar et al., 2020). Thus, when mutations occur and the amino acid composition changes, this can alter its affinity for its receptor and the neutralizing capability of prior immunity.

There are several examples of how the mutation of a few amino acids within the RBD of a coronavirus S protein can facilitate a species jump or more efficient transmission within a species. For example, studies of the SARS-CoV RBD revealed that two amino acid substitutions conferred greater affinity for human ACE2 to a palm civet isolate of the virus (Li, 2015). Similarly, two amino acid substitutions in the RBD of HKU4, a bat coronavirus that is closely related to MERS-CoV, enabled the virus to utilize human DPP4 when it was unable to before. In the case of SARS-CoV-2, changes to the RBD have resulted in new outbreaks of novel viral variants which are capable of evading prior immunity and, in some cases, increased virulence or transmissibility (Magazine et al., 2022). Every encounter with a new host is an opportunity for host factors to select for mutations in the spike protein that may expand host range or increase transmission efficiency.

4.2 Introduction to deer mice

4.2.1 The genus *Peromyscus*

The genus *Peromyscus* is classified in the rodent family Cricetidae along with true hamsters and lemmings, and contains over 50 species and 200 subspecies of deer mice (Carleton, 1989a). It is likely that deer mice represent the most populous mammalian genus in North America, and their geographic range extends across the entire continent (Figure 4.2.). Deer mice have frequent contact with humans and livestock via cohabitation and are often regarded pests. However, deer mice also serve many essential ecological roles in the environments they inhabit.

On farms in the Midwest, they perform the valuable service of consuming waste grain and weed seeds, which helps keep fields clear for planting the following year (Berl et al., 2017). They are also an indispensable prey animal for many other animals such as snakes, foxes, coyotes, other small carnivores, and birds of prey (Kirkland and Layne, 1989a).

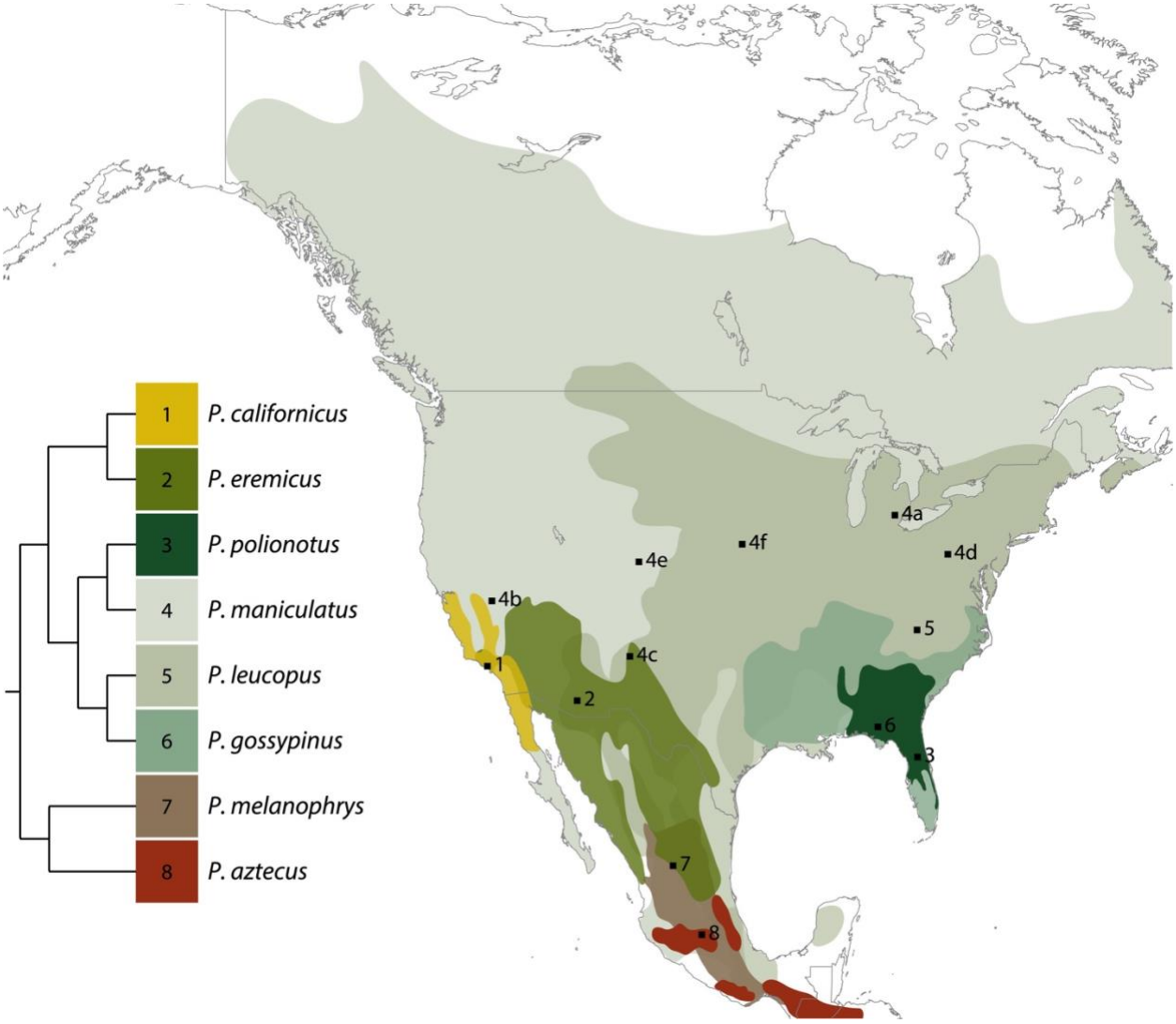

Figure 4.2 The geographic range of 8 laboratory-maintained species of deer mice in North America. *P. maniculatus* has the widest geographic range of the deer mouse species. Phylogenetic tree indicates the relationship of the 8 species shown. *P. californicus* and *P. polionotus* inhabit more niche habitats and are thus less widely distributed.
Nicole L Bedford, Hopi E Hoekstra (2015) The Natural History of Model Organisms: Peromyscus mice as a model for studying natural variation eLife 4:e06813 https://doi.org/10.7554/eLife.06813

The phylogeny of deer mice is currently debated. Most relevant is the discussion of the species *P. maniculatus,* the species group commonly known as the North American deer mouse, and the recent recommendation that it be split into two species; *P. maniculatus* (the western deer mouse) and *P. sonoriensis* (the eastern deer mouse) (Greenbaum et al., 2019).

4.2.2 Laboratory use of deer mice

Deer mice have been used in a research setting for over a century (Field et al., 2007). The Peromyscus Genetic Stock Center was established in 1985 and has increased research access to peromyscine mice. Deer mice have many advantages as an animal model. First, they are easy to maintain in a laboratory setting. They have an extended life span compared to the laboratory mouse (*M. musculus*), living up to 8 years in captivity (Sacher and Hart, 1978). This has made them an attractive model for studies on aging and other long-term studies. A major advantage of deer mice as a laboratory animal model is also one of its greatest disadvantages: genetic polymorphism. Laboratory stocks of deer mice are more outbred than the nearly genetically homogenous laboratory mouse, as inbreeding of deer mice leads to reduced fertility and viability (Joyner et al., 1998). However, the genetic heterogeneity of deer mice also makes them a more “life-like” animal model, as individuals might not respond the same to treatments as the laboratory mouse may.

4.2.3 Deer mice as reservoirs of human pathogens

4.2.3.1 Hantaviruses

Hantaviruses, from the negative-stranded RNA virus family *Hantaviridae*, are endemic and cause disease across the world. Rodents, especially rats, mice, voles, shrews, and lemmings, serve as the principal reservoirs for all hantaviruses identified to date. In North America, deer mice serve as the reservoir for Sin Nombre hantavirus, which was responsible for an outbreak

of hantavirus cardiopulmonary syndrome in 1993 (Hjelle et al., 1994; Schmaljohn and Hjelle, 1997). The virus is transmitted to humans either by the bite of an infected deer mouse or by inhalation of aerosolized urine or feces from infected deer mice. The pathogenicity of different hantavirus species varies greatly, from mild clinical disease to hemorrhagic manifestations and renal failure, with a current case fatality rate of about 35% (de St Maurice et al., 2017).

4.2.3 Borrelia burgdorferi

Lyme disease, caused by infection with the spirochete *Borrelia burgdorferi*, is one of the most important vector-borne diseases in the world. It is estimated that 476,000 people contract Lyme disease each year in the United States alone (CDC, 2022). Deer mice are the reservoir of *B. burgdorferi* in the United States (Peavey and Lane, 1995). Ticks in the genus *Ixodes*, the vector of *B. burgdorferi*, feed on deer mice in the larval and nymph stages and become infected with the spirochete. In the adult stage, the ticks then go on to feed on larger animals and humans, transmitting the bacteria.

4.3 Coronaviruses in New World rodents: Unexplored potential reservoirs

Since the identification of bats as the reservoir of SARS-like-CoVs in 2005, bats have been a target of much surveillance for coronaviruses. Despite rodents also being reservoirs for coronaviruses including murine coronavirus, swine acute diarrhea coronavirus, and the ancestral host of BCOV, surveillance efforts in rodents have not been as emphasized (Lau et al., 2015a; Lau et al., 2015b; Maru and Sato, 1982; Nelson, 1952). Surveillance efforts in China and southeast Asia have identified alphacoronaviruses and betacoronaviruses in wild and urban pest species of rodents (Ge et al., 2017; Lau et al., 2015a; Li et al., 2021; Miot et al., 2022; Tsoleridis et al., 2016; Wang et al., 2020; Wang et al., 2015; Wu et al., 2021; Wu et al., 2018). While the circulation of coronaviruses is a known entity in China and southeast Asia,

surveillance for coronaviruses in the new world, and especially in new world rodents, is sparse. One survey following the outbreak of SARS-CoV-2 on mink farms in Utah sampled various animals found near the affected mink farms. One deer mouse (out of 47 sampled) was found to be infected with a betacoronavirus most closely related to betacoronavirus 1, which contains subspecies endemic in human populations (Ip et al., 2021). The same survey found a number of alpha- and betacoronaviruses in house mice as well. The close contact of rodents with humans, peridomestic, and domestic animals, and their wide geographic distribution make them an ecologically ideal reservoir for human pathogens in the Americas, warranting further investigation to the current circulation of coronaviruses as well as their potential to host coronaviruses in a laboratory setting.

Chapter 5: SARS-CoV-2 infection, neuropathogenesis, and transmission among deer mice: Implications for reverse zoonosis to New World rodents[1]

5.1 Introduction

Coronavirus disease-19 (COVID-19) emerged in late 2019 in China and the etiologic agent was identified as a novel betacoronavirus, severe acute respiratory syndrome coronavirus-2 (SARS-CoV-2) (Huang et al., 2020; Zhou et al., 2020b; Zhu et al., 2020b). Both SARS-CoV and SARS-CoV-2 use angiotensin converting enzyme 2 (ACE2) as a cellular entry receptor in humans (Letko et al., 2020; Zhou et al., 2020b). The virus likely originated from insectivorous *Rhinolophus* spp. horseshoe bats. Some evidence suggests it may have undergone recombination in the receptor binding domain via an intermediate host prior to its spillover into humans (Lau et al., 2020; Zhou et al., 2020b). However, other evidence suggests the virus has not undergone recombination in its receptor binding domain (Boni et al., 2020) and may have transmitted to humans directly from bats or via another intermediate host. To date, only a few mammalian species have been identified as susceptible, including cynomolgus macaques, ferrets, felines, American mink, Egyptian rousette bats and canines (Chan et al., 2020b; Imai et al., 2020; Oreshkova et al., 2020; Rockx et al., 2020; Schlottau et al., 2020a; Shi et al., 2020a; Sia et al., 2020b). Human ACE2-transgenic mice are also susceptible, unlike wildtype laboratory mice and rats (Bao et al., 2020b).

---

[1] Fagre, A., Lewis, J., Eckley, M., Zhan, S., Rocha, S. M., Sexton, N. R., Burke, B., Geiss, B., Peersen, O., Bass, T., Kading, R., Rovnak, J., Ebel, G. D., Tjalkens, R. B., Aboellail, T., & Schountz, T. (2021). SARS-CoV-2 infection, neuropathogenesis and transmission among deer mice: Implications for spillback to New World rodents. *PLoS pathogens*, *17*(5), e1009585. https://doi.org/10.1371/journal.ppat.1009585

A significant concern is the potential for spillback of SARS-CoV-2 into native wildlife species that could allow the virus to become endemic by the establishment of secondary reservoir hosts outside of Asia (Franklin and Bevins, 2020). Middle East respiratory syndrome coronavirus (MERS-CoV) likely transmitted from bats to dromedary camels in North Africa and established a secondary reservoir that accounts for most human outbreaks of MERS which repeatedly occur each year (Memish et al., 2013; Milne-Price et al., 2014). A recent report identified 20 important contact residues in human ACE2 for SARS-CoV-2 spike protein binding and suggested members the rodent Cricetidae family may also be susceptible (Luan et al., 2020). Experimental challenge of Syrian hamsters, a cricetid rodent whose ACE2 shares 18 of these 20 critical residues, resulted in moderate, nonlethal pulmonary disease resembling human COVID-19 but without mortality (Chan et al., 2020b; Imai et al., 2020; Sia et al., 2020b).

Peromyscine rodents are also members of Cricetidae (subfamily Neotominae, genus *Peromyscus*) and are distributed throughout North America. There are 56 recognized species in the genus, and some serve as reservoir hosts for diverse zoonotic agents, including hantaviruses, *Borrelia burgdorferi*, *Babesia* spp., and Powassan virus (Barbour, 2017). Deer mice (*P. maniculatus*) are the most studied and abundant mammals in North America and are frequently contacted by mammalogists during field studies (Bedford and Hoekstra, 2015). They are also abundant in regions where American mink (*Neovison vison*) are farmed, raising the possibility of contact with infected American mink or fomites (e.g., mink food) that may be contaminated with SARS-CoV-2. The ACE2 receptor of deer mice shares 17 of the 20 critical residues for SARS-CoV-2 binding, suggesting that deer mice may be susceptible to infection with SARS-CoV-2. Because of these features, we challenged deer mice to determine if they are susceptible and whether they can transmit the virus through multiple passages.

5.2 Materials and Methods

5.2.1 Virus and Cells

SARS-CoV-2 (isolate 2019-nCoV/USA-WA1, NR52281) was provided by BEI Resources. Virus was passaged twice on Vero E6 cells (ATCC CRL-1586) in 2% FBS-DMEM containing 10,000 IU/ml penicillin and streptomycin at 37°C under 5% CO_2 to generate stock virus used in these experiments. Virus was stored at -80°C. All work with infectious virus was performed at BSL-3 with approval from the Colorado State University Institutional Biosafety Committee.

5.2.2 Animal Procedures

Deer mice (*Peromyscus maniculatus nebrascensis*) of both sexes and of 6 months of age were kindly provided by Dr. Ann Hawkinson at the University of Northern Colorado. This colony was established with deer mice captured near Whitewater, CO in 2000 (Schountz et al., 2004). All animal work was approved by the Colorado State University Institutional Animal Care and Use Committee (protocol #993).

Deer mice were intranasally inoculated under inhalation isoflurane anesthesia with $2x10^4$ $TCID_{50}$ SARS-CoV-2. On days 3, 6 and 14, three inoculated deer mice were euthanized, and one sham-inoculated deer mouse was euthanized on day 3 and the other two on day 14. Necropsies were performed for tissue RNA, virus isolation, and histopathology and immunohistochemistry.

To assess contact transmission, three deer mice were inoculated as described above. The next day, the deer mice were added to a cage with three naive contact deer mice (passage 1). Oral swabs were collected daily to determine infection status via qPCR. As the contact deer mice became PCR^+ they were moved into another cage containing two additional naive contact deer mice (passage 2).

5.2.3 Virus Detection

Swabs in virus transport medium were vortexed thoroughly and centrifuged to pellet cellular debris. RNA was extracted from swab supernatant using the QiaAmp Viral RNA kit (Qiagen) according to the manufacturer's instructions. Tissues were homogenized and RNA extracted using RNeasy Mini kit (Qiagen) following manufacturer instructions. For detection of viral RNA, a one-step real-time RT-PCR E gene assay was employed using the GoTaq 1-Step RT-qPCR kit (Promega). The Berlin E gene primer/probe/plasmid standard (IDT Technologies) kit was used to quantify viral copy numbers (Corman et al., 2020). For virus isolation from lungs, the lower third of left lungs were homogenized in 500 µl of 10% FBS-DMEM with a stainless steel bead and a TissueLyser II (Qiagen). Samples were diluted 10^{-3} and inoculated on Vero E6 cells and scored for CPE 4 days later.

5.2.4 Production of recombinant SARS-CoV-2 nucleocapsid protein

Truncated SARS-CoV-2 nucleocapsid (N) protein (AA133-416) was produced to reduce non-specific binding during antibody production (Chen et al., 2015; Terry et al., 2020; Yu et al., 2005). A bacteria-codon optimized gBlock for the truncated protein was produced by IDT DNA Technologies and cloned into a pET28a bacterial expression with a C-terminal 6xHis tag using the NEBuilder Assembly Kit (New England Biolabs). Recombinant protein was expressed in BL21(DE3) pLysS *E. coli* and purified by nickel affinity and size exclusion chromatography essentially as previously described (Geiss et al., 2009), with the exception of the use of 50 mM HEPES buffer (pH 7.4) and 500 mM NaCl throughout purification to reduce aggregation. Purity and identity of purified nucleocapsid protein was determined by SDS-PAGE and mass spectrometry at the CSU Proteomics and Metabolomics Core, respectively.

5.2.5 Enzyme-linked immunosorbent assay

ELISA was performed by coating plates with 200 ng/100 µl recombinant N protein diluted in PBS (pH 7.2) overnight, then washed 3x with PBS. Plates were blocked with SuperBlock T20 (Thermo Scientific) for 30 minutes and washed. Heat inactivated serum samples (60°C 60 min) were diluted 1:100 in PBS, then serially diluted 2-fold and incubated with antigen for 1 hr at room temperature then washed 3x PBS-0.25% TWEEN-20/3x PBS. Goat anti-*Peromyscus leucopus* IgG(H&L)-HRP conjugate (SeraCare) at 1:1,000 was incubated for 1 hour followed by PBS-TWEEN-20/PBS washing. ABTS substrate (Thermo Fisher) was added and after 15 min absorbance (405 nm) recorded. The titers we determined by the reciprocal of the greatest dilution that was 0.200 OD above the mean of the negative control serum samples.

5.2.6 Western blot

For western blot detection, infected Vero cell supernatants were subject to centrifugal filter concentration with molecular weight cutoff of 300 kDa (Pall Microsep 300K Omega). Enriched virus was inactivated with 2% sodium dodecyl sulfate (SDS) and protein concentration determined with a Pierce BCA protein assay kit (Thermo Scientific) according to manufacturer's instructions. Eight micrograms of protein per lane were separated by 12% SDS polyacrylamide gel electrophoresis and blotted onto Immobilon-P nylon membranes (Millipore). After transfer, the blots were sectioned by lane, blocked, and individual lanes incubated with 1:100 dilutions of the deer mouse sera or with house mouse anti-nucleocapsid monoclonal antibody overnight. Primary antibodies from deer mice were detected with goat anti-*P. leucopus* IgG-HRP and developed with the TMB membrane peroxidase substrate system (3,3',5,5'-tetramethylbenzidine, KPL). Images were scanned with a Visioneer One Touch 9420 scanner at a gamma value of 1.0, and all contrast adjustments were uniformly applied using Adobe Photoshop.

5.2.7 Serum neutralization test

Serum neutralization was performed starting at 1:10 dilution with 2-fold dilution series. An equal volume of SARS-CoV (100 $TCID_{50}$) was added (final dilution of 1:20) and incubated for 1 hr at 37°C. The mixture was plated on Vero E6 cells and scored for CPE after 6 days. The titer was reciprocal of the greatest dilution that conferred 100% protection.

5.2.8 Immune Gene Expression Profiling

Deer mouse immune gene expression profiling has been previously described (Schountz et al., 2014). Briefly, primers (Supplementary Figure 5.1) for various immune genes were used to amplify cDNA collected from lungs using QuantiNova reverse transcription and SYBR Green I PCR kits (Qiagen). The $\Delta\Delta C_T$ method was used with normalization within sample on GAPDH (ΔC_T) and fold-change calculated for each gene against the means of the 3 sham inoculated control deer mice ($\Delta\Delta C_T$). Statistical assessment was performed using Kruskal-Wallis test (ANOVA) with Prism software (GraphPad, Inc.)

5.2.9 Histopathology

Three deer mice were humanely euthanized at 3-, 6- and 14 dpi and after retrieval of lungs and spleens, the remaining deer mice carcasses were fixed in 10% neutral buffered formalin (10% NBF) after opening abdominal and thoracic cavities to allow for gross inspection and formalin penetration. Fixed specimens were transferred after at least 3 days from BSL-3 facility to the Colorado State University Diagnostic Laboratories, BSL-2 for trimming. Skulls were bisected (hemi skulls) and decalcified in semiconductor grade formic acid and EDTA (Calfor, Cancer Diagnostics, USA) for 2-3 days. Oral cavity, salivary glands, olfactory bulb, cerebrum, cerebellum, and brain stem were thoroughly inspected for gross lesions. Decalcified skulls and visceral organs were processed, embedded in paraffin wax and 4-5 µm sections were stained

with hematoxylin and eosin for blinded evaluation by the pathologist using Nikon i80 microscope (Nikon Microscopy).

5.2.10 Immunohistochemistry

Sections from hemi skulls and visceral organs were stained using ultraView universal alkaline phosphatase red detection kit. Heat-induced epitope retrieval was performed on a Leica Bond-III IHC automated stainer using Bond Epitope Retrieval solution for 20 minutes. Viral nucleocapsid antigen was detected with a purified rabbit polyclonal antibody. Labeling was performed on an automated staining platform. Fast Red was used as chromogen and slides were counterstained with hematoxylin. Immunoreactions were visualized by a single pathologist in a blinded fashion. In all cases, normal and reactive mouse brain sections incubated with primary antibodies was used as a positive immunohistochemical control. Negative controls were incubated in diluent consisting of Tris-buffered saline with carrier protein and homologous nonimmune sera. All sequential steps of the immunostaining procedure were performed on negative controls following incubation.

5.2.11 Immunofluorescence Staining and Tissue Imaging

Paraffin embedded tissue sections were stained for SARS-CoV-2 nucleocapsid protein (1:500), microtubule-associated protein 2 (Abcam; ab32454; 1:500), ionized calcium binding adaptor molecule 1 (Abcam; ab5076; 1:50)/glial fibrillary acidic protein (Sigma; 3893;1:500) using a Leica Bond RXm automated staining instrument following permeabilization using 0.01% Triton X diluted in Tris-buffered saline (TBS). Blocking was performed with 1% donkey serum diluted in TBS. Sections were stained for DAPI (Sigma) and mounted on glass coverslips in ProLong Gold Antifade mounting medium and stored at ambient temperature until imaging. Images were captured using an Olympus BX63 fluorescence microscope equipped with a motorized stage

and Hamamatsu ORCA-flash 4.0 LT CCD camera. Images were collected and regions of interest quantified with Olympus cellSens software (v 1.18) using an Olympus X-line apochromat 10X (0.40 N.A.), 20X (0.8 N.A.) or 40X (0.95 N.A.) air objectives, or Uplan Flour X100 oil immersion (1.3 N.A.) objective.

5.2.12 Next-generation sequencing library preparation for positive NP samples

Viral RNA from positive deer mouse samples was prepared for Next-generation sequencing. Briefly, cDNA was generated using SuperScript IV Reverse Transcriptase enzyme (Invitrogen) with random hexamers. PCR amplification was performed using ARTIC network V3 tiled amplicon primers in two separate reactions by Q5 High-fidelity polymerase (NEB). First-round PCR products were purified using Ampure XP beads (Beckman Coulter). Libraries were prepared using the Nextera XT Library Preparation Kit (Illumina) according to manufacturer protocol. Unique Nextera XT i7 and i5 indexes for each sample were incorporated for dual indexed libraries. Indexed libraries were again purified using Ampure XP bead (Beckman Coulter). Final libraries were pooled and analyzed for size distribution using the Agilent High Sensitivity D1000 Screen Tape on the Agilent Tapestation 2200, final quantification was performed using the NEBNext Library Quant Kit for Illumina (NEB) according to manufacture protocol. Libraries were then sequenced on the Illumina MiSeq V2 using 2 x 250 paired end reads.

5.2.13 Deep sequencing analysis

Next-generation sequencing data were processed to generate consensus sequences for each viral sample. MiSeq reads were demultiplexed, quality checked by FASTQC, paired-end reads were processed to removed Illumina primers and quality trimmed with Cutadapt, duplicate reads were removed. Remaining reads were aligned to SARS-CoV-2 reference sequence by Bowtie2

(GenBank: MT020881.1). Alignments were further processed, and quality checked, using Geneious software, consensus sequences were determined and any gaps in sequences were filled in with the reference sequence. Consensus sequences were aligned in Geneious. Based upon the insertion that was identified in the passage 2 deer mice, a PCR assay was developed to detect the presence of the insert using a forward primer (5'-AGTGCGTGATAAGCTGAGAAGT-3'; 12 nt insert sequence underlined) and reverse primer (5'-TAACCCACATAATAAGCTGCAGC) that generated a 183 bp product. A control forward primer (5'-GCACACGCCTATTAATTTAGTGC-3') for detection of both wild-type (201 bp) or insert (213 bp) vRNA was designed 5' to the insert primer.

5.2.14 Modeling deer mouse-passaged SARS-CoV-2 spike protein

The Phyre2 structure modeling engine (Kelley et al., 2015) was used in the One-to-One Threading expert mode to generate a model of the deer mouse passage spike protein with the KLRS insert using the C chain of PDB entry 6VYB. The resulting model showed the insert is located at a surface loop on the N-terminal domain composed of residues 216-219 and predicts that this loop is enlarged to accommodate the 4-residue insertion. To illustrate the location of this insertion relative to the ACE2 receptor (Figure 4C), the structure of human ACE2 bound to the spike receptor binding domain (RBD), PDB entry 6VW1, was superposed on the up-conformation RBD from the B chain of the spike trimer (Shang et al., 2020; Walls et al., 2020).

5.3 Results

5.3.1 Deer mice are susceptible to SARS-CoV-2 infection.

To test susceptibility, nine young adult deer mice 6 months of age of both sexes were intranasally challenged with $2x10^4$ $TCID_{50}$ of SARS-CoV-2 and three were held as unchallenged controls. Three deer mice each were euthanized on days 3, 6 and 14 post inoculation (dpi) to

assess infection, and one sham-inoculated deer mouse was euthanized on day 3 whereas the other two were euthanized on day 14. On days 3 and 6, gross substantial pulmonary consolidation and hemorrhage were observed in the cranial and middle portions of both lungs. Viral RNA was detected in the lungs of all deer mice euthanized on days 3, and two of three on day 6, but virus was isolated from only the day 3 deer mice (Figure 5.1A-B). Virus and viral RNA was detected in olfactory bulbs of two deer mice on day 3 but not on subsequent days (Figure 5.1C-D). IgG to recombinant nucleoprotein was detected by ELISA only on day 14 (Figure 5.1E; GMT=504), and low titer neutralizing antibody (GMT=25) was initially detected on day 6 that significantly increased on day 14 (GMT=160, Figure 5.1C), suggesting neutralizing antibody on day 6 was likely IgM that prevented virus isolation in the day 6 deer mice. Antibody to multiple viral antigens was detected in all 9 of the inoculated deer mice by western blot (Supplementary Figure 5.1), indicating an early antibody response.

5.3.2 SARS-CoV-2 induces immune gene transcription in the lungs of infected deer mice.

Examination of 41 immune response genes (Schountz et al., 2014) (Supplementary Figure 5.1) identified several that were elevated in the lungs during infection. Eight innate immune response genes (IFNα, IFNβ, Tbk1, Oas2, Cxcl10, Pycard, Isg15, Tlr7) were significantly elevated during acute infection but then subsided by 14 dpi; IFNβ expression was elevated but not significantly so (Figure 5.2A-H), indicating activation of antiviral defenses that declined as the virus was controlled. IL-6 expression was not elevated; high levels of IFN and IL-6 have been associated with severe COVID-19 (Wan et al., 2020). Expression of CD8β was substantially elevated on days 3 and 6, whereas CD4 expression was less elevated; both returned to nominal levels by day 14 (Figure 5.2I-J). IFNγ expression was not detected in the lungs of the sham inoculated deer mice; however, it was detected at low levels in one deer mouse at 3 dpi (Cq=35) and two deer mice at 6 dpi (Cq=32, 35). Although IL-2 and IL-13 were not detected, receptors for each were significantly elevated (Figure 5.2K-L). IL-21 expression was greatest among the cytokines

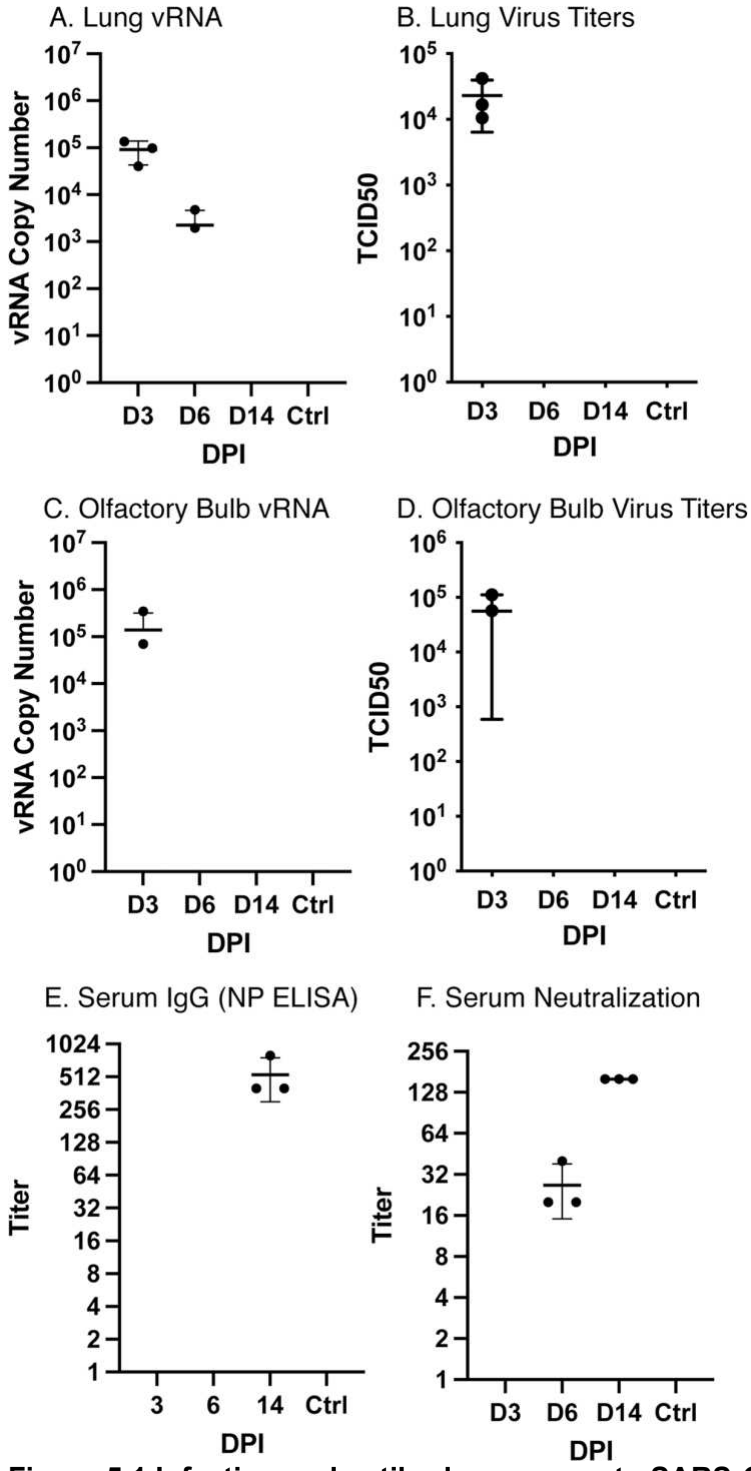

Figure 5.1 Infection and antibody response to SARS-CoV-2. (A) Viral RNA was detected in lungs of infected deer mice to day 6, and (B) virus was recovered only on day 3. (C) Two of three deer mice had detectable vRNA in their olfactory bulbs and (D) virus was isolated from each. (E) IgG antibodies were detected to nucleocapsid protein on day 14, (F) with neutralizing antibody detected on days 6 and 14. Each time point represents samples collected from 3 euthanized deer mice per group. Error bars represent the standard deviation of the mean and geometric mean antibody titers.

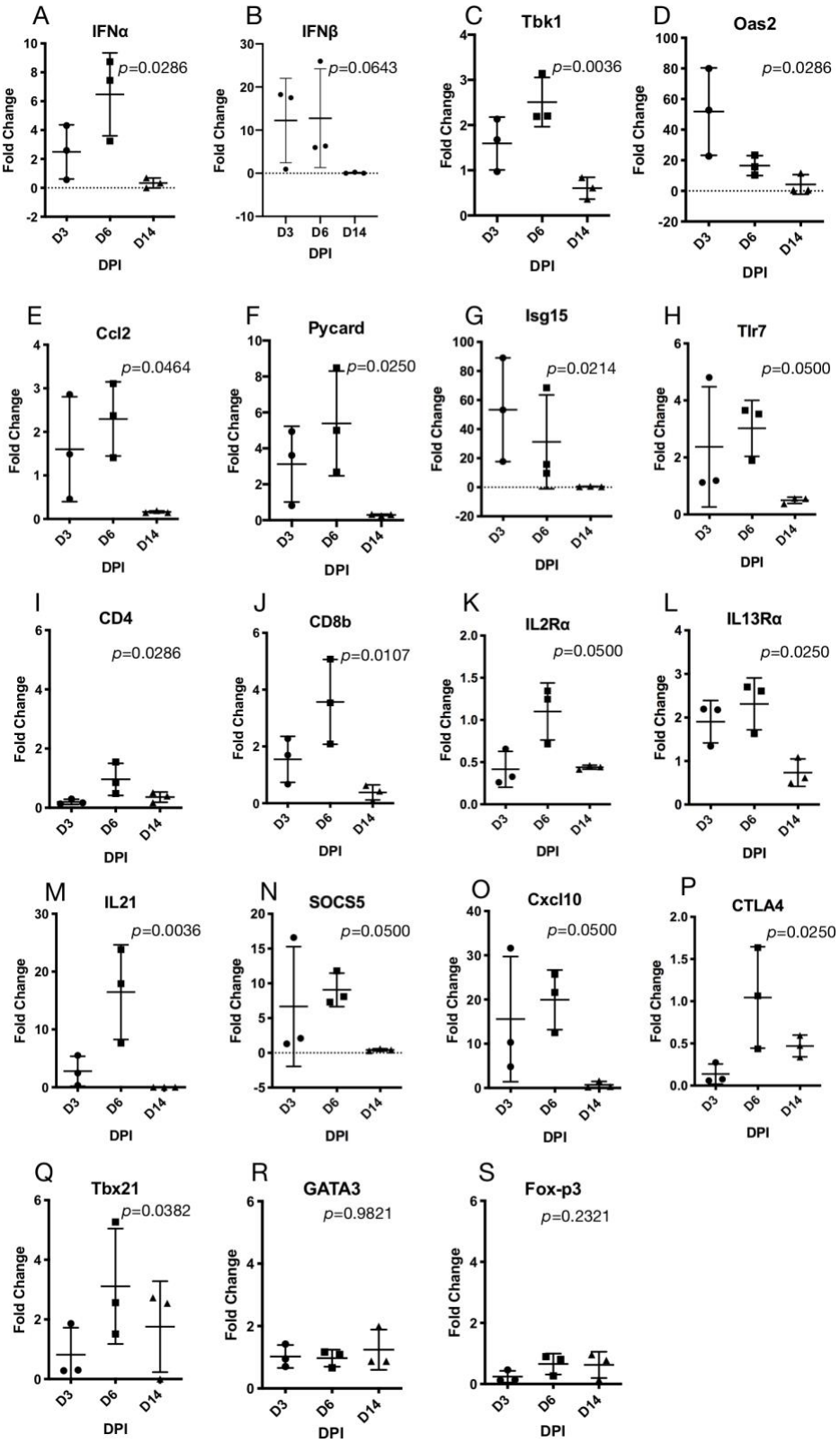

Figure 5.2 Immune gene expression in lungs of infected deer mice. Gene profiling showed elevated expression of several antiviral innate immune response genes 3 and 6 dpi (A-H) and evidence of T cell infiltration and inflammatory type I immune response 6 dpi (I-S).

examined with up to 25-fold increase 6 dpi (Figure 5.2M). SOCS5, Cxcl10 and CTLA4 were each significantly elevated on day 6 (Figure 5.2N-P). The type I inflammatory immune response transcription factor Tbx21 (T-bet) was significantly elevated, but not the type II GATA3 or regulatory T cell Foxp3 transcription factors (Figure 5.2Q-S), suggestive of a pro-inflammatory type I immune response in the lungs of infected deer mice.

5.3.3 Histopathology

Histologically, at 3 dpi, multifocal immunoreactivity was seen in occasional vibrissae with no associated inflammation in mystacial pad. Hemi skulls showed severe necrosuppurative to fibrinopurulent inflammation in nasal meatuses, maxillary sinuses and ethmoturbinates. Fibrinoid vascular necrosis obliterated the walls of medium-sized veins in ethmoturbinates. Severe ulceration and desquamation of the main olfactory epithelium (MOE) manifested in vomeronasal organ (VMO) and septum. Intense infiltrates of neutrophils surrounded and occasionally involved centrifugal afferent sensory branches of olfactory (CNI), ethmoidal, and maxillary nerves (Figure 5.3A). Multifocal inflammation extended to the submucosa of maxillary and ethmoid sinuses at 6 dpi. Abundant viral antigen was detected in the sloughed necrotic mucosal epithelium intermixed with numerous intact and degenerate neutrophils, macrophages and variable amounts of fibrin. Lingual fungiform and circumvallate papillae were surrounded by neutrophils, which clustered on necrotic gustatory buds. The tongue was mildly swollen due to dissecting edema and neutrophilic interstitial glossitis in all 3 deer mice at 3 dpi. Abundant viral antigen was present in the nasal passages spanning sustentacular, olfactory and basal cells of MOE in all 3 of the deer mice at 3 dpi (Figure 5.3B) and less prominently in lingual mucosa, hard palate and oropharynx. Branches of chorda tympani, greater superficial petrosal and glossopharyngeal nerves (CNIX) were variably degenerate or minimally inflamed. Pterygopalatine (parasympathetic ganglion deep within pterygoid fossa in the upper jaw), petrosal and lateral geniculate nuclei (in tympanic bulla) and trigeminal ganglion were

multifocally degenerate and surrounded and/or infiltrated by small numbers of neutrophils in 2 of the deer mice at 6 dpi. Virus antigen was present in the ganglia (trigeminal ganglion, Figure 5.3C) at 3 and 6 days of infection (Supplementary Figure 5.2-5.3). The glomerular layer of the main olfactory bulb (MOB) was spongiotic and immunoreactive at 3 dpi (Figure 5.3E). Laminar neuronal degeneration and scattered necrotic neurons were observed in anterior olfactory nucleus in the brain of one of the most affected deer mice at 6dpi. Histioneutrophilic inflammation manifested in frontal lobe of the brain of one of the deer mice by 6 dpi (Figure 5.3D-E). In inflamed areas of the MOB, viral antigen was also detected in cytoplasm of microglial and mitral cells (Figure 5.3F-I). Viral antigen within the olfactory bulb (Figure 5.3J) remained prominent from 3 dpi to 6 dpi. In accordance with the olfactory bulb, detection of the virus was observed 3 dpi and 6 dpi in the nasal turbinates (Fig. 3K). Interestingly, marked increase in SARS-CoV-2 antigen was observed at the 6 dpi timepoints within trigemimal nerve (Fig. 3L), indicating that the virus was capable of invading nervous fibers in the subacute phase of the disease. This then allowed access to rostral most brain regions by the 6 dpi time-point resulting in glial phenotypic changes inducing microcytosis. Less severe glial reactions and immunoreactivity were present multifocally within brain stem at the level of lateral sulcus nucleus (NTS), optic chiasm, hypothalamus, and thalamic parabrachial nucleus (PbN), ventral posteromedial nucleus (VPM) culminating in gustatory cortex. Neuronal cell bodies in the affected regions of olfactory lobe, brain stem, thalamus, hypothalamus and insula showed variable immunoreactivity against viral nuclear capsid. Individual neurons were shrunken with angular borders, hypereosinophilic cytoplasm and pyknotic nuclei. Retinal ganglionic and inner nuclear layers showed multifocal immunoreactivity (Supplementary Figure 5.4-5.6). There were no significant histologic lesions in peripheral or central nervous systems at 14 dpi. Calvarial bone marrow showed multifocal cytoplasmic immunoreactivity in myeloid precursors, including megakaryocytes, at 6 dpi (Supplementary Figure 5.7). Inflammation and mucosal desquamation were mild to moderate in trachea and main stem bronchi showed mild to moderate

immunoreactivity, respectively, at 3 dpi. Immunoreactivity was also detected in mononuclear and stellate, antigen presenting cells in reactive tracheobronchial and hilar lymph nodes at 6 dpi. Extensive histioneutrophilic and hemorrhagic bronchointerstitial pneumonia manifested at 3- and 6-days dpi along with leukocytoclastic vasculitis involving main and medium sized branches of the pulmonary artery along with marked peribronchiolar and perivascular lymphoid hyperplasia (Supplementary Figure 5.8). Terminal bronchioles and adjacent alveoli contained infiltrates of moderate to large numbers of macrophages and neutrophils intermixed with multifocal extravasated erythrocytes. Abundant viral antigen was detected in individual bronchiolar lining epithelial cells and scattered alveolar lining cells. Some inflammatory foci were interspersed by multinucleate syncytial cells. Perivascular mild neutrophilic infiltrates were present around main blood vessels at the base of the heart and around renal hilar vessels and nerves at 6 dpi (Supplementary Figure 5.10). Other visceral organs did not show significant pathologies. Occasional multinucleate cells of epithelial and histiocytic origin were scattered amongst inflammatory infiltrates. Inflammation significantly subsided at 14 dpi where lungs showed mild pulmonary fibrosis and residual pneumonia. Hemorrhage was less prominent to absent in lungs of infected deer mice by 14 days. Lamina proprial cellularity of the small intestine, particularly duodenum and ileum, moderately increased by 6 dpi and immunoreactivity was detected in crypt epithelium and mature enterocytes along with occasional submucosal macrophages (Supplementary Figure 5.9).

5.3.4 Experimentally infected deer mice can transmit SARS-CoV-2 conspecifically.

To assess transmission, 3 deer mice were intranasally inoculated with $2x10^4$ $TCID_{50}$ of virus and the next day they were moved to a new cage containing 3 naive contact deer mice. Oral swabs, but not rectal swabs, of the three contact deer mice (DM5, DM6, DM7) became $vRNA^+$ on days 2, 5, and 5 post-contact (P1, days 3 and 6 of the study, Table 5.1). As they became $vRNA^+$, the P1 deer mice were transferred to a third cage containing 2 additional naive contact deer mice

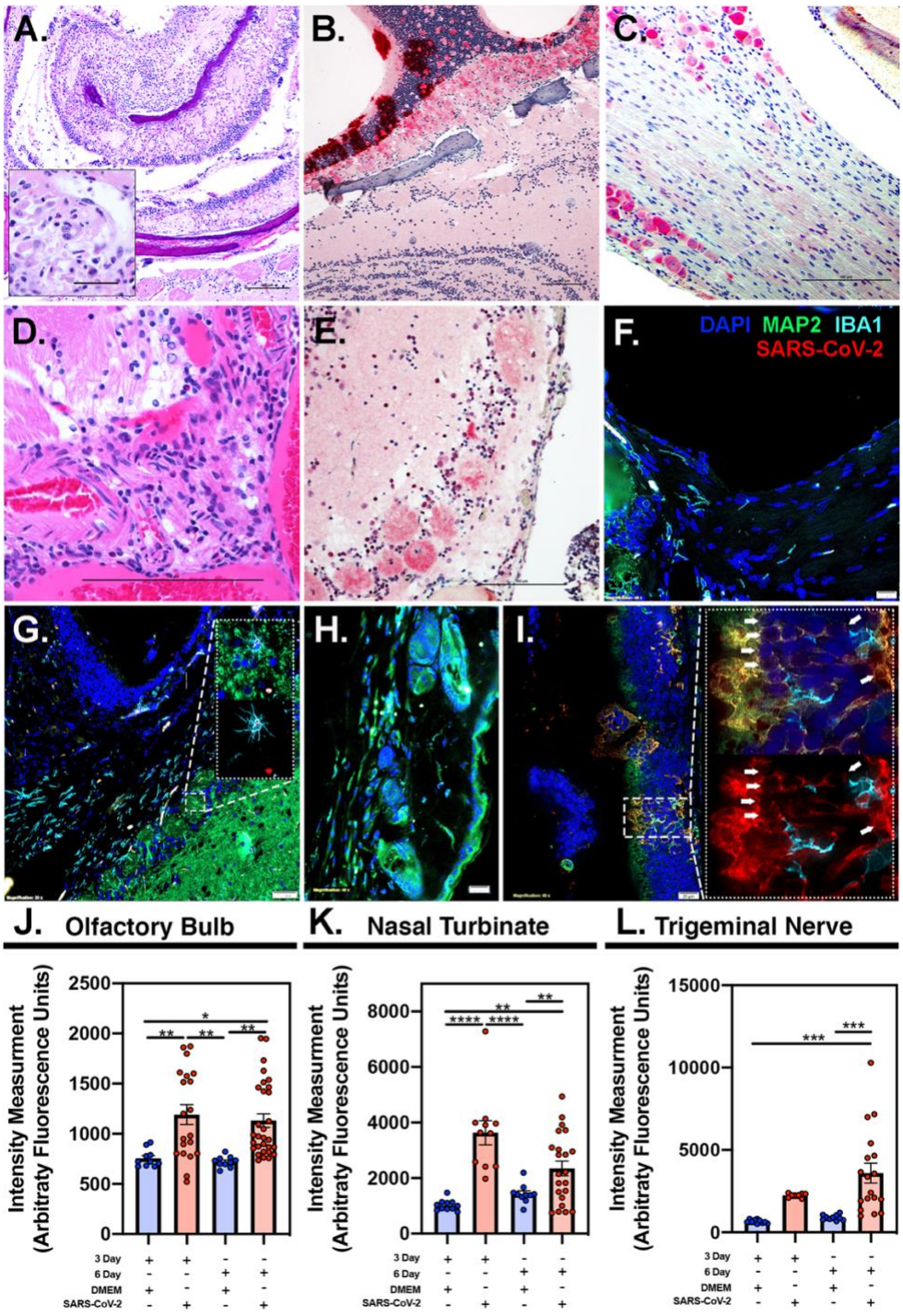

Figure 5.3 Histopathology and immunohistochemistry of SARS-CoV-2 in skull and brain of deer mice at 3- and 6- days post-infection. (A) Acute fibrinosuppurative and ulcerative sinusitis in ethmoturbinates with degeneration and inflammation of branches of olfactory, ethmoidal, and maxillary sensory nerves (fibrinoid vascular necrosis – inset) (B) Transmural SARS-CoV-2 immunoreactivity (Fast Red staining) in MOE, 3 dpi. (C) Prominent immunoreactivity in trigeminal ganglionic neurons with mild glial reaction at 6 dpi. (D) Disruption of the BBB with associated histioneutrophilic meningoencephalitis, 6 dpi (E) Viral transmission to the glomerular layer of the MOB, 6 dpi. (F) Immunofluorescence imaging depicting entry of centrifugal afferents to the olfactory bulb at the cribriform plate in uninfected control deer mice 6

dpi showing no viral immunoreactivity in any neurons or glial cells. Neurons were identified with antibodies against microtubule associated protein (MAP2, green), microglia with anti-ionized calcium-binding adaptor molecule 1 (IBA1, cyan), anti-SARS-CoV-2 (red) and nuclei were counterstained with DAPI (blue). (G) Multifocal SARS-CoV-2 antigen was detected by 6 dpi within neurons and microglia of the afferent nerves and in the glomerular layer of the olfactory bulb (arrows; 100X high-magnification inset microglial cell). Examination of the trigeminal nerve and ganglion in (H) uninfected control with no immunoreactivity and (I) infected deer mice revealing neuroinvasion of SARS-CoV-2, with extensive co-localization of the virus within $MAP2^+$ neurons proximal to activated microglia, 6 dpi. 100X high-magnification insets depict co-localization of SARS-CoV-2 with $MAP2^+$ neurons (top panel, arrows), as well as the same image without MAP2 to better highlight the extent of neuronal staining with SARS-CoV-2. SARS-CoV-2 quantification by fluorescence intensity within given regions of interest (ROI) are represented in the olfactory bulb (J), nasal turbinates (K), and trigeminal nerve (L) showing the increase in viral load. Scale bars equal 100 μm (n=2/group) *p<0.0332, **p<0.0021, ***p<0.0002, ****p<0.0001.

(P2). The P2 deer mice (DM8, DM9) had detectable vRNA from oral swabs 5 days after contact (day 8 of the study), demonstrating that sustained transmission can occur. The inoculated and P1 deer mice were held until day 28 post contact, at which time all had antibodies detectable by western blot (Supplementary Figure 5.1). The P2 contact deer mice were euthanized on day 14 of the transmission study to provide a passage 2 viral stock. Viral RNA (Figure 5.4A) was detected up to 21 days post inoculation, whereas infectious virus (Figure 5.4B) was detected up to 14 days post inoculation. Each of the inoculated deer mice in the transmission study lost weight in the first 4-6 days before regaining weight, as did one passage 1 deer mouse (DM6) and both passage 2 deer mice (DM8, DM9) but to a lesser extent (Figure 5.4C).

5.3.5 Purifying selection for a 4 amino acid insert in the spike protein occurs in deer mice.

The viral genome sequence was determined by NGS using oral swab samples from the two P2 deer mice and compared to the input virus sequence. A 4-residue insertion, KLRS, occurred in the N-terminal domain (NTD) of the spike protein, at residues 216-219 (nt 22,208-22,219) (Figure 5.5A) and was observed in all reads (150 reads for DM8, 140 reads for DM9). A structural model shows this insertion is located in a solvent-accessible loop that is distant from the RBD that interacts with ACE2 (Figure 5.5B). The surface location of the KLRS insert at a

Table 5.1 Detection of viral RNA in oral swabs. Values = vRNA copy numbers. Gray boxes, no sample collected. Neg, no vRNA detected by PCR. Euth, day of euthanasia of deer mice DM8 and DM9

dpi	DM1	DM2	DM4	DM5	DM6	DM7	DM8	DM9
1	3.3E+05	3.2E+05	3.0E+05					
2	8.1E+04	3.0E+05	1.3E+03	Neg	Neg	Neg		
3	8.2E+03	1.3E+03	4.3E+02	2.7E+05	Neg	Neg		
4	4.4E+03	1.1E+03	1.2E+04	7.8E+05	Neg	Neg	Neg	Neg
5	2.8E+05	1.8E+03	4.6E+02	3.9E+03	Neg	Neg	Neg	Neg
6	3.2E+03	3.1E+03	1.3E+04	6.0E+03	1.2E+05	2.6E+03	Neg	Neg
7	2.0E+04	1.9E+04	7.9E+03	1.1E+05	2.7E+07	2.9E+03	Neg	Neg
8	1.1E+03	2.8E+02	8.6E+03	6.2E+04	1.4E+03	3.7E+02	7.7E+02	3.1E+04
9							3.7E+02	1.0E+04
10	4.7E+02	5.3E+00	2.3E+02	7.2E+02	1.8E+03	2.2E+00	9.0E+02	5.1E+03
14	1.3E+01	1.6E+01	3.3E+01	4.5E+02	9.0E+02	9.0E+02	Euth	Euth
21	Neg	1.9E+02	2.6E+02	Neg	Neg	1.3E+02		
28	Neg	Neg	Neg	Neg	Neg	Neg		
	Inoculated			Contact P1			Contact P2	

location away from the RBD may suggest interactions with an unknown co-receptor, and notably mouse coronavirus 1 (formerly mouse hepatitis virus) uses the NTD as a receptor binding domain (Li, 2016). It may be that the passage 2 deer mice were both infected by the passage 1 deer mouse DM5 (Table 1) that was introduced to the P2 cage when vRNA was initially detected in DM5 oral swabs 4 days prior to introduction of the other two passage 1 deer mice (DM6, DM7). However, the passage 2 deer mice did not become PCR^+ until 2 days after DM6 and DM7 deer mice were added to the P2 cage, thus it cannot be conclusively determined which P1 deer mice transmitted the virus to the P2 deer mice.

Although the insertion was not detected in the NGS data for the input virus, which was sequenced at 8x coverage, conventional PCR using the forward primer containing the 12 nt insertion confirmed that the insert was present at low levels in the inoculum virus and at very

low levels in the virus obtained from BEI Resources (Supplementary Figure 5.11). PCR with the insert primer also showed that all 17 infected deer mice in this study had at least some insert virus, implying a strong purifying selection during passage. In addition, two synonymous mutations occurred in the Orf7 (codon 5, CUU > CUA) and nucleocapsid (codon 145, CAC > CAU) genes in the P2 virus.

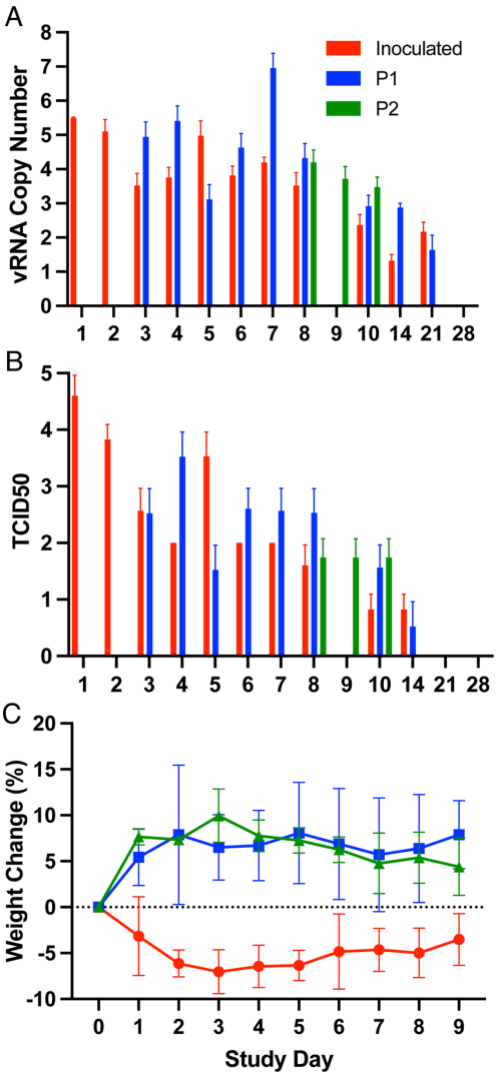

Figure 5.4 Abundance of viral RNA in oral swabs and weight loss in deer mice infected with SARS-CoV-2. (A) Probe-based PCR was used to detect levels of E gene RNA and quantified against an E gene plasmid standard (Integrated DNA Technologies). Transient weight loss occurred in some deer mice inoculated with SARS-CoV-2. (B) Virus isolation from oral swabs of infected deer mice. *P2 contact deer mice were euthanized on day 10 to prepare P2 virus stock. Deer mice were weighed each day during the transmission study (C). All three inoculated deer mice, one passage 1 deer mouse (DM6) and both passage 2 (DM8, DM9) deer mice lost weight followed by recovery.

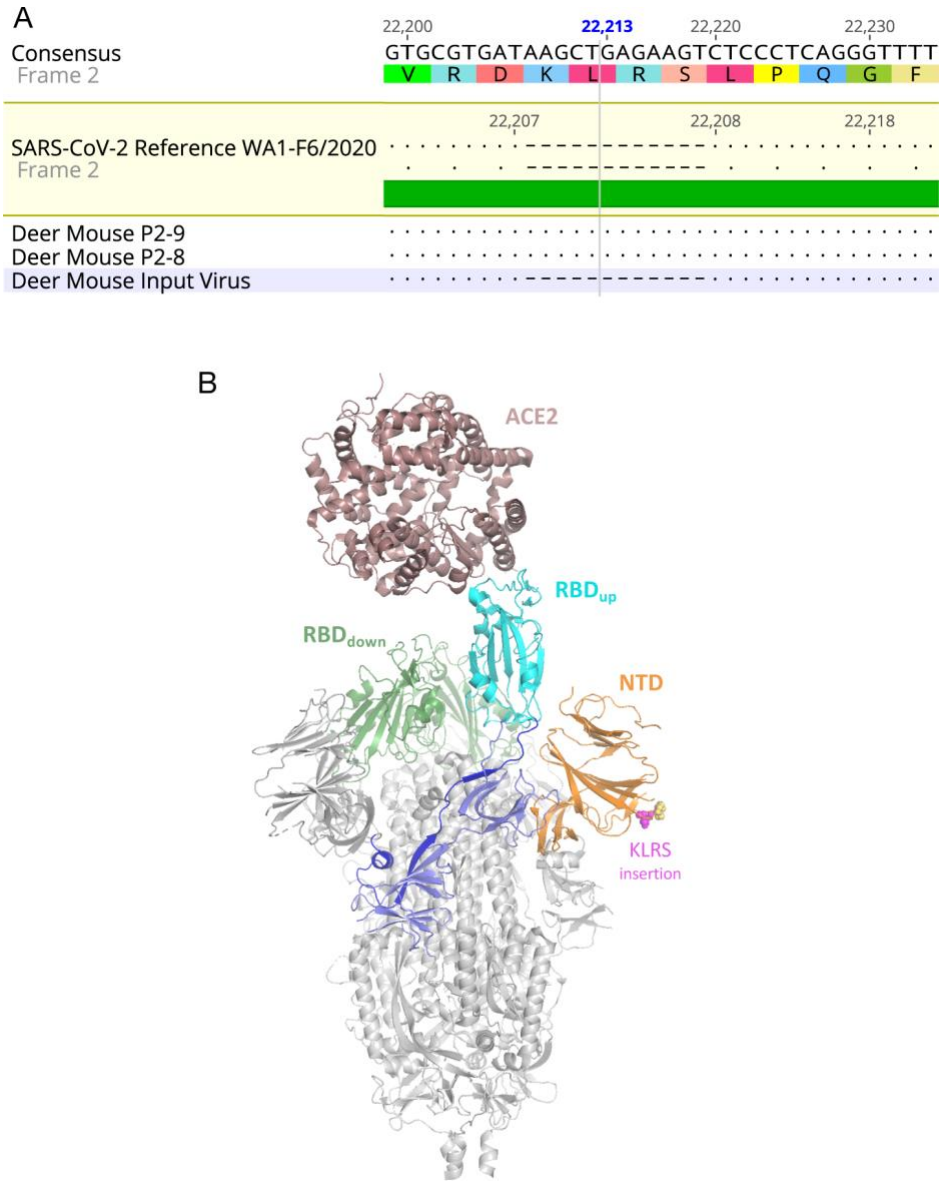

Figure 5.5 Spike protein insertion after serial passage in deer mice. (A) Passage of SARS-CoV-2 led to fixation of a 4-residue insertion in the N-terminal domain. Oral swabs of both DM8 and DM9 passage 2 deer mice (P2-8, P2-9, respectively) were submitted to RNA-Seq and an insertion was detected in all reads spanning residues 216-219 (nt 22,208-22,209, hatches) of the spike protein, implying a strong purifying selection for the insert during passage. (B) Homology model of the spike protein-human ACE2 complex showing the location of the KLRS insertion observed in the P2 virus. Model was generated by threading the deer mouse P2 spike protein sequence into the EM structure of the open-state SARS-CoV-2 spike protein (PDB: 6VYB) and colored as follows: Core (grey), N-terminal domain (NTD, orange) with KLRS insert as magenta spheres and native loop residues as yellow spheres, interdomain linker (blue), receptor binding domain (RBD, cyan for one up-conformation copy, green for two down-conformation copies), SD1/SD2 domains (light blue). The structure of the human ACE2 receptor (brown) was then superposed on the up-confirmation RBD using the crystal structure of the RBD-ACE2 complex (PDB: 6VW1).

5.4 Discussion

The order Rodentia has more than 2,200 species and the divergence of families Cricetidae (hamsters, voles, lemmings, and New World mice and rats) and Muridae (Old World mice, rats and gerbils) occurred about 18.5 mya (Steppan and Schenk, 2017). Cricetidae has more than 600 species, including at least 70 species in the North American subfamily Neotominae (Steppan and Schenk, 2017) that include deer mice and other peromyscines. Few cricetid ACE2 sequences are available, but the 20 critical residues of ACE2 that interact with the RBD of SARS-CoV-2 (Luan et al., 2020) suggest other cricetid rodents are likely susceptible. In addition to *Peromyscus* species, two other neotomids from different genera have ACE2 similarities that suggest they are susceptible; the northern grasshopper mouse (*Onychomys torridus*) with 18/20 identities, and the desert woodrat (*Neotoma lepida*) with 17/20 identities. Experimental challenges of these species will be necessary to determine their susceptibility, and which will shed light on diversity of North American species that may be susceptible to SARS-CoV-2. ACE2 residues are less human-like (15 of 20 residues) in the cricetid North American prairie vole (*Microtus ochrogaster*; subfamily Arvicolinae) and South American long-tailed pygmy rice rat (*Oligoryzomys longicaudatus*; subfamily Sigmodontinae), suggesting they are less likely to be susceptible. The laboratory house mouse (family Muridae) is not susceptible and it has 13 of the 20 critical ACE2 residues (Luan et al., 2020).

The respiratory pathology that occurred demonstrates that deer mice are a suitable small animal model for the study of SARS-CoV-2 disease. Neutralizing antibody was detected on day 6 post challenge, which corresponded with an inability to isolate infectious virus from lungs or olfactory bulbs, suggesting rapid antibody control of the virus. The ELISA, which is IgG-specific, detected high titer antibody on day 14, but not day 6, suggesting the neutralizing antibody on day 6 was exclusively IgM. No deer mouse anti-IgM detection antibodies are available, thus it is not

possible to definitively demonstrate IgM reactivity. Despite this seroconversion and neutralization, we isolated virus from oral swabs of some deer mice to 14 days post infection.

Elevated inflammatory immune signatures by qPCR also suggested that a proinflammatory adaptive immune response may contribute to the pathogenesis of disease, which is also thought to be a significant component of COVID-19 morbidity and mortality (Cao, 2020). The elevated expression of CD8β, Tbx21 transcription factor and IL-21, and low but significant expression of IL-2Rα, suggest CTL infiltration and activation (Sutherland et al., 2013). We did not detect robust IFNγ or IL-6 expression, both of which are associated with fatal COVID-19 (Wan et al., 2020), which may account for why the deer mice did not have significant disease or death. Although gene expression is suggestive of biological responses, the inability to detect the proteins encoded by these genes in deer mice limits interpretation of gene expression results. New approaches for detection and quantification of immune proteins will be required to further scrutinize the host response in deer mice.

Neurological manifestations and neuropathogenesis of human coronaviruses have been dwarfed by the respiratory component of the diseases (Iroegbu et al., 2020). Understanding the underlying mechanisms of neuroinvasion was among the main goals of this study. Involvement of peripheral nerves of a 3-year-old girl spontaneously coinfected with HCoV 229E and OC43 resulted in acute flaccid paralysis (AFP), inability to masticate or swallow, speech loss and total lack of muscle tone and deep muscle reflexes (Turgay et al., 2015). In deer mice, the presence of virus in the peripheral cranial nerves, ganglia and the brain suggests a wide spectrum of neurological consequences that could precipitate parasympathetic and sympathetic clinical symptoms such as xerostomia, epiphora, trigeminal neuralgia, confusion, and more consistently hyposmia/anosmia and hypogeusia/ageusia (Biadsee et al., 2020; Wu et al., 2020b). Bidirectional trans-neuronal dissemination in the medulla can result in rapid death if the more

vital neighboring respiratory center becomes infected. SARS-CoV-2/deer mouse infection studies may clarify the complex relationship between sensory losses, chronic pain and compromise to the BBB and immune system of affected COVID-19 patients. If cervical ganglia are infected, autonomic dysfunction, and potential myogenic effect in addition to brain stem injury could lead to global brain ischemia due to electrographic myocardial injury and constriction of cervical and skull arterial blood supply (Tahsili-Fahadan and Geocadin, 2017). Collective pathology and immunohistochemistry results point to two different mechanisms that SARS-CoV-2 may utilize to enter the central nervous system. Similar to herpesviruses, early in the course of the disease at 3 dpi, the virus appeared to invade the brain in a retrograde axonal transmission along gustatory, olfactory and trigeminal pathways, bypassing the BBB (From the American Association of Neurological Surgeons et al., 2018). Penetration routes can occur through damaged olfactory epithelium or via infected monocytes through compromised BBB later in the course of the disease. The neuropathology induced in this animal model makes it more suitable to further elaborate on neuropathogenesis of COVID-19 when compared to the Syrian hamster model which develop marked respiratory disease (Rosa et al., 2021).

Deer mice are among the most widely studied rodents in North America and are frequently collected by mammalogists conducting field work. Outbreaks of SARS-CoV-2 on farms in several U. S. states (2020) has resulted in the deaths of thousands of American mink (*Neovison vison*) and escape of other infected mink (Shriner et al., 2021). Many of these farms are located in deer mouse habitat, thus the risk of transmission to deer mice that inhabit mink barns or escape of SARS-CoV-2-infected mink, could lead to spillback to rodents. There is now evidence that wild mink in Utah have become infected with SARS-CoV-2, likely via contact with caged or escaped mink (DeLiberto, 2020). This heightens concerns that deer mice or other neotomid rodents could serve as secondary reservoirs of SARS-CoV-2 in North America. Dromedary camels, which are secondary reservoirs of MERS-CoV, had detectable vRNA in oral swab

samples for up to 35 days in an experimental infection study (Adney et al., 2014). All contact deer mice in this study became infected with detection of vRNA in oral swabs as early as 2 days after contact, and inoculated deer mice had detectable vRNA to 21 days, suggesting that sustained transmission among wild deer mice is possible. The susceptibility of two cricetid rodents, deer mice and Syrian hamsters, also raises the possibility that cricetid rodents could have served as intermediate hosts in spillover to humans and/or recombination events between coronaviruses. As a precedent for recombination, alphacoronaviruses have been detected in cricetid rodents in Europe, including bank voles (*Myodes glareolus*) and field voles (*Microtus agrestis*), and in those studies each of the alphacoronaviruses possessed spike genes derived from betacoronaviruses (Tsoleridis et al., 2019). Considering that cricetid rodents are also found in Asia, it must be considered that they could have served as intermediate hosts for SARS-CoV-2 prior to spillover into humans (Lau et al., 2020).

The weight loss of the three inoculated deer mice could be reflective of a higher dose inoculum, or greater virulence of the wildtype virus that was abundant in the inoculum relative to the NTD insertion virus and will require further investigation. No SARS-CoV-2 sequences in Genbank have this insertion, thus it may not have relevance to human infection. It remains unclear whether this insertion rose in frequency to near fixation due to bottlenecks during transmission and/or systemic spread of the virus, or to positive selection. Ongoing studies will address this issue.

Deer mice and other peromyscine rodents have been used in biomedical research for many decades, including for their roles as reservoir hosts of zoonotic agents (Barbour, 2017; Botten et al., 2000; Schountz et al., 2007), and aging and diabetes studies (Havighorst et al., 2017), both of which are comorbidities associated with higher mortality rates in humans (Wu et al., 2020a). They can live eight years in captivity, about four times longer than laboratory mice and Syrian

hamsters, making them particularly suitable as a model organism to examine the effects of age and SARS-CoV-2 infection, and the durability of immunity to infection and vaccination. Moreover, as an outbred model, deer mice are more likely to reflect the diverse outcomes of infection observed in humans (e.g., neuropathology), in contrast to those that occur in highly inbred laboratory mice and Syrian hamsters (Adler, 1948).

We have examined SARS-CoV-2 infection in Syrian hamsters using the same virus stock and dose described in this study (Fagre et al., 2020). While both Syrian hamsters and deer mice show bronchointerstitial pneumonia that is thought to be a significant reason for the severe COVID-19 in some human patients, total lung area affected in hamsters seems to be larger, precipitating respiratory clinical signs. The elements of pulmonary inflammation in both species seem to be the same including early necrotizing and later proliferative bronchiolitis, leukocytoclastic vasculitis and proliferative pneumonia with formation of syncytial cells. Lethality of the respiratory disease in both experimental models is lacking, but in deer mice the expression of IFNγ and IL-6 does not markedly change in the course of acute and subacute phases of the disease, which may in part explain why the infected deer mice recovered without an overt or severe respiratory disease. At 6 dpi, lymphocytic infiltrates around respiratory ducts and blood vessels in this study seemed to intensify in deer mice, which is concordant with increased expression of the T cell genes (Figure 5.2) and a decline in viral replication (Figure 5.1).

Although no manifest behavioral signs were observed in the current study, SARS-CoV-2 infectious virus was detected in the brains of infected deer mice. Presence of infectious virus in the autonomic nervous system of the deer mice that survived the acute infection is in line with the COVID-19 complications seen in some human patients, especially the sympathetic and parasympathetic long-term complications. Infection of the CNS is not indicative of a lethal

outcome in most human patients. Infection of autonomic nervous system of Syrian hamsters and autonomic instability is less documented when compared to the deer mice used in the current model.

Collectively, the present study offers a novel animal model for the study of SARS-CoV-2 pathogenesis that has many similarities to the Syrian hamster, but also some differences. The availability of alternative models may facilitate efforts to understand tissue and organ specific pathogenesis to identify commonalities and differences that may shed light on mechanisms of SARS-CoV-2 pathogenesis

Chapter 6: SARS-CoV-2 infects multiple species of North American deer mice

6.1 Introduction

Severe acute respiratory syndrome coronavirus-2 (SARS-CoV-2), the virus that causes Coronavirus disease-19 (COVID-19), emerged in late 2019 in Wuhan, China with rapid global spread resulting in millions of deaths (Zhu et al., 2020a). Molecular evidence suggests the zoonotic origin of SARS-CoV-2 is horseshoe bats of the genus *Rhinolophus,* which carry many SARS-related coronaviruses (Hu et al., 2017). COVID-19 remains an ongoing pandemic with hundreds of millions of cases and substantial global economic impacts.

The long-term pandemic status of COVID-19 is partially facilitated by the periodic emergence of new variants of SARS-CoV-2 that overcome immunity from vaccination or prior infection. The emergence of the omicron variant of SARS-CoV-2 in November 2021 sparked a new wave of infections globally due to its increased ability to infect convalescent and vaccinated individuals (Dejnirattisai et al., 2021). The rapid accumulation of spike protein mutations that led to the omicron variant has led to the hypothesis that its progenitor may have acquired mutations during adaptation to a non-human host, perhaps rodents (Sun et al., 2022; Wei et al., 2021). The potential for new variants to emerge because of adaptation to non-human hosts must be considered, and therefore identification and characterization of prospective non-human hosts is necessary to ensure preparedness.

Several mammalian species have been shown to be susceptible to infection with SARS-CoV-2, including tree shrews, Syrian hamsters, ferrets, cats, Egyptian fruit bats, mink, North American

deer mice, and several species of non-human primates (Fagre et al., 2021a; Griffin et al., 2021; Lu et al., 2020; Oude Munnink et al., 2021; Schlottau et al., 2020b; Shi et al., 2020b; Sia et al., 2020a; Zhao et al., 2020). Of note was the human-to-mink transmission of SARS-CoV-2 on mink farms in several countries, which resulted in localized human outbreaks of a mink-adapted SARS-CoV-2 variant (Oude Munnink et al., 2021). This exemplifies the need to examine animals living in close proximity to humans for their potential to act as hosts to SARS-CoV-2.

In our previous work, we determined that one subspecies of North American deer mice (*Peromyscus maniculatus nebrascensis*) is susceptible to experimental infection with SARS-CoV-2 and capable of transmission to naïve conspecifics for at least two passages. Another group reported similar findings in another subspecies of deer mouse (*P. m. rufinus*) (Griffin et al., 2021). Deer mice are common peridomestic rodents that occupy a wide geographical range in North America (Carleton, 1989b; Lawlor and Hall, 1982) and are the principal reservoir hosts of Sin Nombre orthohantavirus (Schmaljohn and Hjelle, 1997) and *Borrelia burgdorferi,* the causative agent of Lyme disease (Bosler et al., 1984). Given their prominence in North American ecosystems, including on and around mink farms, it is feasible that SARS-CoV-2 could be introduced into wild deer mouse populations.

In this work, we expand the evidence of peromyscine rodent susceptibility to infection with a human isolate of SARS-CoV-2 to include two additional subspecies of the North American deer mouse group, including the Sonora white-footed mouse (*P. m. sonoriensis*) and the prairie deer mouse (*P. m. bairdii*). We also demonstrate susceptibility of two additional deer mouse species, the Oldfield mouse (*P. polionotus subgriseus*) and the California mouse (*P. californicus*), suggesting that rodents in genus *Peromyscus* are broadly susceptible to SARS-CoV-2. The examined species also expand the geographical range in which susceptible deer mice exist,

increasing the risk of zooanthroponotic transmission of SARS-COV-2 from humans to wild rodents.

6.2 Materials and Methods

6.2.1 Viruses

SARS-CoV-2 (isolate 2019-nCoV/USA-WA1, NR52281) was obtained from BEI Resources. Virus was passaged twice on Vero E6 cells (ATCC CRL-1586) in 2% FBS-DMEM containing penicillin and streptomycin at 37°C under 5% CO_2 to generate stock virus used in these experiments. Virus was stored at −80° C. All work with infectious virus was performed at BSL-3 with approval from the Colorado State University Institutional Biosafety Committee.

6.2.2 Animal procedures- multi-species study

All rodent work was approved by the CSU Institutional Animal Care and Use Committee (protocol 993). Deer mice were intranasally inoculated under inhalation of isoflurane anesthesia with $1x10^4$ (*P. bairdii*), $1.5x10^4$ (*P. sonoriensis*), or $2×10^4$ (*P. polionotus* and *P. californicus*) $TCID_{50}$ SARS-CoV-2 (dose based on appropriate inoculation volume for body size). On days 3, 6 and 15 post-challenge, all animals were orally swabbed and weighed, and three inoculated mice of each species were euthanized by inhalation anesthesia and thoracotomy followed by cardiac exsanguination. Oral swabs and weights were taken for remaining mice on day 10 post-challenge. Control rodents were euthanized on day 0 using procedure described above. Necropsies were performed on all mice and samples (blood, lung) were collected for viral RNA detection (by RT-qPCR), virus isolation, and serology. Remaining whole carcasses were fixed in 10% neutral buffered formalin for histopathology and immunohistochemistry. For the California mouse study, all mice were intranasally inoculated under inhalation isoflurane anesthesia with $2×10^4$ $TCID_{50}$ SARS-CoV-2 and four were euthanized as controls on either day

3 or 10 post-challenge. All mice were orally swabbed, weighed, and observed for clinical signs daily. Necropsies were performed on mice euthanized on days 3, 6, and 10 post-challenge, and tissues (blood, lung) were collected for viral RNA detection (by RT-qPCR), virus isolation, and serology. Remaining whole carcass was fixed in 10% neutral buffered formalin for histopathology and immunohistochemistry

6.2.3 Sample collection and processing

Swabs were stored in 200 µL of viral transfer media (VTM) at -80º C until being processed and analyzed. Swabs were vortexed for 10 seconds followed by centrifugation at 1,500 rcf for 10 minutes to pellet any debris. Resulting supernatant was used in downstream assays. Tissues were stored in 500 µL of VTM and either flash frozen in LN_2 and stored at -80º C until processing and analysis (multi-species experiment) or immediately processed following collection and stored at -80º C until analysis (California mouse experiment). Processing of tissue samples included homogenization on a TissueLyser II (Qiagen) at 50hz for 5 minutes followed by centrifugation at 10,000 rcf to pellet debris. The resulting supernatants were used in downstream analysis, including infectious virus isolation and RNA extraction for viral RNA quantification. Blood was collected in a serum separator tube, allowed to clot for 20-30 minutes, and then centrifuged at 20,000 rcf for 90 seconds. Serum was collected and stored at -80º C until analysis.

6.2.4 $TCID_{50}$ of tissues and swabs

Supernatant from swabs or lung homogenate was plated in triplicate on 96-well plates seeded with Vero E6 cells in a 10-fold dilution series from 10^0 to 10^{-3}. Samples that were above the limit of detection were re-plated in triplicate on 96-well plates seeded with Vero E6 cells in a 10-fold

dilution series from 10^{-2} to 10^{-5}. All plates were scored four days post-infection and titers were calculated using the Reed-Meunch method (Reed and Muench, 1938).

6.2.5 Viral RNA in tissues and swabs

RNA was extracted from swab or tissue supernatant using the Mag-Bind Viral DNA/RNA 96 Kit (Omega Biotek) on the KingFisher FLEX System (ThermoFisher Scientific) according to manufacturer's instructions. Reverse transcriptase quantitative PCR (RT-qPCR) was run using the GoTaq RT-qPCR System (Promega) with the IDT E Assay First Line Screening primers and probe (Cat # 10006804) on a LightCycler 96 System (Roche, Cat# 05815916001).

6.2.6 Serum neutralization assay

Serum neutralization was performed starting at a 1:10 dilution with a 2-fold dilution series. An equal volume of SARS-CoV-2 containing 100 $TCID_{50}$s was added (final serum dilution of 1:20) and incubated for 1 hr at 37° C. The mixture was plated on Vero E6 cells and scored for cytopathic effect after five days. The titer was the reciprocal of the greatest dilution that conferred 100% protection.

6.2.7 ELISA

Recombinant SARS-CoV-2 nucleocapsid antigen in PBS was coated onto 96-well plates overnight at 4° C. Plates were washed 3x with PBS-0.5% TWEEN-20 and 3x with PBS between each step, then blocked with 0.5% gelatin in PBS for 30 min. Serum samples were diluted 2-fold in 0.5% BSA-PBS starting 1:100 and incubated for 2 hours at room temperature. Detection antibody, anti-*Peromyscus leucopus* IgG H&L-HRP (SeraCare), was diluted 1:1000 and incubated for 1 hour, followed by ABTS substrate. Plates were read at 405 nm and samples

were considered positive if the OD was 0.200 above the mean of the negative control serum samples (uninfected deer mice).

6.2.8 Histopathology and immunohistochemistry

After samples were collected for molecular analysis, the entire carcass was fixed in 10% neutral buffered formalin. Representative samples from the lungs, liver, heart, and the entire head (sagittal section) were collected and routinely processed for histopathology. Tissues were labeled with hematoxylin and eosin (H&E) for histologic analysis. Anti-SARS-CoV-2 immunohistochemistry was performed on embedded lung tissue from a representative subset of lung tissues at days 3 and 4 post-challenge, selected based on virus detection by RT PCR, using rabbit anit-SARS-CoV-2 nucleocapsid antibody [NP1189] (ProSci) as a primary antibody with hematoxylin counterstain.

6.3 Results

6.3.1 Infectious virus was detected in each species of deer mouse

To investigate the susceptibility of different deer mouse species and subspecies, nine young, adult deer mice from each species or subspecies and of both sexes were intranasally challenged with SARS-CoV-2. Three unchallenged controls from each species group were euthanized and necropsied on day zero of the experiment. Three challenged mice from each species group were euthanized and necropsied on days 3, 6, and 15 post-challenge with one additional oral swab taken at day 10. Infectious virus was detected in 1/9 oral swabs from each species group on day 3 post-challenge, and viral RNA was detected in most lung samples from mice euthanized on days 3 and 6 post-challenge (Table 6.1). Viral RNA was detected in oral swabs of all challenged mice on day 3, and infectious virus was detected in oral swabs from 3/4 species on day 3 post-challenge (prairie deer mouse, California mouse, and Oldfield mouse).

Three of the four species (prairie deer mouse, Sonora white-footed mouse, and Oldfield mouse) had detectable neutralizing antibodies on day 15 post-challenge, with an average geometric mean titer of 87 (SD ± 39). California mouse samples for this time point were compromised by mold contamination.

Table 6.1 Detection of viral RNA (vRNA) and infectious virus in lungs and oral swabs and serology. Values represented as number of positive samples out of total number of samples.

Prairie deer mouse					
days post-challenge	vRNA in lung	infectious virus in lung	vRNA in oral swab	infectious virus in oral swab	neutralizing antibodies
3	3/3	2/3	9/9	1/9	0/3
6	3/3	1/3	6/6	0/6	0/3
10	N/A	N/A	3/3	0/3	N/A
15	0/3	0/3	0/3	0/3	2/3
Sonora white-footed mouse					
Days post-challenge	vRNA in lung	infectious virus in lung	vRNA in oral swab	infectious virus in oral swab	neutralizing antibodies
3	2/3	0/3	9/9	1/9	0/3
6	2/3	1/3	5/6	0/6	0/3
10	N/A	N/A	1/3	0/3	N/A
15	1/3	0/3	0/3	0/3	2/3
Oldfield mouse					
Days post-challenge	vRNA in lung	infectious virus in lung	vRNA in oral swab	infectious virus in oral swab	neutralizing antibodies
3	3/3	0/3	9/9	1/9	0/3
6	3/3	1/3	4/6	0/6	0/3
10	N/A	N/A	3/3	0/3	N/A
15	0/3	0/3	0/3	0/3	2/3
California mouse					
Days post-challenge	vRNA in lung	infectious virus in lung	vRNA in oral swab	infectious virus in oral swab	neutralizing antibodies
3	3/3	0/3	9/9	1/9	0/3
6	3/3	1/3	4/5	0/6	0/3
10	N/A	N/A	1/2	0/3	N/A
15	0/2	0/2	0/2	0/3	N/A

6.3.2. Clinical signs

No clinical signs were observed in the prairie deer mouse or Oldfield mouse at any timepoint in the study. The Sonora white-footed mice lost weight over the 15 day challenge study, despite a lack of other clinical signs (Figure 6.1). On day 3 post challenge, two California mice (1 female, 1 male) were observed to have ruffled fur, a hunched posture, and lethargic behavior. When the California mice were examined on day 4, the male appeared to have improved whereas the female was moribund and was humanely euthanized for necropsy. This mouse had hepatomegaly and prominent hepatic reticular pattern. It was suspected that the mouse was suffering from hepatic lipidosis (or, in humans, non-alcoholic fatty liver disease (NAFLD)). Three other California mice had a grossly prominent hepatic reticular pattern and hepatomegaly upon necropsy, including the male that displayed clinical signs on day 3. California mice lost significantly more weight 3 days post-challenge than any other group. To further investigate California mice as a model for SARS-CoV-2 disease, additional California mice were infected with SARS-CoV-2. Serial necropsies were performed on days 3, 6, and 10 post-challenge. No clinical signs were observed in these mice for the duration of the study.

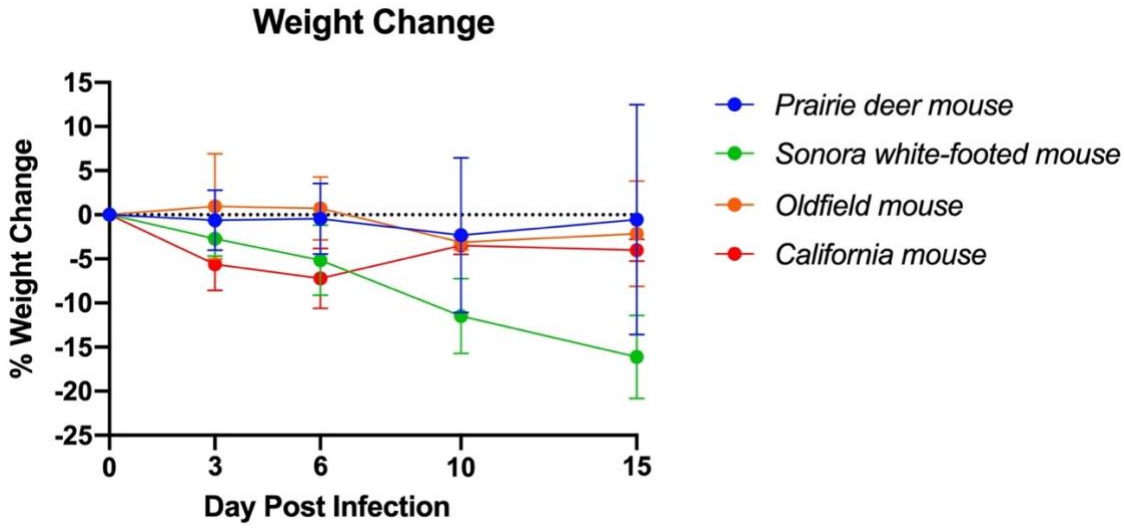

Figure 6.1 Weight change of deer mouse species during SARS-CoV-2 infection. On day 3 post-challenge, the California mice had significantly greater weight loss than the prairie deer mouse (p=0.004), Sonora white-footed mouse (p=0.027), and Oldfield mouse (p=0.010). At 6 days post-challenge, the California mouse had significantly greater weight loss than the prairie deer mouse (p=0.016) and the Oldfield mouse (p=0.005).

6.3.3 California mice become infected with SARS-CoV-2

We further developed California mice as an animal model of SARS-CoV-2 infection following our observation of clinical disease in two mice during our initial investigation. The SARS-CoV-2 challenged group showed significantly greater weight loss than the uninfected controls at days 1 and 3 post-challenge (Figure 6.2). At day 10 the control mice had a significant decrease in weight compared to infected controls. The cause of the weight loss is unknown. As the infected mice had all cleared detectible infectious virus by day 10, the weight loss in the control group at this time point was not significant to the conclusions of this study. RT-qPCR and virus isolation indicated that the mice became infected, with viral RNA detected through day 10 post-challenge in oral swabs and lungs (Figures 6.3A, 6.3C). Infectious virus was detected in oral swabs on days 1, 2, and 3 post-challenge (average $3.16 \times 10^2 \pm 2.93$ $TCID_{50}$/mL, Figure 6.3B) and in all day 3 lungs (average $6.60 \times 10^4 \pm 6.39 \times 10^4$ $TCID_{50}$/mL, Figure 6.3D). Serum IgG to nucleocapsid was detected in all mice at 10 days post-challenge (geometric mean titer 400, 95%CI [180,887] Figure 6.3E), and neutralizing antibody was detectable in 5 of 6 mice (geometric mean titer 92, 95% CI [45,189], Figure 6.3F).

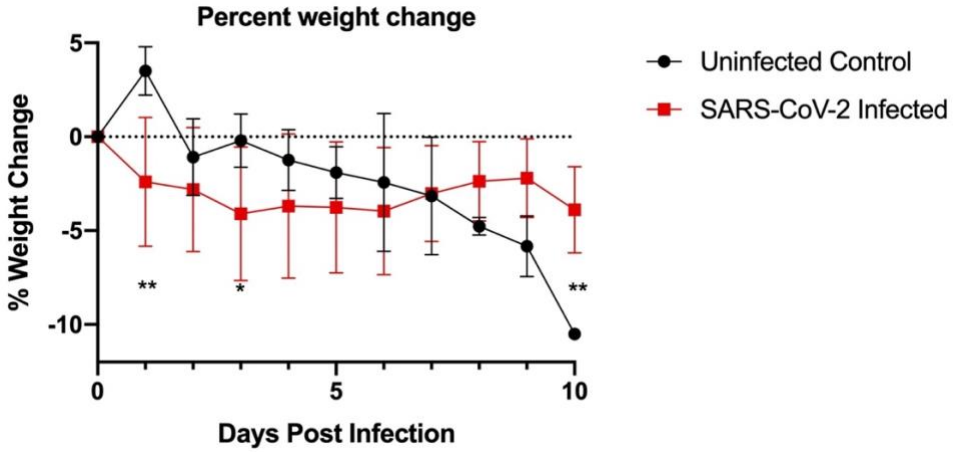

Figure 6.2 California mouse (P. californicus insignis) weight change during SARS-CoV-2 infection. SARS-CoV-2-challenged California mice had significantly greater weight loss on day 1 post-challenge (p=0.003) and day 3 post-challenge (p=0.047) as compared to the uninfected controls. The uninfected control group had significantly more weight loss than the challenged group at day 10 post-challenge (p=0.008).

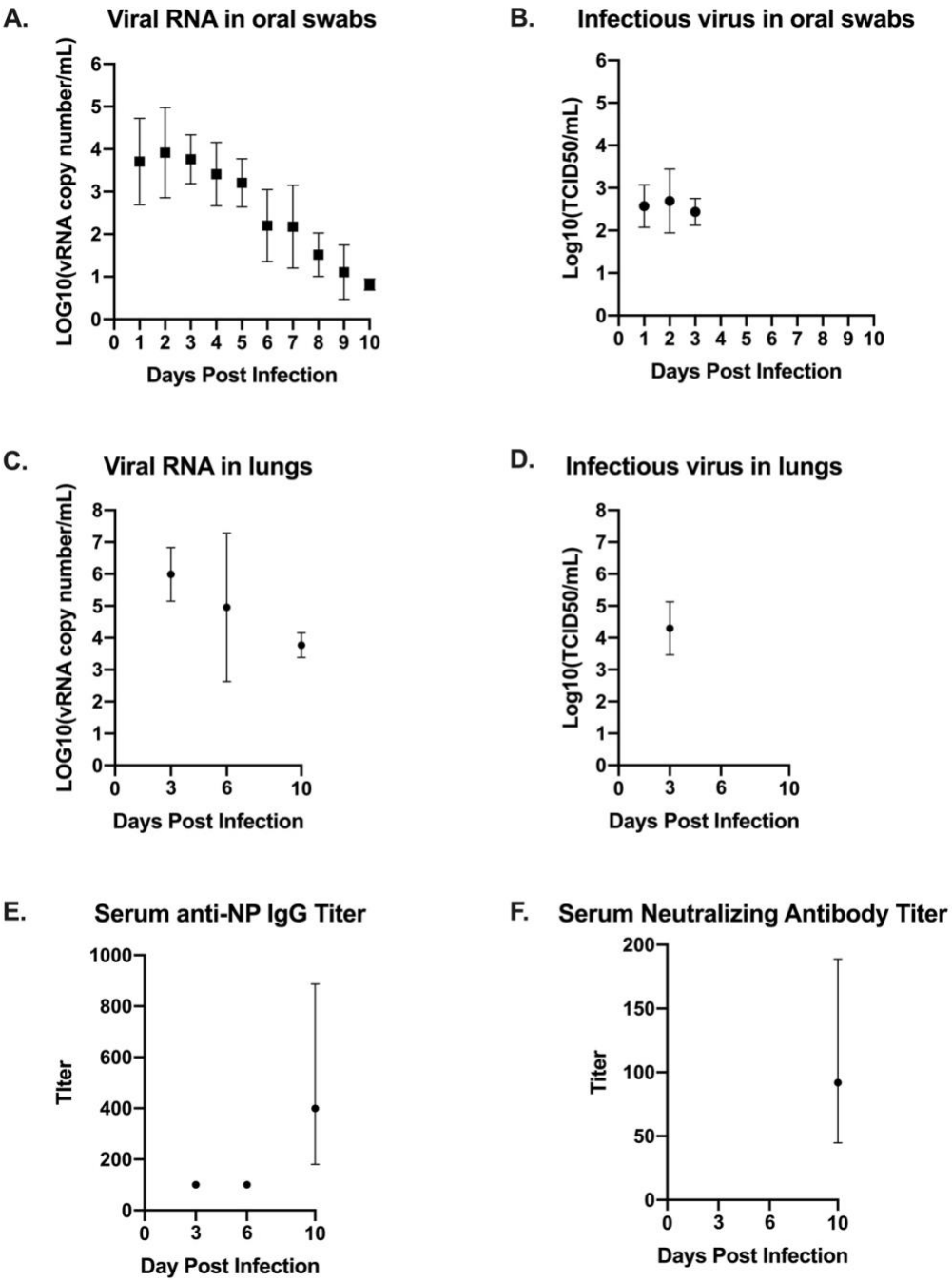

Figure 6.3 Virus detection and serology for California mice (P. californicus insignis). Oral swabs collected daily (days 0–10 post-challenge) were tested for viral RNA (A) and infectious virus (B). Lung homogenate collected from mice euthanized on days 3, 6, and 10 post-challenge were also tested for viral RNA (C) and infectious virus (D). Serum collected from mice on days 3, 6, and 10 post-challenge was evaluated for quantification of serum IgG determined by indirect ELISA (E) and serum neutralizing antibody titer determined by serum neutralization assay (F).

6.3.4 Histopathology and Immunohistochemistry

Lung, liver, spleen, nasal skin and mucosa, and heart from all mice were evaluated for pathology. The most severe inflammation was observed in the lungs and nasal passages in all species. The nasal skin and mucosa, heart, and liver did not show histologic differences in any of the groups. Lung was the most affected tissue and infected mice showed variable severity of interstitial lymphohistiocytic and fibrinous pneumonia with edema, reactive vascular endothelium with neutrophilic margination and perivasculitis, and rarely minimal to mild bronchial epithelial hyperplasia (Figure 4A-B). Necrosuppurative rhinitis was the second most common finding in infected mice (Figure 4C). Other observed pathology included mild lymphohistiocytic myocarditis, microvascular hepatic lipidosis, necrotizing and lymphohistiocytic dermatitis of the muzzle and lymphoplasmacytic perineuritis. Lesions in all species, when present, were most severe at day 3 post-challenge versus days 6/10/15. Pneumonia was present in all groups but was minimal to mild in the Sonora white-footed mouse. Immunohistochemistry for anti-SARS-CoV-2 nucleocapsid had minimal rare positive labeling of bronchiolar epithelium in mice with virus detectible by RT-PCR (Figure 4D).

In six of the twelve California mice, there was hepatic lipidosis that ranged from mild to severe. The mouse that became moribund during the study demonstrated the most severe hepatic lipidosis histologically (Figure 6.5A). Lymphohistiocytic pneumonia in this mouse was minimal to mild but there was increased bronchial epithelial hyperplasia compared to other animals and this animal had the strongest anti-SARS-CoV-2 IHC labeling of the hyperplastic epithelium and scattered histiocytes (6.5B-C).

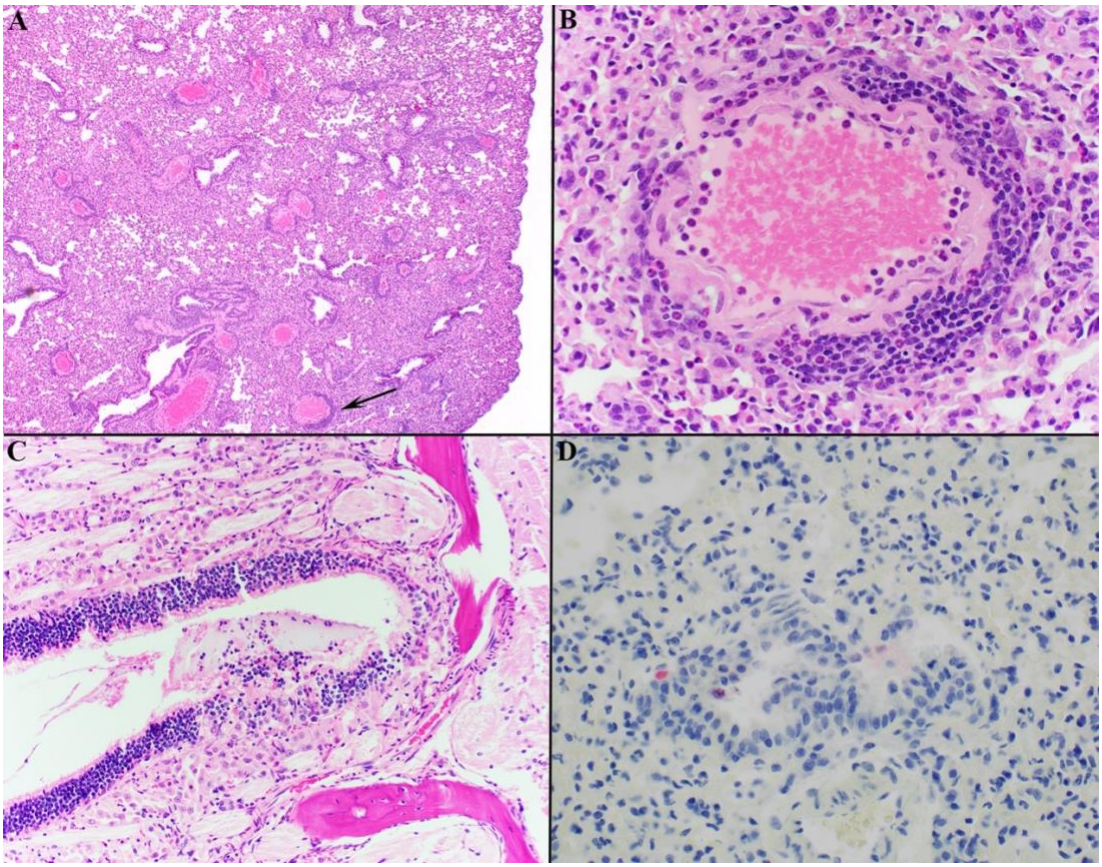

Figure 6.4 Histology of representative lesions in SARS-CoV-2 infected Peromyscus spp. Interstitial lymphohistiocytic pneumonia (A; Oldfield mouse) was the most common finding with multifocal vessels with segmental reactive endothelium, neutrophilic margination, and perivasculitis (A; Black arrow. Magnified in B). Necrosuppurative rhinitis was the second most common finding (C; California mouse). Anti-SARS-CoV-2 IHC shows rare positive labeling (red) of bronchial epithelial cells within the lungs (D; Sonora white-footed mouse). Hematoxylin counterstain.

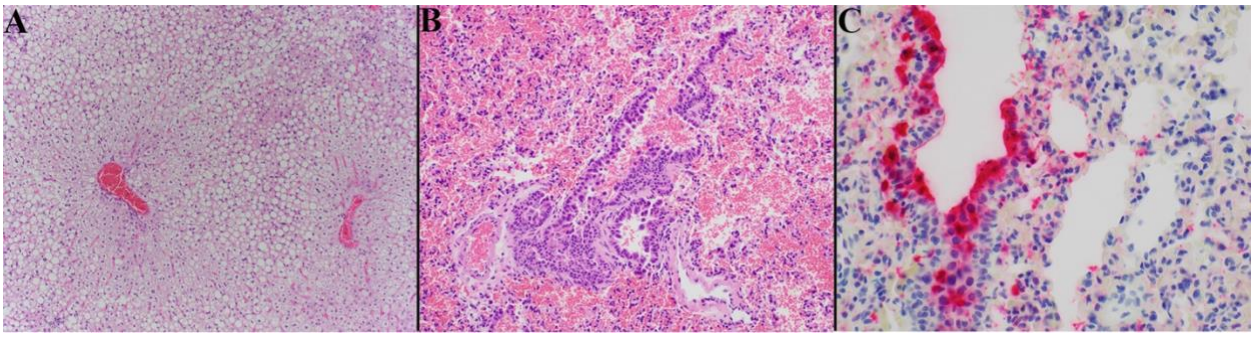

Figure 6.5 Photomicrographs of California mouse liver and pulmonary lesions. A single California mouse became moribund and at necropsy was found to have hepatomegaly. Histopathology showed severe diffuse distention of hepatocytes by lipid vacuoles consistent with hepatic lipidosis (A). The lungs of this animal exhibited only minimal to mild lymphohistiocytic pneumonia with moderate hyperplasia of the bronchiolar epithelium (B) but there was marked anti-SARS-CoV-2 positive labeling (red) of hyperplastic bronchial epithelium and histiocytes (C). Hematoxylin counterstain.

6.4 Discussion

The North American genus *Peromyscus*, collectively known as deer mice, contains more than 50 species and has been studied extensively for their use as animal models of human disease and for their ability to host and transmit medically important pathogens (Kirkland and Layne, 1989b). Many peromyscine rodents live in peri-domestic habitats, encountering humans through shared habitats as well as during outdoor activities (e.g. camping, field research). The experiments described here, along with previous work, confirm that three species of deer mice (the North American deer mouse, the Oldfield mouse, and the California mouse) and two subspecies of the North American deer mouse are susceptible to experimental SARS-CoV-2 infection with a human isolate of the virus (Fagre et al., 2021a; Griffin et al., 2021). There is some uncertainty as to the phylogenetic classification of the subspecies of deer mice used in this work, as it was proposed in 2019 by Greenbaum *et al.* that the North American deer mouse (*P. maniculatus*) be split into the eastern deer mouse (*P. maniculatus*) and western deer mouse (*P. sonoriensis*) (Greenbaum et al., 2019). This taxonomic change would increase the number of confirmed susceptible deer mouse species to four.

Experimental infection resulted in asymptomatic infection in all species other than the California mouse, of which two individuals displayed clinical signs and one required euthanasia. Interestingly, the moribund California mouse that was euthanized early had significant immunostaining for SARS-CoV-2 nucleocapsid in the lungs but minimal histological signs of pneumonia, whereas asymptomatic animals in this study had more signs of pneumonia and very little immunostaining. This could indicate that immunosuppression or immunocompromise played a role in the infection outcome for that animal. For most animals, infection lasted through day 10 post-challenge, and by day 15 neutralizing antibodies were present in all species. The mostly asymptomatic and short-lived nature of SARS-CoV-2 infection in the observed species

warrants investigation into their potential use as animal models for asymptomatic infection. The weight loss in some uninfected California mice was striking; however, this species is monogamous and we have observed loss of appetite after disruption of breeding pairs, particularly males, in the USC breeding colony. The separation of these animals after arrival at CSU may have contributed to weight loss. Additionally, the life span of deer mice, which can live up to 8 years in captivity vs ~2 years for laboratory mice (transgenic human ACE2) and Syrian hamsters (*Mesocricetus auratus*) (Sacher and Hart, 1978) that are also used for SARS-CoV-2 studies, potentiates them as models for immune durability in vaccine and reinfection studies.

The California mouse has been studied as a model for several obesity-related conditions including type II diabetes mellitus and NAFLD (Krugner-Higby et al., 2011; Krugner-Higby et al., 2000). California mice spontaneously develop these conditions when consuming a high-fat diet. In this study, we determined that California mice can be experimentally infected with SARS-CoV-2, with evidence of infectious virus in the lungs, oral shedding, and seroconversion. Both California mice that exhibited clinical signs in this study had hepatic lipidosis as determined by blinded pathological review, indicating that obesity-related conditions may have similar consequences in California mice as in humans during SARS-CoV-2 infection. NAFLD has been shown to predict COVID-19 progression and severity and COVID-19-related liver injury in human patients (Ji et al., 2020; Mushtaq et al., 2021). Therefore, the California mouse may be a suitable comorbidity model for NAFLD or other obesity related conditions and SARS-CoV-2. A larger study using California mice that have been fed a high-fat diet could address questions about liver dysfunction and SARS-CoV-2 disease, along with metabolic testing of the animals to confirm the conditions.

Peromyscine rodents and Syrian hamsters belong to the family Cricetidae. Deer mice and Syrian hamsters develop similar disease; however, California mice are the first small animal model to develop significant disease upon SARS-CoV-2 infection, other than transgenic mice that express human ACE2. This study used the WA1 isolate of SARS-CoV-2, thus future studies should examine other variants of concern, particularly delta variants that can cause more severe disease in humans. Considering their long lifespans, their outbred nature, availability of annotated genomes for several species, ready availability, and easy laboratory management, peromyscine rodents may serve as superior models to existing small animal models used in SARS-CoV-2 studies.

Chapter 7: Concluding remarks

Newly recognized viruses emerge from wildlife species into humans regularly, and risk factors such as climate change, habitat destruction, cohabitation, and agriculture provide continuous and growing fronts on which these exchanges may occur. The majority of epidemics due to viral pathogens are of a zoonotic origin, including Zika virus, dengue virus, Ebola virus, Marburg virus, Nipah virus, Hendra virus, SARS-CoV, MERS-CoV, and most recently SARS-CoV-2. Considering these outbreaks, surveillance of common reservoir hosts such as bats and rodents has increased, particularly in regions where virus spillovers have been previously documented such as Southeast Asia and Africa. However, little attention has been given to potential threats in the New World.

In my dissertation work, I reviewed and consolidated the literature and data on surveillance for and detection of PMVs in New World bats. The literature shows that PMVs are present in bats in the western hemisphere and have particularly high prevalence in vampire bats. The literature also revealed that standardization of data collection and reporting practices would greatly strengthen the knowledge of PMV prevalence and influencing factors. Next, I demonstrated the susceptibility of Jamaican fruit bats, a widespread and populous New World bat species, to a henipavirus infection. Primary cells from 7 different bats supported CedV replication, at least one primary cell line was susceptible to NiV, HeV, and CedV, and a susceptibility experiment resulted in viral shedding and seroconversion in three bats. NiV and HeV were able to suppress the innate immune response in the primary cells whereas CedV was not. It has been hypothesized that the V and W proteins of NiV and HeV, which are interferon antagonists, are responsible for the severe pathology in humans and animal models. This seems supported by studies of V knockout NiV infection in hamsters and ferrets, which survived infection with the

mutant virus. However, the V protein is capable of suppressing the innate immune response of cells from black flying foxes, the natural reservoir that does not develop disease (Virtue et al., 2011). The ability of NiV and HeV to antagonize the interferon response in Jamaican fruit bat cells does not provide any indication as to whether Jamaican fruit bats would develop disease or not if infected with these viruses, and *in vivo* experiments should be performed to determine the nature of infection in this model. Such an experiment would provide more complete insight into the role that these New World bats might play in henipavirus ecology in the Americas. The ability of V and W to suppress the bat immune response also reveals that there is a different pathogenic determinant that is yet to be discovered, most likely a host factor that governs the response to infection which is different in flying foxes than in animal disease models. Is this difference that bats have more control mechanisms in place to prevent an overactivation of the immune response? Examination of the innate immune response to NiV and HeV in bats cells revealed a typical mammalian response, as have similar studies *in vivo* and *in vitro* (Chen et al., 2020; Virtue et al., 2011; Woon et al., 2020). Perhaps the viruses have different tissue tropism in bats? The few experimental infections of bats with henipaviruses have not reported nervous system or respiratory involvement, with virus primarily detected in kidneys and urine, whereas virus can be detected in the brain and/or central nervous system and lungs of all disease models. Careful study of bat reservoir models alongside disease models may reveal such differences.

The work here established that Jamaican fruit bats can be infected by CedV. However, with a sample size of three, this study is not enough to characterize Jamaican fruit bats a model for CedV infection. Additional studies with larger sample size and necropsy at earlier timepoints will be necessary to determine important infection characteristics such as tissue tropism, immune gene expression in target tissues, seroconversion timeline, transmissibility, and the influence of sex, reproductive status, and environmental factors.

The emergence of SARS-CoV-2 and resulting pandemic saw a shift in focus across the board of scientific research to address the public health crisis, and my dissertation work was not exempt. The alignment of ACE2 sequences from a multitude of species and known susceptibility of Syrian hamsters, a cricetid rodent, revealed that deer mice may be a potential animal model as well as a susceptible wildlife species in North America, and our lab had the resources to address this. The wide geographic spread, peridomestic lifestyle, frequent contact with field biologists, long domestic lifespans, and prior use as lab animals made deer mice a necessary and attractive subject for studying SARS-CoV-2. This work demonstrates that several species and subspecies of deer mice are competent hosts and models of SARS-CoV-2. The eastern deer mouse was capable of sustained natural transmission to naïve conspecifics through cohousing. The majority of infected deer mice did not exhibit clinical signs, though upper and lower respiratory tract pathology was frequently observed at early timepoints. The exception was the California deer mouse. Two infected California deer mice exhibited clinical signs, and one was euthanized for humane reasons. Histopathology revealed that these individuals had severe fatty liver, a condition that is easily induced in California deer mice by feeding a high fat diet (Krugner-Higby et al., 2011; Krugner-Higby et al., 2000; Krugner-Higby et al., 2006). While the small sample size of this study precludes any conclusions, it could be hypothesized that the comorbidity of fatty liver in California deer mice leads to more severe disease and fatality during SARS-CoV-2 infection. This model warrants further investigation, as fatty liver is known to be a risk factor in COVID19 severity, and a laboratory animal model would allow investigations into the treatment for such patients (Ji et al., 2020; Mushtaq et al., 2021).

The susceptibility of deer mice to SARS-CoV-2 is an important finding because a major concern in the COVID19 pandemic has been the potential for SARS-CoV-2 to spillback into wildlife and establish endemicity or acquire adaptations which lead to the emergence of new variants. The

emergence of variants has facilitated the prolonged pandemic, as new variants are often capable of some degree of immune escape.

The roles of animals outside of “human pathogen host” must be remembered and respected during research and surveillance efforts. Bats have been vilified as reservoirs of human pathogens, and as a result there have been attempts to exterminate bat populations in parts of the world. However, such efforts have resulted in the opposite of the desired effect: bats repopulate the targeted area and have higher viral prevalence than before (Amman et al., 2014). Another important consideration is how important bats are to the ecosystems they are a part of, providing many essential ecosystem services that benefit natural habitats as well as humans. Therefore, future surveillance and research efforts need to also have a focus on bat conservation by using available data and predictive modelling to selectively sample regions and species with a high probability of virus circulation and using non-invasive, minimal handling procedures to reduce the impact of research efforts on the bats (Becker et al., 2022; Giles et al., 2021a). Surveillance efforts should also include a strong emphasis on viral isolation from positive samples so that new potentially zoonotic viruses can be characterized in the laboratory using molecular, cellular, and animal modeling methods.

Appendix I: Supplementary Material

Supplementary Table 2.1. Summary of the individual level data provided in each study. A section is only marked "Y" if that information is available for all samples.

Study	Species	Date (year)	Date (month)	Location (country)	Location (specific)	Sample type	Age	Sex
Anthony 2013	Y	N	N	Y	Y	Y	N	N
Campos, unpublished	Y	Y	N	Y	Y	Y	N	N
Cibulski 2021	Y	Y	Y	Y	Y	Y	N	N
Cuevas-Romero 2021	Y	Y	N	Y	Y	Y	N	N
Darcissac 2021	Y	Y	N	Y	Y	Y	N	Y
De Souza 2021	Y	Y	Y	Y	Y	Y	N	Y
Drexler 2012	Y	Y	N	Y	N	N	N	N
Hagmaier 2007	Y	Y	N	Y	N	N	N	N
Hause 2021	Y	Y	Y	Y	Y	N	N	N
Larsen 2022	Y	Y	Y	Y	Y	Y	N	N
Lee 2021	Y	Y	N	Y	Y	Y	Y	Y
Loh, unpublished	Y	Y	N	Y	Y	Y	N	N
PREDICT, unpublished	Y	Y	Y	Y	Y	Y	N	N
Rasche, unpublished	Y	Y	N	Y	N	N	N	N
Schulz 2020	Y	Y	Y	Y	Y	Y	N	N
Wells 2022	Y	Y	N	Y	N	Y	N	N
Wray 2016	Y	Y	Y	Y	Y	Y	N	N
Summary	17/17	16/17	7/10	17/17	13/17	13/17	1/17	3/17

Supplementary Table 2.2. P-values of chi-square test comparing prevalence of PMVs in New World bats by diet type. Values were calculated in R using the prop.test function to calculate chi-square and p-value for prevalence.

	Frugivorous	Insectivorous	Nectarivorous
Haematophagus	2.20E-16	2.20E-16	1.03E-08
Frugivorous		1.73E-05	0.5858
Insectivorous			0.09205

Supplementary Table 2.3. P-values of chi-square test comparing prevalence of PMVs in New World bats by family. Values were calculated in R using the prop.test function to calculate chi-square and p-value for prevalence.

	Mormoopidae	Phyllostomidae	Vespertillionidae
Molossidae	0.686	0.003748	0.07188
Mormoopidae		0.00439	0.04687
Phyllostomidae			0.6481

Supplementary Table 3.1. Primer and probe sequences used in RT-qPCR for detection and quantification of CedV/CedPV, NiV, and HeV RNA. Primers are listed 5' to 3'.

Virus	Forward Primer	Reverse Primer	Probe
CedPV /CedV	TGCATTGAGCGAA CCCATATAC	GCACGCTTCTTGACA GAGTTGT	/56-FAM/TCCCGAGAA/ZEN/ACCC TCTGTGTTTGA/3IABkFQ/
NiV	GTACTCAACCATG AATGAACAGTTG	CTTTAAAGGACACAG TTTAATATCCAATG	/56-FAM/CTTAGGACC/ZEN/CAGG TCCATAA/3IABkFQ/
HeV	CTTCGACAAAGAC GGAACCAA	CCAGCTCGTCGGACA AAATT	/56-FAM/TGGCATCTT/ZEN/TCATG CTCCATCTCGG/3IABkFQ/

Supplementary Table 3.2. Primer sequences used in qPCR arrays for NiV-HeV-CedPV qPCR arrays. Primers are listed 5' to 3'.

Primer	Sequence
CARD9 F'	AAG GAG CAC CTC TCA CTG ACC C
CARD9 R'	CCG CTT CCT GCG GTA GTT CTC
CASP1 F'	CAC GTC TTG CCC TCA TTA TCT
CASP1 R'	CTT CTA GCA GCT TCT CCA TAC C
CASP10 F'	CCT TAC CGG AGA AAG CTG TGT AT
CASP10 R'	TTG GGT CCC TCG TCT TTC TTT C

CASP8 F'	CAA GGA GAT CGC CAA ATG TAA AC
CASP8 R'	GGA CCC TCT TCT CCA TCT CTA T
CCL5 F'	CGC CAT ATG CCT CCG ACA CC
CCL5 R'	CAC ACC TGG CGC TTC TTT CGG
CXCL10 F'	ACG CTG TAC CTG CAT CAG TAT TA
CXCL10 R'	TCT TGT CCA CGT GTT GAG ATC A
CYLD F'	CTG CCA GAA GAT GGA GCT CTT
CYLD R'	GGA GTC GTC TTT GCC GTA CTT
DDX58 F'	GAA CCC ACG GAG ACA ACA AGA
DDX58 R'	CTG CCT CTG GTC TGG ATC ATT T
DHX58 F'	ATT CAC CTG CGA CGC TAC AA
DHX58 R'	GCA CGC TCC CTC TCA TAG AAA T
EPHRIN B2 F'	TTG AGC AGG TGA TTG GAG CA
EPHRIN B2 R'	CTT CTC GGT GTA GCC CGA TTT
EPHRIN B3 F'	ACG GAG AAG CTG CAG CAA TA
EPHRIN B3 R'	TCG ATC TCC TTG GCA AAC TCC
GAPDH F'	GAA GGT AGT GAA GCA GGC ATC T
GAPDH R'	GAG GAG TGG GTG TCA CTG TTA AA
HERC5 F'	AAG GAT GGG CTC CTG TTT ACA T
HERC5 R'	CCA ACA AGC TCA GTC ACC AAA C
IFIT1 F'	CAT CCT TGG GTT CGT CTA CAA
IFIT1 R'	CTA AGG AAC ACA TCC CAC AGA G
IFIT2 F'	GGA AAG AGA GGA GTT GCA GGA A
IFIT2 R'	TGC ATA GAG GCA GGC AAG ATA G
IFIT3 F'	ACA GGT GTG CGA GAA GTA TTC C
IFIT3 R'	GCC CTT TCA TTT CGC TTT CCT C
IFIT5 F'	CCA CTA CCA CTA TGG CCG TTT
IFIT5 R'	GGG ATG ACC TGT CTT TGA CCT T
IFNa F'	CCA GTT CCA GAA GGC TCA A
IFNa R'	CTT GTC CCA AGC AGC AAA G
IFNb F'	CAG CCT CTT GGA CTC TCA TAA A
IFNb R'	GAG CAT CTC ATG GAT GAC CAA TA
IFNL3 F'	GAA GCC TCT GTG ACA TTC AAC CT
IFNL3 R'	TCA GAC ACA CAG GTC TCC ACT
IL15 F'	CTG AAT CTG GCT GCA AAG AAT G
IL15 R'	TGG CGT GTT GAT GAA CAT TTG
IL15Ra F'	GAA CTC CAG GGA ACG GTA TAT TT
IL15Ra R'	TGT CCA CTG GGT AAT GTT TGT
IL18 F'	GAT GCT GAC TGC GAA GGT AAT G
IL18 R'	ACA GAG ATT GTT ACT GCC ATG C
IL1a F'	GTG AGT GCC CAA AGT GAA GA

IL1a R'	TGC CAT GAT GTT CCC AGA AG
IL1b F'	CAT TGT CTG CTC ACA GGA CTT
IL1b R'	AAG TGT CAT CCC ACA TGC TAT C
IL6 F'	CAC TCA CCT CTC CAG ACC AAA T
IL6 R'	TCT CGT GGT TGT CAC ACA TCT T
IRF1 F'	CAC CAG TGA CCT GTA CAA CTT
IRF1 R'	GTA ATT TCC CTT CCT CGT CCT C
IRF3 F'	CAG GAG GAC TTT GGC ATC TT
IRF3 R'	AGA CCT GAA ATT CCG CTT CC
IRF7 F'	AGA AGC AGC TGC AGT ACA C
IRF7 R'	CAC CTC CCA GTA GAC CTT ACA
IRF9 F'	GCT GAG CCC TAC AAG GTG TAT C
IRF9R'	CAC AGA GCT GTG GTG TCT CTT T
ISG20 F'	CCT GAA AGG CAA GCT GGT
ISG20 R'	GCT GTA GTT GCT CAT GTT CTC T
MAVS F'	GCC TTA CTT GTC TTG CCT CA
MAVS R'	GCT GTT GAA GAG TTC CCA GAT A
MX2 F'	GGT GGA GAG GGA AAT CAA CAA
MX2 R'	TGA TGC CGG GAA GAT CAA TAA G
NOD2 F'	CCA GGA GTT TCT CTT CGT CTT C
NOD2 R'	GCC AAC AGC AGT GTT CAA AG
PKR F'	GAT TGG AGA CTT TGG ACT TGT AAC
PKR R'	GAT CTG TTC TGG GCT CAT GTA
PYCARD F'	GAA GCT GCT CAA CTC GGG GG
PYCARD R'	ACG CAC TCG AAG GTG TTG GG
STAT1 F'	ATG CCG GCA ACA GAA CCA ACG
STAT1 R'	ACC AGG CTG GCA TAA CTG GGT
STAT2 F'	CAT ACT AGG TGT GGT GCA AGA G
STAT2 R'	CTG GTG CCG ACT GTG AAA TA
TBK1 F'	GGG ATG CGA TGG TTG ATA GAA
TBK1 R'	TCT GAG GCA GAA ATC CAA TGT
TLR7 F'	TCC CTT TAC CTG GAT GGA AAT C
TLR7 R'	GTT GAG GGA GAA GAT GCT GTT A
TNF F'	CAG CTG CAG TGG AAG AAT CA
TNF R'	GAC CTG GGA GTA GAT GAG GTA TAG
TRIM25 F'	CAG CAA GTT CGA CAC CAT TTA C
TRIM25 R'	CAG GGC AAG TTC AAT CTC CT
TRIM5 F'	GAG AGA AAC TCC TGC TCT TCT G
TRIM5 R'	CCT GGA GTT TCT CCT TGT ACT C
ZC3HAV1 F'	CTC AGC GCC TGG AGT TCA T
ZC3HAV1 R'	TCT CGC AGG TAG TGA TAG TCC TT

Supplementary Table 5.1. Primers used for SYBR Green qPCR gene expression profiling. Primers used for the amplification of deer mouse genes for the PCR expression array. Each primer is listed 5' to 3'.

Gene	Forward	Reverse
Gapdh	GGTGCCAAAAGGGTCATCATCTC	GCAGGAAGCGTTGCTGATAATCTTG
Foxp3	AAGCAGATCACCTCCTGGATGAG	TAGCACCCAGCTTCTCCTTTTCC
Gata3	AGTCCGCATCTCTTCACCTTCC	GGCACTCTTTCTCATCTTGCCG
Tbx21	GCCAACCCAAGGATATGGT	GAATGTGGGCTTCATGCTC
CD4	GGTTGAAATGAAGGACCCTGAGG	CCTCTGGATGAAACCTGGATTTTGG
CD8a	AAGAAGAGCGGATTGGACTTCG	AGATGAGAGTGATGACCAGGGACAG
TCRb	CAATAACATCACCTACTGCCTGAGC	GTAAGCCCATAGAACTGGACTTGG
TGFb	CGTGGAACTCTACCAGAAATACAGC	TCAAAAGACAACCACTCAGGCG
Ifng	GGCTATTTCTGGCTGTTACTGCC	ATCCCCGACATCTGAGCTACTTG
Il4	CCCCGTGCTTGAAGAACAATTC	GGACTCATTCCCAGTACAGCTTTTC
Il4ra	AGAACCCTGTTCCCAACCA	TTGGATGGCAACTCCATGT
Il13	TGCAAACCCATCTACAAGACCC	GCCACTTCGATTTTGGTATCCG
Il13ra1	TGGTGTTCTTCCTGATGCTG	AGCGCTTCGCTCCAATTA
IL21	AACTCAAGCCAGCAAACACAGG	GCTGCTTTTTCTCAGCCTTGG
IL23	AGAAATGATGTCCCCCGTATCC	CAGACCTTGGTGGATTCTTTGC
Il2ra	TGCCACATTCAAAGCCCT	CCAACTCCTTTGTTCTTCGG
Socs1	TGAGATCGCGAAGAACCTG	GGAAGGGGAAGGAACTTCA
Socs5	CGGTTTGGGGACCATTTTA	TCAATCCCCGTTCTGCAT
Tnf	TGTAGCCCACGTTGTAGCAAACC	CTGGTTGTCTTTGAGATCCATGC
Zeb1	CCCAACAAACAGCTGCAA	ATCCACAGCCCCATCAAA
CD80	CATTGTGTGTCGCGTTGTGT	TGTCGGGGTCACCTCAGTTA
CD86	CTTACCTTGCCAGCTCTGCT	TGCCCTAGACCTGAGTGTGA
Ctla4	CTTGTCTTGGAGTCCCGAGG	ATGGCTTTGGAGAAGGTCGG
Ccl2	CAGACGTACACAAGAAAACTGGACC	GTCAAGTTCGCATTCAAAGGTGC
Ccl3	AGCCAGGTGTCATTTTCCTAACC	CAGCTCAGTGATGTATTCTTGGACC
Ccl5	CCACGTCAAGGAGTATTTCTACACC	TCCTGAACCCACTTCTTCTTTGG
Cxcl10	CACTGTCAGCACCATGAACC	GGGATTCCTTGAGTCCCACT
IFNg	GGCTATTTCTGGCTGTTACTGCC	ATCCCCGACATCTGAGCTACTTG
TGFb	CGTGGAACTCTACCAGAAATACAGC	TCAAAAGACAACCACTCAGGCG
Il10	TAAGGGTTACCTGGGTTGCCAAG	CAAATGCTCCTTGATTTCTGGGC
Il12a	TCCAAAAACCTGCTGAGGACCAC	AATCAACGTCTTCAGGAGTGCAG
Il12b	TGTTCTCATGGGCTGATCC	GGCAGCCTTGGTTGAAAA
Il6	CCATCCAACTCATCCTGAAAGC	CCACAGATTGGTACACATAGGCAC
Ifna2	ACTCATCTGCTGCTTGGGA	TTGCAGGTCTTTGAGCTGG
Ifnb1	TGCCTTCGTCATCCAAGAG	TCTCATTCCACCCAGTGCT

Irf3	TAGAAAAGGAAGCCCCAGC	TGGTGCCAACACTGGTTTC
Isg15	AGAGTTCCTGGTGTCCCTGA	ACACCAGTCTTCTGGGCAAT
Mavs	GCAACTAGGGAACCAGGACA	AAGCACTGTACCCAGCCAAC
Tbk1	TCTCGAATAGCCAGCACCTT	CTCACCAGCTCAATCAACCA
TLR7	CCTGGTTGCCTGAATCTTTC	TGAGCAATGGCAGCTGTTAG
Oas2	TGGACGAGTTCGACATTGC	AAGATGCAGAGCTGCTGGT
Pycard	ACCAGCACAGACAAGCACTG	GTCAGCACACTGCCAAACAG

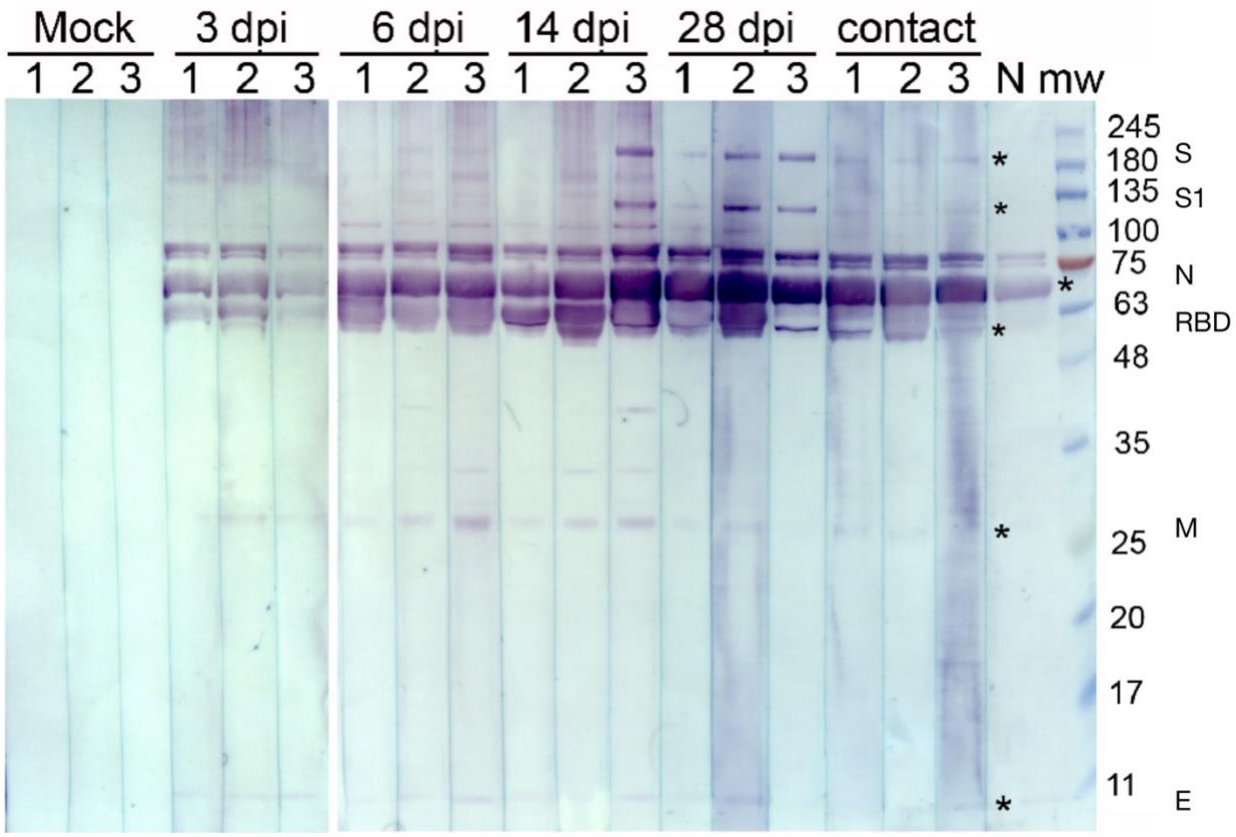

Supplementary Figure 5.1. Serum response to SARS-CoV-2 structural proteins by infected deer mice. Protein from virus-enriched supernatants from SARS-CoV-2-infected Vero E6 cells, 8 µg protein per lane, were separated by SDS gel electrophoresis, and individual lanes from western blots were probed with 1:100 dilutions of sera from groups of three mock and infected deer mouse sera at times post infection as indicated and from contact controls at 28 dpi post exposure to infected animals. Prepared monoclonal antibody to the nucleocapsid protein served as control (N). Asterisks indicate predicted and known positions of structural proteins based on molecular weight: spike protein (S), cleaved spike 1 (S1), nucleocapsid (N), cleaved receptor binding domain (RBD), membrane (M), and envelope (E).

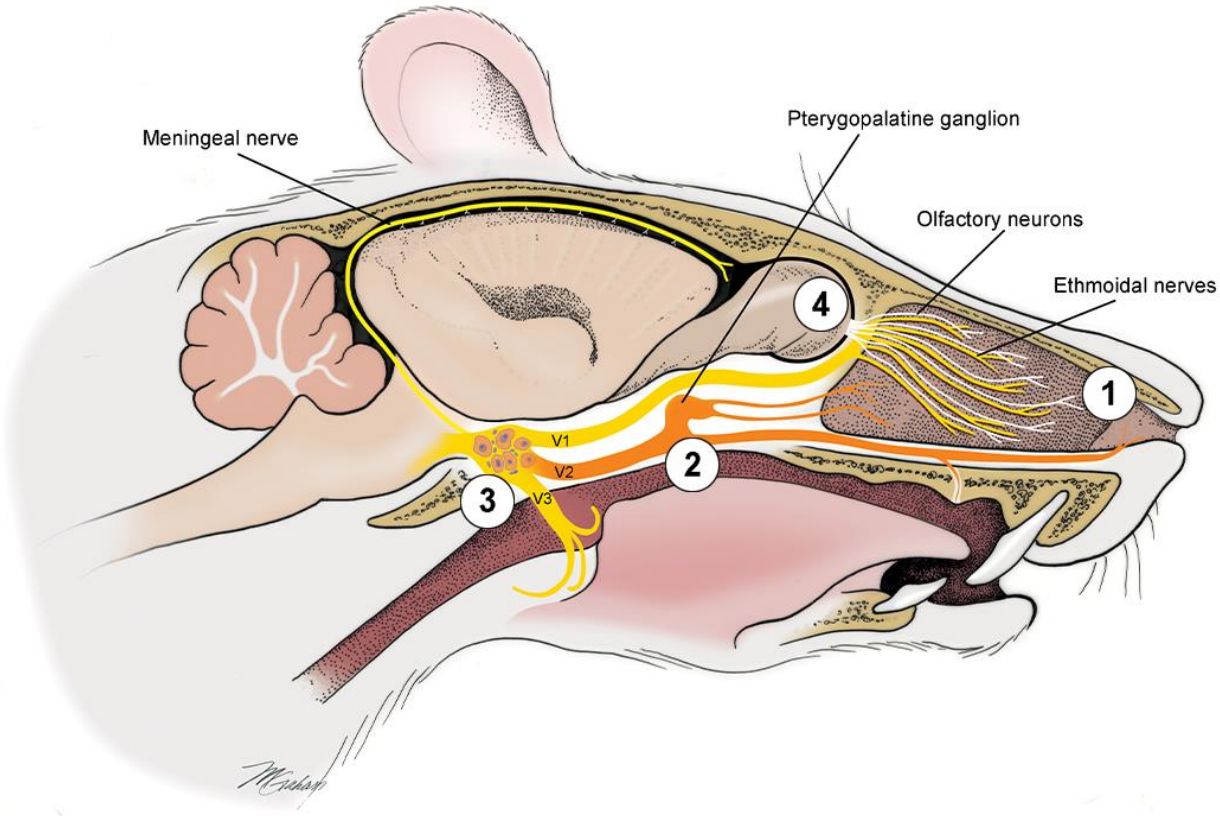

Supplementary Figure 5.2. Mouse olfactory (1, 4) and trigeminal pathways (2,3). The three major sensory branches of trigeminal nerve: ophthalmic (V1), maxillary, mainly formed by union between posterior nasal and rhinopalatine nerves (V2) and thickest branch, mandibular nerve (V3). Viral spread occurs via sympathetic and/or parasympathetic fibers into corresponding pterygopalatine and trigeminal ganglia (2 and 3, respectively). SARS-CoV-2 dissemination may be facilitated by transmission of disrupted olfactory epithelium and the olfactory neurons (1) to finally infect the main olfactory bulb (4) at 6 dpi as detailed below. Meningeal nerve was also inflamed at that time (Veronesi et al., 2020).

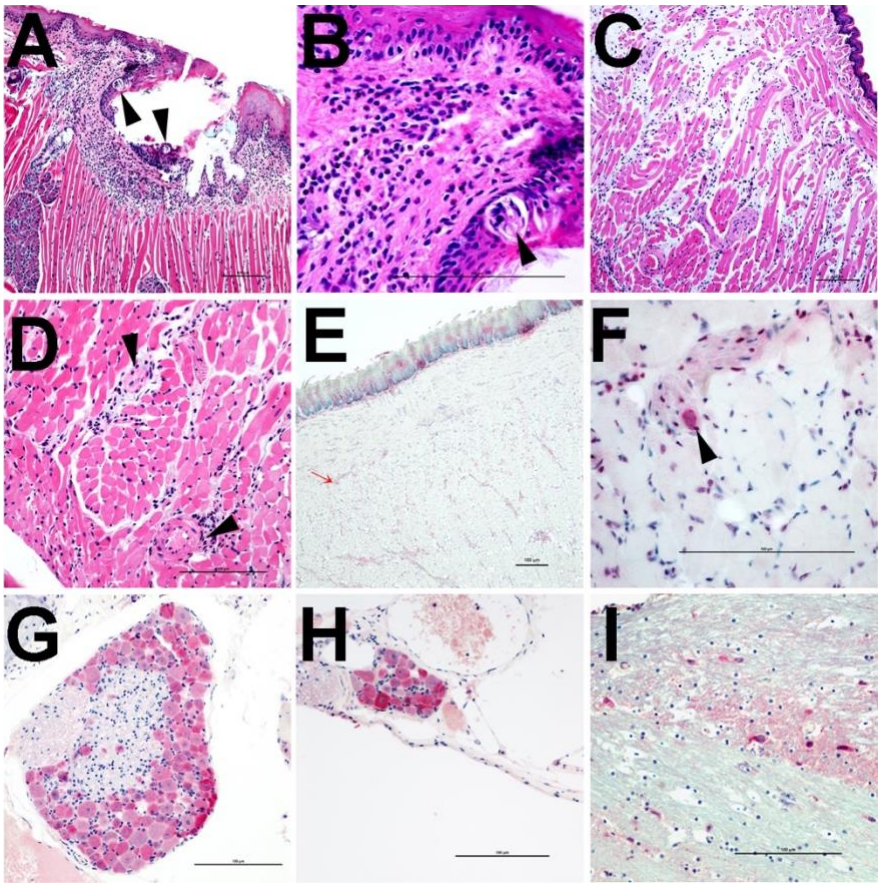

Supplementary Figure 5.3. Necrosis of circumvallate and foliate papillae at posterior tongue, 3 dpi (A) with close-up view of neutrophils clustering around a taste bud (arrowheads) (B). Dissecting edema dispersing lingual skeletal muscles apart, 3 dpi (C). Interstitial suppurative glossitis extending into branches of chorda tympani nerve (arrowhead) at anterior tongue, 3 dpi (D). Multifocal viral immunostaining is showing lingual mucosa and submucosa with occasional immunoreactivity in a hypertrophied neuronal cell body in one of chorda tympani nerve branches, 6 dpi (E). Close-up view of the hypertrophied neuron in lingual parenchyma (F, arrowhead). Geniculate nucleus in tympanic bulla showing strong immunoreactivity in ganglionic neurons (cell bodies) of greater superficial petrosal and chorda tympani nerve fibers, 6 dpi (control negative inset). Petrosal ganglion with attached CN IX shows strong immunoreactivity in corresponding ganglionic neurons 6 dpi. Strong immunoreactivity is seen in scattered neurons and glial cells mainly microglia in the area of the nucleus of the solitary tract (NST) (I). Bars = 100 µm.

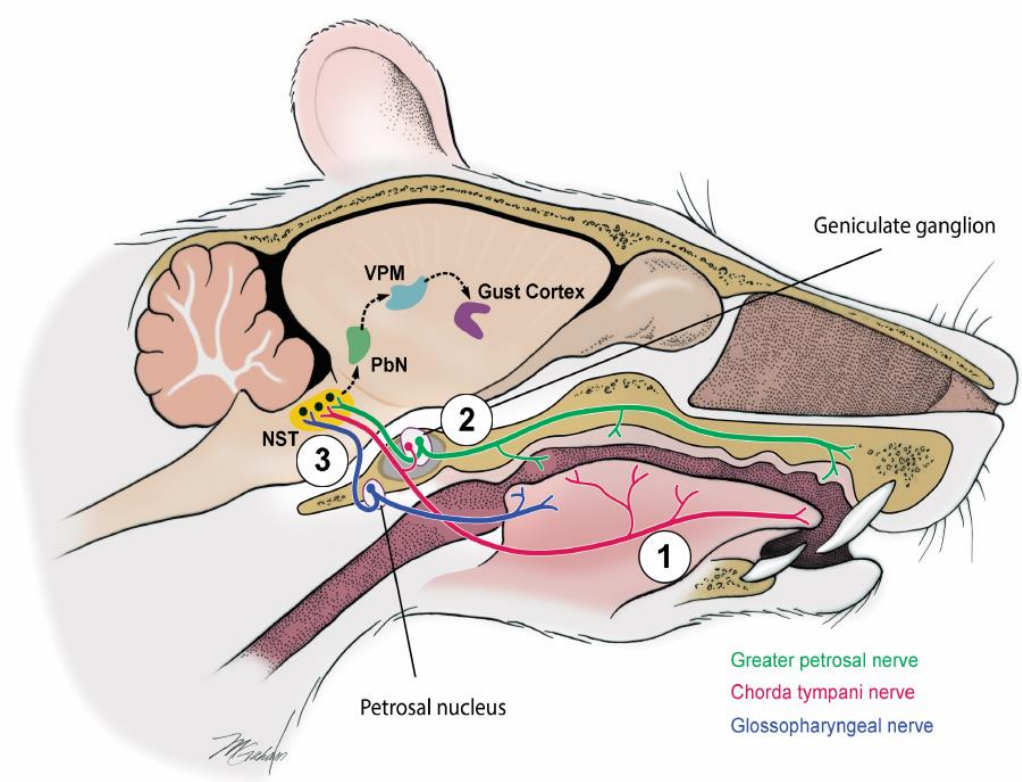

Supplementary Figure 5.4. Schematic illustration depicting gustatory nerves carrying taste information from the soft palate and tongue to brain stem of the deer mouse. Chorda tympani nerve on anterior tongue (red) (1) along with greater superficial petrosal nerve (green) (2) located on the soft palate conduct taste information from taste buds to cell bodies in the geniculate ganglion located within tympanic bulla. The glossopharyngeal nerve (CN IX, blue) conducts taste information from the circumvallate and posterior foliate papillae on posterior tongue to petrosal ganglion on the medial aspect of tympanic bulla. Information from taste ganglia is then transmitted into the nucleus tractus solitarius (NTS) (3) in medulla oblongata. In the medulla, taste responses are processed and then carried through parabrachial nucleus (PbN) and thalamic ventral posteromedial nucleus (VPM) to the primary gustatory nucleus in the insula. Perception of flavors is integrated with other avenues of sensation, particularly olfaction (8, 9). Temporary to persistent loss of taste is the one of the most consistent and common clinical symptoms reported in patients suffering from the mild form of COVID-19 (10). Pathologies of different components of the mouse gustatory system are following in Fig. S3A-I.

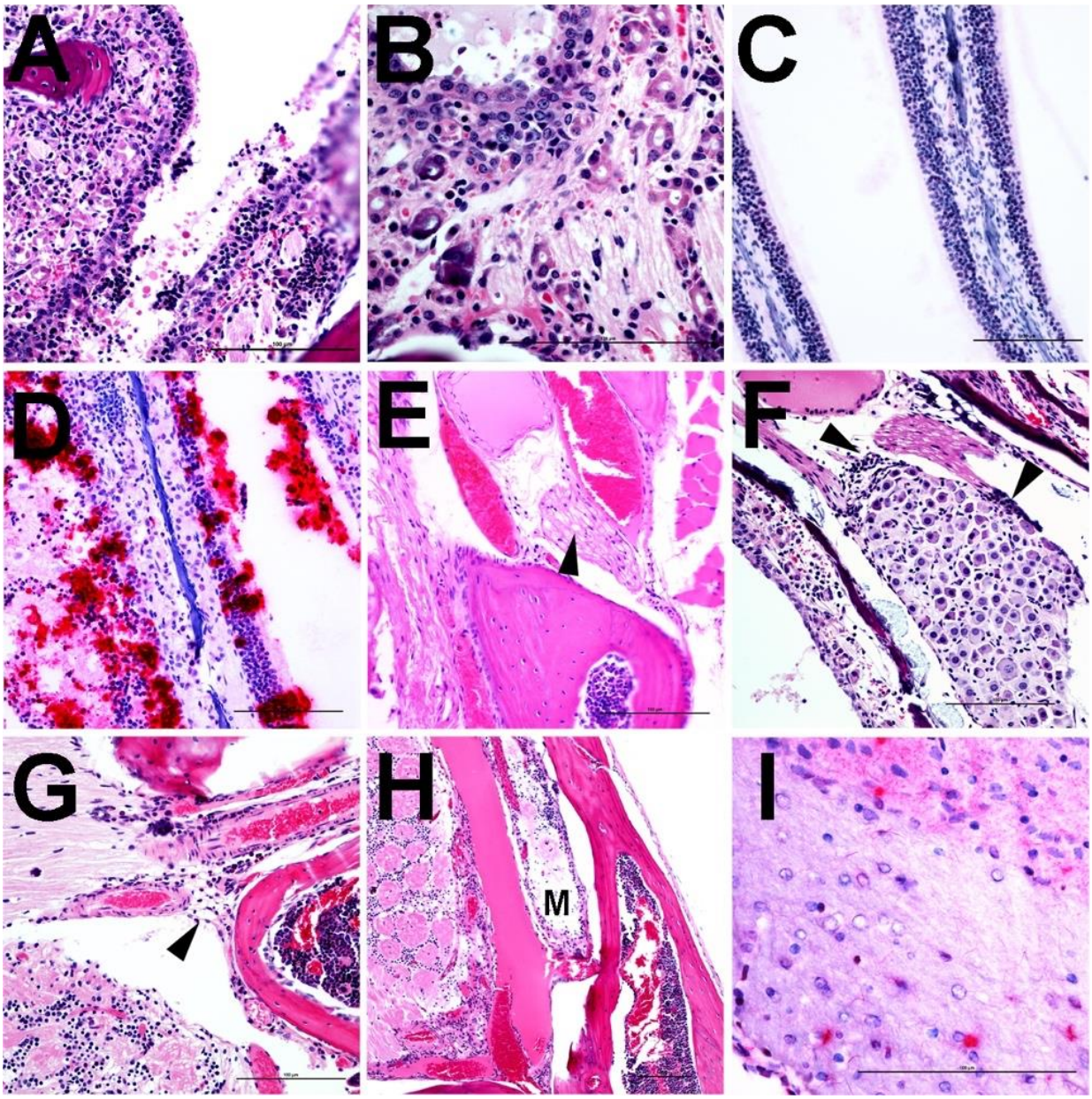

Supplementary Figure 5.5. Massive necrosis and ulceration of MOE with expansion of submucosa by fibrinosuppurative exudate, 3 dpi (A). Close-up of embedded nerve branches, which appear rarefied by extensive status spongiosus and minimal infiltration of neutrophils, 3 dpi (B). Maxillary sinuses from a control deer mouse show intact lining epithelium with no immunoreactivity (C), 3 dpi. Marked immunoreactivity is seen in lining and detached MOE, 3 dpi (D). Branches of facial nerve show moderate axonopathy (E, arrowhead). Pterygopalatine ganglion is multifocally cuffed by neutrophils with variable degeneration of the constituent neurons, 3 dpi (F). Ethmoidal nerves percolating cribriform plate showing multifocal suppurative neuritis and perineuritis (G, arrowhead). Severe congestion of meningeal vessels and rarefaction of meningeal nerve with histioneutrophilic perineuritis/meningitis , 3 dpi (H). Optic chiasm and hypothalamus show multifocal neuronal immunoreactivity, 6 dpi (I). Bars = 100 µm.

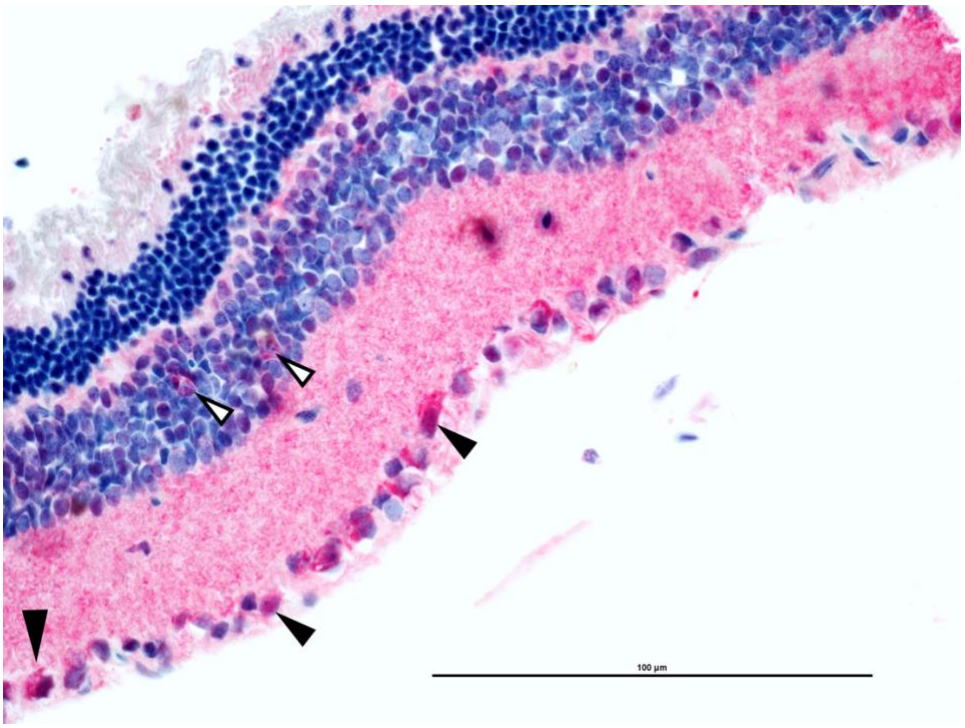

Supplementary Figure 5.6. Retinal ganglionic cell bodies show multifocal immunoreactivity extending into inner plexiform layer (black arrowheads) and scattered bipolar cells in the inner nuclear layer (white arrowheads), 3 dpi. Bar = 100 µm.

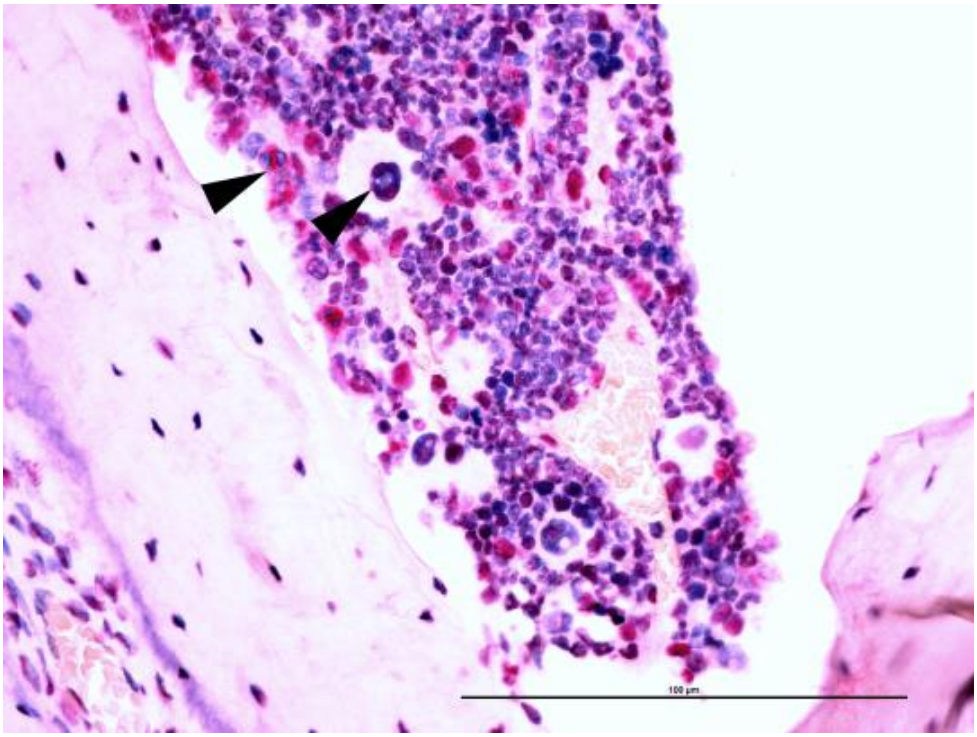

Supplementary Figure 5.7. Calvarium bone marrow show strong cytoplasmic immunoreactivity in myeloid precursors, including monocytes (upper arrowhead) and megakaryocytes (lower arrowhead), 6 dpi. Bar = 100 µm.

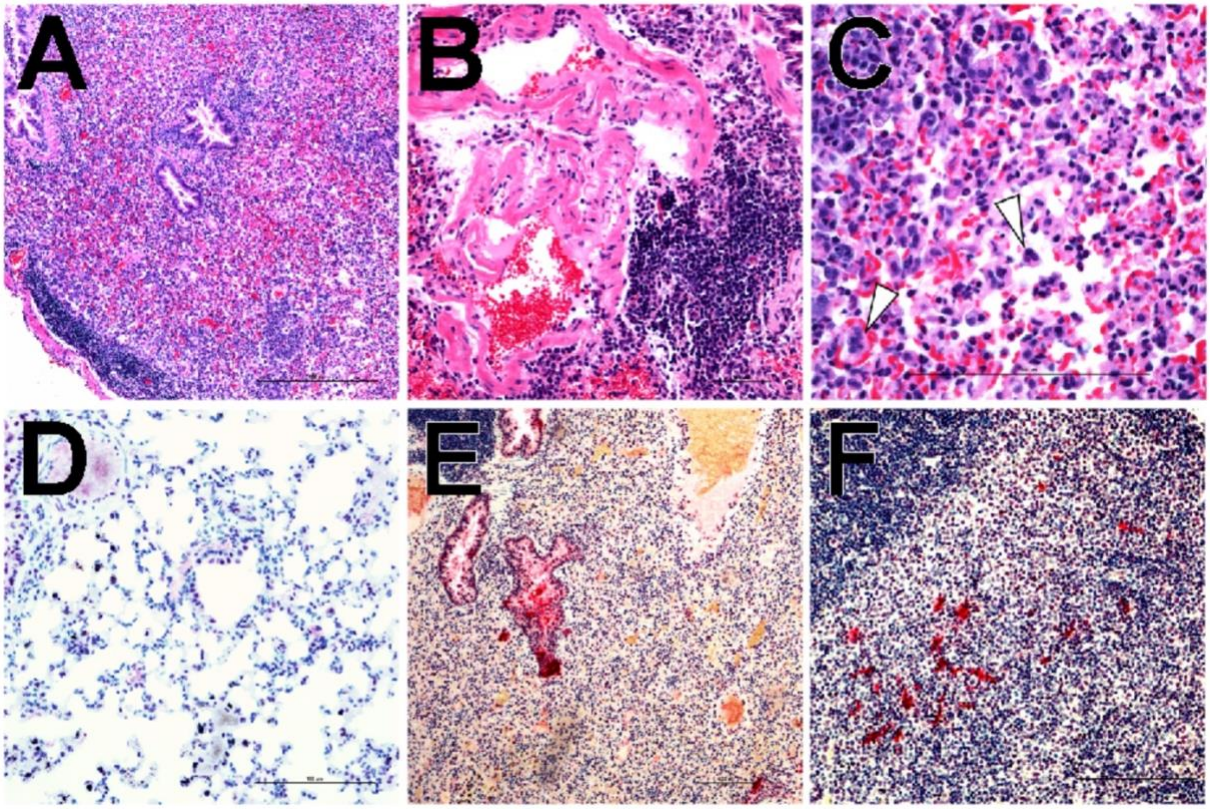

Supplementary Figure 5.8. Grossly consolidated lung portions show massive infiltration of pulmonary parenchyma by numerous neutrophils and macrophages with peribronchiolar lymphoid hyperplasia (A). Main branches of pulmonary artery are infiltrated by neutrophils and cuffed by lymphoid follicles (B). Syncytial and histiocytic giant cells are dispersed among inflammatory cells expanding pulmonary interstitium and filling alveolar spaces (C). Lungs from a control mouse is within normal histologic limits with no immunoreactivity (D). Multifocal prominent bronchiolar and milder parenchymal immunostaining is seen in lungs 3 and 6 dpi (E). Mononuclear cells, macrophages, and antigen-presenting cells showing scattered cellular immunostaining in the paracortex (T-zone) area, 3 and 6 dpi (F). Bars = 100 μm.

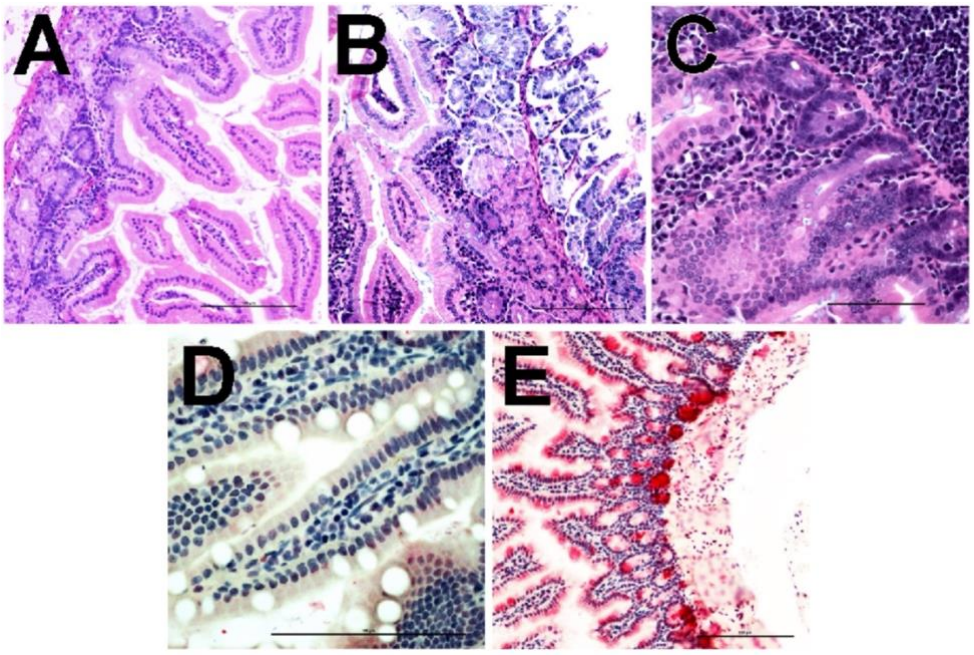

Supplementary Figure 5.9. Duodenum at 3 dpi shows mild focal histioneutrophilic duodenitis (A). Duodenum and ileum show moderate histioneutrophilic and lymphoplasmacytic enteritis (B and C). Small intestine from negative control deer mouse shows minimal nonspecific staining in goblet cells lining intestinal villi (D). Small intestine at 3 dpi shows marked immunoreactivity in the cytoplasm and apical border of mature enterocytes, crypt cells and scattered submucosal mononuclear cells consistent with macrophages (E). Bars = 100 µm.

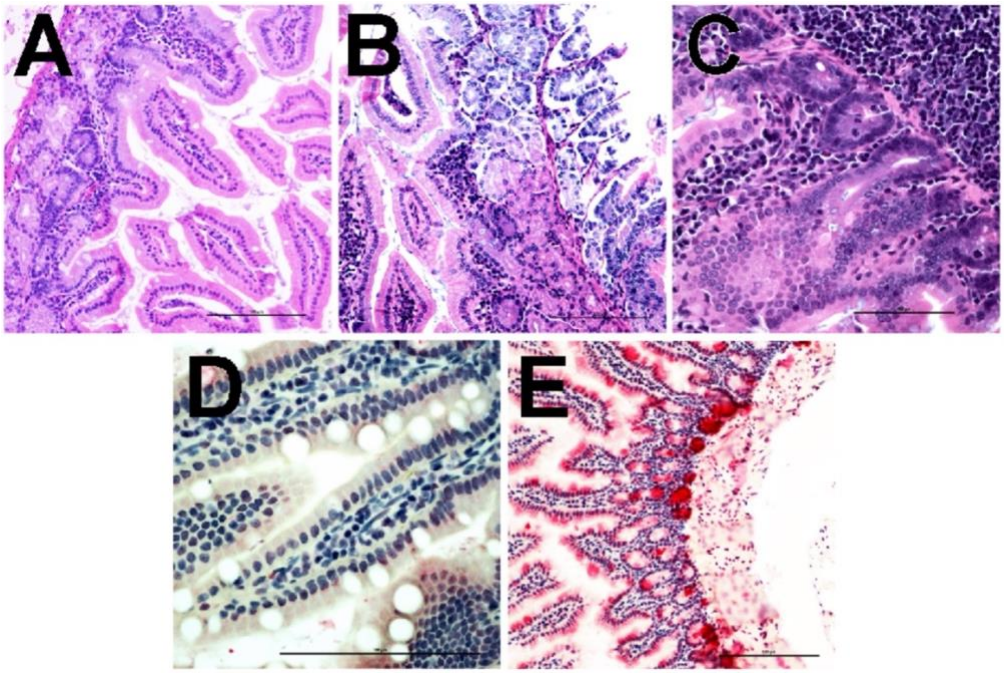

Supplementary Figure 5.10. Heart at 6 dpi, left subvalvular endocardium and myocardium shows minimal lymphocytic interstitial myocarditis (A) and more significant atrial suppurative perivascular myocarditis in right atrium (B). Kidney hilus shows mild perivascular suppurative inflammation that encircles small branches of renal nerves (C). Bars = 100 µm.

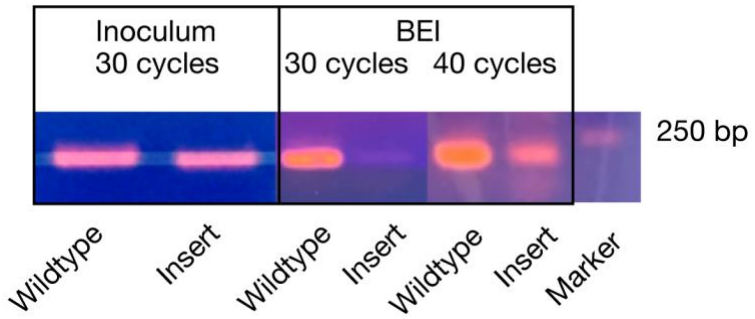

Supplementary Figure 5.11. Detection of spike protein insert sequence by PCR. Forward primers were designed to amplify the wildtype or insert spike sequences. WT and insert were detected in both the deer mouse inoculum virus (Vero E6 passage 2) and original sourced BEI Resources virus. The BEI Resources virus had low amplification at 30 cycles that became greater at 40 cycles.

Supplementary Table 6.1. P-values of multiple unpaired T-tests performed between species groups. Group notation is as follows: P. m. bairdii (A), P. m. sonoriensis (B), P. polionotus (C), P. californicus (D). Comparisons with $P<0.05$ were considered significant.

day post-challenge	A vs B	A vs C	A vs D	B vs C	B vs D	C vs D
3	0.128	0.509	0.004	0.101	0.027	0.010
6	0.068	0.610	0.016	0.023	0.393	0.005
10	0.179	0.884	0.871	0.029	0.089	0.694
15	0.124	0.857	0.744	0.034	0.043	0.703

References

(2020). COVID-19 and Animals (Centers for Disease Control and Prevention).
Adler, S. (1948). Origin of the golden hamster Cricetus auratus as a laboratory animal. Nature *162*, 256.
Adney, D.R., van Doremalen, N., Brown, V.R., Bushmaker, T., Scott, D., de Wit, E., Bowen, R.A., and Munster, V.J. (2014). Replication and shedding of MERS-CoV in upper respiratory tract of inoculated dromedary camels. Emerg Infect Dis *20*, 1999-2005.
Aguilar Pierlé, S., Zamora, G., Ossa, G., Gaggero, A., and Barriga, G.P. (2022). The Myotis chiloensis Guano Virome: Viral Nucleic Acid Enrichments for High-Resolution Virome Elucidation and Full Alphacoronavirus Genome Assembly. Viruses *14*.
Alves, D.M.C.C., Diniz-Filho, J.A.F., da Silva e Souza, K., Gouveia, S.F., and Villalobos, F. (2018). Geographic variation in the relationship between large-scale environmental determinants and bat species richness. Basic and Applied Ecology *27*, 1-8.
Ambat, A.S., Zubair, S.M., Prasad, N., Pundir, P., Rajwar, E., Patil, D.S., and Mangad, P. (2019). Nipah virus: A review on epidemiological characteristics and outbreaks to inform public health decision making. Journal of Infection and Public Health *12*, 634-639.
Amman, B.R., Carroll, S.A., Reed, Z.D., Sealy, T.K., Balinandi, S., Swanepoel, R., Kemp, A., Erickson, B.R., Comer, J.A., Campbell, S.*, et al.* (2012). Seasonal pulses of Marburg virus circulation in juvenile Rousettus aegyptiacus bats coincide with periods of increased risk of human infection. PLoS Pathog *8*, e1002877.
Amman, B.R., Nyakarahuka, L., McElroy, A.K., Dodd, K.A., Sealy, T.K., Schuh, A.J., Shoemaker, T.R., Balinandi, S., Atimnedi, P., Kaboyo, W.*, et al.* (2014). Marburgvirus resurgence in Kitaka Mine bat population after extermination attempts, Uganda. Emerg Infect Dis *20*, 1761-1764.
Baker, M.L., Tachedjian, M., and Wang, L.F. (2010). Immunoglobulin heavy chain diversity in Pteropid bats: evidence for a diverse and highly specific antigen binding repertoire. Immunogenetics *62*, 173-184.
Banerjee, A., Rapin, N., Bollinger, T., and Misra, V. (2017). Lack of inflammatory gene expression in bats: a unique role for a transcription repressor. Sci Rep *7*, 2232.
Bao, L., Deng, W., Huang, B., Gao, H., Liu, J., Ren, L., Wei, Q., Yu, P., Xu, Y., Qi, F.*, et al.* (2020a). The pathogenicity of SARS-CoV-2 in hACE2 transgenic mice. Nature *583*, 830-833.
Bao, L., Deng, W., Huang, B., Gao, H., Liu, J., Ren, L., Wei, Q., Yu, P., Xu, Y., Qi, F.*, et al.* (2020b). The pathogenicity of SARS-CoV-2 in hACE2 transgenic mice. Nature.
Bao, L., Song, Z., Xue, J., Gao, H., Liu, J., Wang, J., Guo, Q., Zhao, B., Qu, Y., Qi, F.*, et al.* (2021). Susceptibility and Attenuated Transmissibility of SARS-CoV-2 in Domestic Cats. J Infect Dis *223*, 1313-1321.
Barbour, A.G. (2017). Infection resistance and tolerance in Peromyscus spp., natural reservoirs of microbes that are virulent for humans. Semin Cell Dev Biol *61*, 115-122.
Barrantes Murillo, D.F., Piche-Ovares, M., Gamboa-Solano, J.C., Romero, L.M., Soto-Garita, C., Alfaro-Alarcón, A., and Corrales-Aguilar, E. (2022). Serological Positivity against Selected Flaviviruses and Alphaviruses in Free-Ranging Bats and Birds from Costa Rica Evidence Exposure to Arboviruses Seldom Reported Locally in Humans. Viruses *14*.
Becker, D.J., Albery, G.F., Sjodin, A.R., Poisot, T., Bergner, L.M., Chen, B., Cohen, L.E., Dallas, T.A., Eskew, E.A., Fagre, A.C.*, et al.* (2022). Optimising predictive models to prioritise viral discovery in zoonotic reservoirs. The Lancet Microbe *3*, e625-e637.
Bedford, N.L., and Hoekstra, H.E. (2015). Peromyscus mice as a model for studying natural variation. Elife *4*.

Berl, J.L., Flaherty, E.A., Danielson, B.J., Kellner, K.F., and Swihart, R.K. (2017). Winter ecology of prairie deer mice (Peromyscus maniculatus bairdii) in cultivated habitats: Implications for agricultural ecosystem services. Agriculture, Ecosystems & Environment *249*, 130-136.
Beyer, R.M., Manica, A., and Mora, C. (2021). Shifts in global bat diversity suggest a possible role of climate change in the emergence of SARS-CoV-1 and SARS-CoV-2. Science of The Total Environment *767*, 145413.
Biadsee, A., Biadsee, A., Kassem, F., Dagan, O., Masarwa, S., and Ormianer, Z. (2020). Olfactory and Oral Manifestations of COVID-19: Sex-Related Symptoms-A Potential Pathway to Early Diagnosis. Otolaryngol Head Neck Surg, 194599820934380.
Bolatti, E.M., Zorec, T.M., Montani, M.E., Hošnjak, L., Chouhy, D., Viarengo, G., Casal, P.E., Barquez, R.M., Poljak, M., and Giri, A.A. (2020). A Preliminary Study of the Virome of the South American Free-Tailed Bats (Tadarida brasiliensis) and Identification of Two Novel Mammalian Viruses. Viruses *12*.
Bonaparte, M.I., Dimitrov, A.S., Bossart, K.N., Crameri, G., Mungall, B.A., Bishop, K.A., Choudhry, V., Dimitrov, D.S., Wang, L.F., Eaton, B.T.*, et al.* (2005). Ephrin-B2 ligand is a functional receptor for Hendra virus and Nipah virus. Proc Natl Acad Sci U S A *102*, 10652-10657.
Boni, M.F., Lemey, P., Jiang, X., Lam, T.T., Perry, B.W., Castoe, T.A., Rambaut, A., and Robertson, D.L. (2020). Evolutionary origins of the SARS-CoV-2 sarbecovirus lineage responsible for the COVID-19 pandemic. Nat Microbiol.
Bosco-Lauth, A.M., Hartwig, A.E., Porter, S.M., Gordy, P.W., Nehring, M., Byas, A.D., VandeWoude, S., Ragan, I.K., Maison, R.M., and Bowen, R.A. (2020). Experimental infection of domestic dogs and cats with SARS-CoV-2: Pathogenesis, transmission, and response to reexposure in cats. Proc Natl Acad Sci U S A *117*, 26382-26388.
Bosler, E.M., Ormiston, B.G., Coleman, J.L., Hanrahan, J.P., and Benach, J.L. (1984). Prevalence of the Lyme disease spirochete in populations of white-tailed deer and white-footed mice. Yale J Biol Med *57*, 651-659.
Bossart, K.N., Zhu, Z., Middleton, D., Klippel, J., Crameri, G., Bingham, J., McEachern, J.A., Green, D., Hancock, T.J., Chan, Y.P.*, et al.* (2009). A neutralizing human monoclonal antibody protects against lethal disease in a new ferret model of acute nipah virus infection. PLoS Pathog *5*, e1000642.
Botten, J., Mirowsky, K., Kusewitt, D., Bharadwaj, M., Yee, J., Ricci, R., Feddersen, R.M., and Hjelle, B. (2000). Experimental infection model for Sin Nombre hantavirus in the deer mouse (Peromyscus maniculatus). Proc Natl Acad Sci U S A *97*, 10578-10583.
Bratsch, S., Wertz, N., Chaloner, K., Kunz, T.H., and Butler, J.E. (2011). The little brown bat, M. lucifugus, displays a highly diverse V H, D H and J H repertoire but little evidence of somatic hypermutation. Dev Comp Immunol *35*, 421-430.
Breed, A.C. (2008). Paramyxoviruses in Bats. Zoo and Wild Animal Medicine, 225-cp223.
Butler, J.E., Wertz, N., Zhao, Y., Zhang, S., Bao, Y., Bratsch, S., Kunz, T.H., Whitaker, J.O., Jr., and Schountz, T. (2011). The two suborders of chiropterans have the canonical heavy-chain immunoglobulin (Ig) gene repertoire of eutherian mammals. Dev Comp Immunol *35*, 273-284.
Calderón, A., Guzmán, C., Oviedo-Socarras, T., Mattar, S., Rodríguez, V., Castañeda, V., and Moraes Figueiredo, L.T. (2021). Two Cases of Natural Infection of Dengue-2 Virus in Bats in the Colombian Caribbean. Trop Med Infect Dis *6*.
Campos, A.C.A., Góes, L.G.B., Moreira-Soto, A., de Carvalho, C., Ambar, G., Sander, A.L., Fischer, C., Ruckert da Rosa, A., Cardoso de Oliveira, D., Kataoka, A.P.G.*, et al.* (2019). Bat Influenza A(HL18NL11) Virus in Fruit Bats, Brazil. Emerg Infect Dis *25*, 333-337.
Cao, X. (2020). COVID-19: immunopathology and its implications for therapy. Nat Rev Immunol *20*, 269-270.

Cappelle, J., Furey, N., Hoem, T., Ou, T.P., Lim, T., Hul, V., Heng, O., Chevalier, V., Dussart, P., and Duong, V. (2021). Longitudinal monitoring in Cambodia suggests higher circulation of alpha and betacoronaviruses in juvenile and immature bats of three species. Sci Rep *11*, 24145.
Carleton, M.D. (1989a). Systematics and evolution (Lubbock: Texas Tech Univ. Press).
Carleton, M.D. (1989b). Systematics and evolution. Advances in the study of Peromyscus, 7-141.
CDC (1999). Update: outbreak of Nipah virus--Malaysia and Singapore, 1999. MMWR Morb Mortal Wkly Rep *48*, 335-337.
CDC (2022). Lyme Disease.
Chan, J.F., Zhang, A.J., Yuan, S., Poon, V.K., Chan, C.C., Lee, A.C., Chan, W.M., Fan, Z., Tsoi, H.W., Wen, L.*, et al.* (2020a). Simulation of the Clinical and Pathological Manifestations of Coronavirus Disease 2019 (COVID-19) in a Golden Syrian Hamster Model: Implications for Disease Pathogenesis and Transmissibility. Clin Infect Dis *71*, 2428-2446.
Chan, J.F., Zhang, A.J., Yuan, S., Poon, V.K., Chan, C.C., Lee, A.C., Chan, W.M., Fan, Z., Tsoi, H.W., Wen, L.*, et al.* (2020b). Simulation of the clinical and pathological manifestations of Coronavirus Disease 2019 (COVID-19) in golden Syrian hamster model: implications for disease pathogenesis and transmissibility. Clin Infect Dis.
Chandler, J.C., Bevins, S.N., Ellis, J.W., Linder, T.J., Tell, R.M., Jenkins-Moore, M., Root, J.J., Lenoch, J.B., Robbe-Austerman, S., DeLiberto, T.J.*, et al.* (2021). SARS-CoV-2 exposure in wild white-tailed deer (Odocoileus virginianus). Proc Natl Acad Sci U S A *118*.
Chen, L., Liu, B., Yang, J., and Jin, Q. (2014). DBatVir: the database of bat-associated viruses. Database (Oxford) *2014*, bau021.
Chen, M., Tachedjian, M., Marsh, G.A., Cui, J., and Wang, L.F. (2020). Distinct Cell Transcriptomic Landscapes Upon Henipavirus Infections. Front Microbiol *11*, 986.
Chen, Y., Chan, K.H., Kang, Y., Chen, H., Luk, H.K., Poon, R.W., Chan, J.F., Yuen, K.Y., Xia, N., Lau, S.K.*, et al.* (2015). A sensitive and specific antigen detection assay for Middle East respiratory syndrome coronavirus. Emerg Microbes Infect *4*, e26.
Chua, K.B., Goh, K.J., Wong, K.T., Kamarulzaman, A., Tan, P.S.K., Ksiazek, T.G., Zaki, S.R., Paul, G., Lam, S.K., and Tan, C.T. (1999). Fatal encephalitis due to Nipah virus among pig-farmers in Malaysia. The Lancet *354*, 1257-1259.
Chua, K.B., Koh, C.L., Hooi, P.S., Wee, K.F., Khong, J.H., Chua, B.H., Chan, Y.P., Lim, M.E., and Lam, S.K. (2002). Isolation of Nipah virus from Malaysian Island flying-foxes. Microbes Infect *4*, 145-151.
Cool, K., Gaudreault, N.N., Morozov, I., Trujillo, J.D., Meekins, D.A., McDowell, C., Carossino, M., Bold, D., Mitzel, D., Kwon, T.*, et al.* (2022). Infection and transmission of ancestral SARS-CoV-2 and its alpha variant in pregnant white-tailed deer. Emerg Microbes Infect *11*, 95-112.
Corman, V.M., Landt, O., Kaiser, M., Molenkamp, R., Meijer, A., Chu, D.K., Bleicker, T., Brunink, S., Schneider, J., Schmidt, M.L.*, et al.* (2020). Detection of 2019 novel coronavirus (2019-nCoV) by real-time RT-PCR. Euro Surveill *25*.
Corman, V.M., Muth, D., Niemeyer, D., and Drosten, C. (2018). Hosts and Sources of Endemic Human Coronaviruses. Adv Virus Res *100*, 163-188.
de Araujo, J., Lo, M.K., Tamin, A., Ometto, T.L., Thomazelli, L.M., Nardi, M.S., Hurtado, R.F., Nava, A., Spiropoulou, C.F., Rota, P.A.*, et al.* (2017). Antibodies Against Henipa-Like Viruses in Brazilian Bats. Vector Borne Zoonotic Dis *17*, 271-274.
de St Maurice, A., Ervin, E., Schumacher, M., Yaglom, H., VinHatton, E., Melman, S., Komatsu, K., House, J., Peterson, D., Buttke, D.*, et al.* (2017). Exposure Characteristics of Hantavirus Pulmonary Syndrome Patients, United States, 1993-2015. Emerg Infect Dis *23*, 733-739.
Dejnirattisai, W., Huo, J., Zhou, D., Zahradník, J., Supasa, P., Liu, C., Duyvesteyn, H.M.E., Ginn, H.M., Mentzer, A.J., Tuekprakhon, A.*, et al.* (2021). Omicron-B.1.1.529 leads to widespread escape from neutralizing antibody responses. bioRxiv, 2021.2012.2003.471045.

DeLiberto, T. (2020). Coronavirus disease 2019 update (536): Animal, USA (Utah) wild mink, first case. In ProMED Digest.
Doliff, R., and Martens, P. (2022). Cats and SARS-CoV-2: A Scoping Review. Animals (Basel) *12*.
Downs, W.G., Anderson, C.R., Spence, L., Aitken, T.H., and Greenhall, A.H. (1963). Tacaribe virus, a new agent isolated from Artibeus bats and mosquitoes in Trinidad, West Indies. Am J Trop Med Hyg *12*, 640-646.
Drexler, J.F., Corman, V.M., Gloza-Rausch, F., Seebens, A., Annan, A., Ipsen, A., Kruppa, T., Müller, M.A., Kalko, E.K., Adu-Sarkodie, Y.*, et al.* (2009). Henipavirus RNA in African bats. PLoS One *4*, e6367.
Drexler, J.F., Corman, V.M., Müller, M.A., Maganga, G.D., Vallo, P., Binger, T., Gloza-Rausch, F., Cottontail, V.M., Rasche, A., Yordanov, S.*, et al.* (2012). Bats host major mammalian paramyxoviruses. Nature Communications *3*, 796.
Edson, D., Peel, A.J., Huth, L., Mayer, D.G., Vidgen, M.E., McMichael, L., Broos, A., Melville, D., Kristoffersen, J., de Jong, C.*, et al.* (2019). Time of year, age class and body condition predict Hendra virus infection in Australian black flying foxes (Pteropus alecto). Epidemiol Infect *147*, e240.
Fagre, A., Lewis, J., Eckley, M., Zhan, S., Rocha, S.M., Sexton, N.R., Burke, B., Geiss, B., Peersen, O., Bass, T.*, et al.* (2021a). SARS-CoV-2 infection, neuropathogenesis and transmission among deer mice: Implications for spillback to New World rodents. PLoS pathogens *17*, e1009585-e1009585.
Fagre, A.C., Lewis, J., Miller, M.R., Mossel, E.C., Lutwama, J.J., Nyakarahuka, L., Nakayiki, T., Kityo, R., Nalikka, B., Towner, J.S.*, et al.* (2021b). Subgenomic flavivirus RNA (sfRNA) associated with Asian lineage Zika virus identified in three species of Ugandan bats (family Pteropodidae). Scientific Reports *11*, 8370.
Fagre, A.C., Manhard, J., Adams, R., Eckley, M., Zhan, S., Lewis, J., Rocha, S.M., Woods, C., Kuo, K., Liao, W.*, et al.* (2020). A Potent SARS-CoV-2 Neutralizing Human Monoclonal Antibody That Reduces Viral Burden and Disease Severity in Syrian Hamsters. Front Immunol *11*, 614256.
Fajgenbaum, D.C., and June, C.H. (2020). Cytokine Storm. N Engl J Med *383*, 2255-2273.
Ferguson, N.M., and Van Kerkhove, M.D. (2014). Identification of MERS-CoV in dromedary camels. Lancet Infect Dis *14*, 93-94.
Field, H.E. (2016). Hendra virus ecology and transmission. Current Opinion in Virology *16*, 120-125.
Field, H.E., Mackenzie, J.S., and Daszak, P. (2007). Henipaviruses: emerging paramyxoviruses associated with fruit bats. Curr Top Microbiol Immunol *315*, 133-159.
Fischer, K., Groschup, M.H., and Diederich, S. (2020). Importance of Endocytosis for the Biological Activity of Cedar Virus Fusion Protein. Cells *9*, 2054.
Focosi, D., and Maggi, F. (2022). Recombination in Coronaviruses, with a Focus on SARS-CoV-2. Viruses *14*.
Franklin, A.B., and Bevins, S.N. (2020). Spillover of SARS-CoV-2 into novel wild hosts in North America: A conceptual model for perpetuation of the pathogen. Sci Total Environ *733*, 139358.
Frieman, M., Yount, B., Heise, M., Kopecky-Bromberg, S.A., Palese, P., and Baric, R.S. (2007). Severe acute respiratory syndrome coronavirus ORF6 antagonizes STAT1 function by sequestering nuclear import factors on the rough endoplasmic reticulum/Golgi membrane. J Virol *81*, 9812-9824.
From the American Association of Neurological Surgeons, A.S.o.N.C., Interventional Radiology Society of Europe, C.I.R.A.C.o.N.S.E.S.o.M.I.N.T.E.S.o.N.E.S.O.S.f.C.A., Interventions, S.o.I.R.S.o.N.S., World Stroke, O., Sacks, D., Baxter, B., Campbell, B.C.V., Carpenter, J.S., Cognard, C., Dippel, D.*, et al.* (2018). Multisociety Consensus Quality Improvement Revised

Consensus Statement for Endovascular Therapy of Acute Ischemic Stroke. Int J Stroke *13*, 612-632.
Ge, X.Y., Yang, W.H., Zhou, J.H., Li, B., Zhang, W., Shi, Z.L., and Zhang, Y.Z. (2017). Detection of alpha- and betacoronaviruses in rodents from Yunnan, China. Virol J *14*, 98.
Geisbert, T.W., Daddario-DiCaprio, K.M., Hickey, A.C., Smith, M.A., Chan, Y.P., Wang, L.F., Mattapallil, J.J., Geisbert, J.B., Bossart, K.N., and Broder, C.C. (2010). Development of an acute and highly pathogenic nonhuman primate model of Nipah virus infection. PLoS One *5*, e10690.
Geisbert, T.W., Feldmann, H., and Broder, C.C. (2012). Animal challenge models of henipavirus infection and pathogenesis. Curr Top Microbiol Immunol *359*, 153-177.
Geiss, B.J., Thompson, A.A., Andrews, A.J., Sons, R.L., Gari, H.H., Keenan, S.M., and Peersen, O.B. (2009). Analysis of flavivirus NS5 methyltransferase cap binding. J Mol Biol *385*, 1643-1654.
Giles, J.R., Peel, A.J., Wells, K., Plowright, R.K., McCallum, H., and Restif, O. (2021a). Optimizing noninvasive sampling of a zoonotic bat virus. Ecol Evol *11*, 12307-12321.
Giles, J.R., Peel, A.J., Wells, K., Plowright, R.K., McCallum, H., and Restif, O. (2021b). Optimizing noninvasive sampling of a zoonotic bat virus. Ecology and Evolution *11*, 12307-12321.
Goh, K.J., Tan, C.T., Chew, N.K., Tan, P.S., Kamarulzaman, A., Sarji, S.A., Wong, K.T., Abdullah, B.J., Chua, K.B., and Lam, S.K. (2000). Clinical features of Nipah virus encephalitis among pig farmers in Malaysia. N Engl J Med *342*, 1229-1235.
Goldstein, T., Anthony, S.J., Gbakima, A., Bird, B.H., Bangura, J., Tremeau-Bravard, A., Belaganahalli, M.N., Wells, H.L., Dhanota, J.K., Liang, E.*, et al.* (2018). The discovery of Bombali virus adds further support for bats as hosts of ebolaviruses. Nat Microbiol *3*, 1084-1089.
Greenbaum, I., Honeycutt, R., and Chirhart, S. (2019). TAXONOMY AND PHYLOGENETICS OF THE PEROMYSCUS MANICULATUS SPECIES GROUP. *71*, 559-575.
Griffin, B.D., Chan, M., Tailor, N., Mendoza, E.J., Leung, A., Warner, B.M., Duggan, A.T., Moffat, E., He, S., Garnett, L.*, et al.* (2021). SARS-CoV-2 infection and transmission in the North American deer mouse. Nature Communications *12*, 3612.
Guillaume, V., Wong, K.T., Looi, R.Y., Georges-Courbot, M.C., Barrot, L., Buckland, R., Wild, T.F., and Horvat, B. (2009). Acute Hendra virus infection: Analysis of the pathogenesis and passive antibody protection in the hamster model. Virology *387*, 459-465.
Hagmaier, K., Stock, N., Precious, B., Childs, K., Wang, L.F., Goodbourn, S., and Randall, R.E. (2007). Mapuera virus, a rubulavirus that inhibits interferon signalling in a wide variety of mammalian cells without degrading STATs. J Gen Virol *88*, 956-966.
Halpin, K., Hyatt, A.D., Fogarty, R., Middleton, D., Bingham, J., Epstein, J.H., Rahman, S.A., Hughes, T., Smith, C., Field, H.E.*, et al.* (2011). Pteropid bats are confirmed as the reservoir hosts of henipaviruses: a comprehensive experimental study of virus transmission. Am J Trop Med Hyg *85*, 946-951.
Halpin, K., Young, P.L., Field, H.E., and Mackenzie, J.S. (2000). Isolation of Hendra virus from pteropid bats: a natural reservoir of Hendra virus. J Gen Virol *81*, 1927-1932.
Hammer, A.S., Quaade, M.L., Rasmussen, T.B., Fonager, J., Rasmussen, M., Mundbjerg, K., Lohse, L., Strandbygaard, B., Jørgensen, C.S., Alfaro-Núñez, A.*, et al.* (2021). SARS-CoV-2 Transmission between Mink (Neovison vison) and Humans, Denmark. Emerg Infect Dis *27*, 547-551.
Harcourt, B.H., Lowe, L., Tamin, A., Liu, X., Bankamp, B., Bowden, N., Rollin, P.E., Comer, J.A., Ksiazek, T.G., Hossain, M.J.*, et al.* (2005). Genetic characterization of Nipah virus, Bangladesh, 2004. Emerg Infect Dis *11*, 1594-1597.

Hause, B.M., Nelson, E., and Christopher-Hennings, J. (2021). Eptesicus fuscus Orthorubulavirus, a Close Relative of Human Parainfluenza Virus 4, Discovered in a Bat in South Dakota. Microbiol Spectr *9*, e0093021.
Havighorst, A., Crossland, J., and Kiaris, H. (2017). Peromyscus as a model of human disease. Semin Cell Dev Biol *61*, 150-155.
Hayman, D.T. (2015). Biannual birth pulses allow filoviruses to persist in bat populations. Proc Biol Sci *282*, 20142591.
He, L., Ding, Y., Zhang, Q., Che, X., He, Y., Shen, H., Wang, H., Li, Z., Zhao, L., Geng, J.*, et al.* (2006). Expression of elevated levels of pro-inflammatory cytokines in SARS-CoV-infected ACE2+ cells in SARS patients: relation to the acute lung injury and pathogenesis of SARS. J Pathol *210*, 288-297.
Hernández, L., da Paz, T., Silva, S., Silva, F., Barros, B., Nunes, B., Casseb, L., Medeiros, D., Vasconcelos, P., and Ribeiro Cruz, A.C. (2022). First Genomic Evidence of a Henipa-like Virus in Brazil.
Hernández, L.H.A.d.P., T.Y.B.; Silva, S.P.D.; Silva, F.S.D.; Barros, B.C.V.D.; Nunes, B.T.D.; Casseb, L.M.N.; Medeiros, D.B.A.; Vasconcelos, P.F.D.C.; Cruz, A.C.R. (2022). First Genomic Evidence of a Henipa-like Virus in Brazil. Preprints.
Hjelle, B., Jenison, S., Torrez-Martinez, N., Yamada, T., Nolte, K., Zumwalt, R., MacInnes, K., and Myers, G. (1994). A novel hantavirus associated with an outbreak of fatal respiratory disease in the southwestern United States: evolutionary relationships to known hantaviruses. Journal of Virology *68*, 592-596.
Hoffmann, M., Zhang, L., Krüger, N., Graichen, L., Kleine-Weber, H., Hofmann-Winkler, H., Kempf, A., Nessler, S., Riggert, J., Winkler, M.S.*, et al.* (2021). SARS-CoV-2 mutations acquired in mink reduce antibody-mediated neutralization. Cell Rep *35*, 109017.
Hooper, P.T., Ketterer, P.J., Hyatt, A.D., and Russell, G.M. (1997). Lesions of experimental equine morbillivirus pneumonia in horses. Vet Pathol *34*, 312-322.
Hu, B., Zeng, L.-P., Yang, X.-L., Ge, X.-Y., Zhang, W., Li, B., Xie, J.-Z., Shen, X.-R., Zhang, Y.-Z., Wang, N.*, et al.* (2017). Discovery of a rich gene pool of bat SARS-related coronaviruses provides new insights into the origin of SARS coronavirus. PLoS pathogens *13*, e1006698-e1006698.
Huang, C., Wang, Y., Li, X., Ren, L., Zhao, J., Hu, Y., Zhang, L., Fan, G., Xu, J., Gu, X.*, et al.* (2020). Clinical features of patients infected with 2019 novel coronavirus in Wuhan, China. Lancet *395*, 497-506.
Imai, M., Iwatsuki-Horimoto, K., Hatta, M., Loeber, S., Halfmann, P.J., Nakajima, N., Watanabe, T., Ujie, M., Takahashi, K., Ito, M.*, et al.* (2020). Syrian hamsters as a small animal model for SARS-CoV-2 infection and countermeasure development. Proc Natl Acad Sci U S A.
Ip, H.S., Griffin, K.M., Messer, J.D., Winzeler, M.E., Shriner, S.A., Killian, M.L., M, K.T., DeLiberto, T.J., Amman, B.R., Cossaboom, C.M.*, et al.* (2021). An Opportunistic Survey Reveals an Unexpected Coronavirus Diversity Hotspot in North America. Viruses *13*.
Iroegbu, J.D., Ifenatuoha, C.W., and Ijomone, O.M. (2020). Potential neurological impact of coronaviruses: implications for the novel SARS-CoV-2. Neurol Sci *41*, 1329-1337.
IUCN (2022). The IUCN Red List of Threatened Species. In Version 2022-1
Jackson, C.B., Farzan, M., Chen, B., and Choe, H. (2022). Mechanisms of SARS-CoV-2 entry into cells. Nature Reviews Molecular Cell Biology *23*, 3-20.
Ji, D., Qin, E., Xu, J., Zhang, D., Cheng, G., Wang, Y., and Lau, G. (2020). Non-alcoholic fatty liver diseases in patients with COVID-19: A retrospective study. Journal of Hepatology *73*, 451-453.
Johnson, N., Aréchiga-Ceballos, N., and Aguilar-Setien, A. (2014). Vampire Bat Rabies: Ecology, Epidemiology and Control. Viruses *6*, 1911-1928.
Joyner, C.P., Myrick, L.C., Crossland, J.P., and Dawson, W.D. (1998). Deer Mice As Laboratory Animals. ILAR Journal *39*, 322-330.

Kading, R.C., and Schountz, T. (2016). Flavivirus Infections of Bats: Potential Role in Zika Virus Ecology. Am J Trop Med Hyg *95*, 993-996.
Kandeil, A., Gomaa, M.R., Shehata, M.M., El Taweel, A.N., Mahmoud, S.H., Bagato, O., Moatasim, Y., Kutkat, O., Kayed, A.S., Dawson, P.*, et al.* (2019). Isolation and Characterization of a Distinct Influenza A Virus from Egyptian Bats. J Virol *93*.
Kelley, L.A., Mezulis, S., Yates, C.M., Wass, M.N., and Sternberg, M.J. (2015). The Phyre2 web portal for protein modeling, prediction and analysis. Nat Protoc *10*, 845-858.
Kepler, T.B., Sample, C., Hudak, K., Roach, J., Haines, A., Walsh, A., and Ramsburg, E.A. (2010). Chiropteran types I and II interferon genes inferred from genome sequencing traces by a statistical gene-family assembler. BMC Genomics *11*, 444.
Kessler, M.K., Becker, D.J., Peel, A.J., Justice, N.V., Lunn, T., Crowley, D.E., Jones, D.N., Eby, P., Sánchez, C.A., and Plowright, R.K. (2018). Changing resource landscapes and spillover of henipaviruses. Ann N Y Acad Sci *1429*, 78-99.
Kirkland, G.L., and Layne, J.N. (1989a). Advances in the study of Peromyscus (Rodentia).
Kirkland, G.L., and Layne, J.N. (1989b). Advances in the study of Peromyscus (Rodentia) (Texas Tech University Press).
Kopecky-Bromberg, S.A., Martínez-Sobrido, L., Frieman, M., Baric, R.A., and Palese, P. (2007). Severe acute respiratory syndrome coronavirus open reading frame (ORF) 3b, ORF 6, and nucleocapsid proteins function as interferon antagonists. J Virol *81*, 548-557.
Krugner-Higby, L., Caldwell, S., Coyle, K., Bush, E., Atkinson, R., and Joers, V. (2011). The effects of diet composition on body fat and hepatic steatosis in an animal (Peromyscus californicus) model of the metabolic syndrome. Comp Med *61*, 31-38.
Krugner-Higby, L., Shadoan, M., Carlson, C., Gendron, A., Cofta, P., Marler, C., and Wagner, J. (2000). Type 2 diabetes mellitus, hyperlipidemia, and extremity lesions in California mice (Peromyscus californicus) fed commercial mouse diets. Comp Med *50*, 412-418.
Krugner-Higby, L., Shelness, G.S., and Holler, A. (2006). Heritable, diet-induced hyperlipidemia in California mice (Peromyscus californicus) is due to increased hepatic secretion of very low density lipoprotein triacylglycerol. Comp Med *56*, 468-475.
Kubota, T., Yokosawa, N., Yokota, S.-i., and Fujii, N. (2002). Association of mumps virus V protein with RACK1 results in dissociation of STAT-1 from the alpha interferon receptor complex. Journal of virology *76*, 12676-12682.
Kubota, T., Yokosawa, N., Yokota, S.-I., Fujii, N., Tashiro, M., and Kato, A. (2005). Mumps virus V protein antagonizes interferon without the complete degradation of STAT1. Journal of virology *79*, 4451-4459.
Kuchipudi, S.V., Surendran-Nair, M., Ruden, R.M., Yon, M., Nissly, R.H., Vandegrift, K.J., Nelli, R.K., Li, L., Jayarao, B.M., Maranas, C.D.*, et al.* (2022). Multiple spillovers from humans and onward transmission of SARS-CoV-2 in white-tailed deer. Proc Natl Acad Sci U S A *119*.
Kunz, T.H., Braun de Torrez, E., Bauer, D., Lobova, T., and Fleming, T.H. (2011). Ecosystem services provided by bats. Annals of the New York Academy of Sciences *1223*, 1-38.
Kunz, T.H., and Fenton, M.B. (2005). Bat ecology (University of Chicago Press).
Laing, E.D., Navaratnarajah, C.K., Silva, S.C.D., Petzing, S.R., Xu, Y., Sterling, S.L., Marsh, G.A., Wang, L.-F., Amaya, M., Nikolov, D.B.*, et al.* (2019). Structural and functional analyses reveal promiscuous and species specific use of ephrin receptors by Cedar virus. Proceedings of the National Academy of Sciences *116*, 20707-20715.
Larsen, H.D., Fonager, J., Lomholt, F.K., Dalby, T., Benedetti, G., Kristensen, B., Urth, T.R., Rasmussen, M., Lassaunière, R., Rasmussen, T.B.*, et al.* (2021). Preliminary report of an outbreak of SARS-CoV-2 in mink and mink farmers associated with community spread, Denmark, June to November 2020. Euro Surveill *26*.
Larson, P.A., Bartlett, M.L., Garcia, K., Chitty, J., Balkema-Buschmann, A., Towner, J., Kugelman, J., Palacios, G., and Sanchez-Lockhart, M. (2021). Genomic features of humoral immunity support tolerance model in Egyptian rousette bats. Cell Reports *35*.

Lau, S.K., Woo, P.C., Li, K.S., Tsang, A.K., Fan, R.Y., Luk, H.K., Cai, J.P., Chan, K.H., Zheng, B.J., Wang, M.*, et al.* (2015a). Discovery of a novel coronavirus, China Rattus coronavirus HKU24, from Norway rats supports the murine origin of Betacoronavirus 1 and has implications for the ancestor of Betacoronavirus lineage A. J Virol *89*, 3076-3092.
Lau, S.K.P., Luk, H.K.H., Wong, A.C.P., Li, K.S.M., Zhu, L., He, Z., Fung, J., Chan, T.T.Y., Fung, K.S.C., and Woo, P.C.Y. (2020). Possible Bat Origin of Severe Acute Respiratory Syndrome Coronavirus 2. Emerg Infect Dis *26*, 1542-1547.
Lau, S.K.P., Woo, P.C.Y., Li, K.S.M., Tsang, A.K.L., Fan, R.Y.Y., Luk, H.K.H., Cai, J.-P., Chan, K.-H., Zheng, B.-J., Wang, M.*, et al.* (2015b). Discovery of a Novel Coronavirus, China Rattus Coronavirus HKU24, from Norway Rats Supports the Murine Origin of Betacoronavirus 1 and Has Implications for the Ancestor of Betacoronavirus Lineage A. Journal of Virology *89*, 3076-3092.
Lawlor, T.E., and Hall, E.R. (1982). The mammals of North America. . Journal of Mammalogy *63*, 718-719.
Lawrence, P., Escudero Pérez, B., Drexler, J.F., Corman, V.M., Müller, M.A., Drosten, C., and Volchkov, V. (2014). Surface glycoproteins of the recently identified African Henipavirus promote viral entry and cell fusion in a range of human, simian and bat cell lines. Virus Res *181*, 77-80.
Lee, B., Ikegame, S., Carmichael, J., Wells, H., Furler, R., Acklin, J., Chiu, H.P., Oguntuyo, K., Cox, R., Patel, A.*, et al.* (2021a). Zoonotic potential of a novel bat morbillivirus. Res Sq.
Lee, S.-H., Kim, K., Kim, J., No, J.S., Park, K., Budhathoki, S., Lee, S.H., Lee, J., Cho, S.H., Cho, S.*, et al.* (2021b). Discovery and Genetic Characterization of Novel Paramyxoviruses Related to the Genus Henipavirus in Crocidura Species in the Republic of Korea. Viruses *13*, 2020.
Letko, M., Marzi, A., and Munster, V. (2020). Functional assessment of cell entry and receptor usage for SARS-CoV-2 and other lineage B betacoronaviruses. Nat Microbiol *5*, 562-569.
Li, F. (2015). Receptor recognition mechanisms of coronaviruses: a decade of structural studies. J Virol *89*, 1954-1964.
Li, F. (2016). Structure, Function, and Evolution of Coronavirus Spike Proteins. Annu Rev Virol *3*, 237-261.
Li, M., Embury-Hyatt, C., and Weingartl, H.M. (2010). Experimental inoculation study indicates swine as a potential host for Hendra virus. Vet Res *41*, 33.
Li, W., Shi, Z., Yu, M., Ren, W., Smith, C., Epstein, J.H., Wang, H., Crameri, G., Hu, Z., Zhang, H.*, et al.* (2005). Bats are natural reservoirs of SARS-like coronaviruses. Science *310*, 676-679.
Li, X., Wang, L., Liu, P., Li, H., Huo, S., Zong, K., Zhu, S., Guo, Y., Zhang, L., Hu, B.*, et al.* (2021). A Novel Potentially Recombinant Rodent Coronavirus with a Polybasic Cleavage Site in the Spike Protein. J Virol *95*, e0117321.
Livak, K.J., and Schmittgen, T.D. (2001). Analysis of relative gene expression data using real-time quantitative PCR and the 2(-Delta Delta C(T)) Method. Methods *25*, 402-408.
Lobova, T.A., C.K. Geiselman & S.A. Mori (2009). Seed dispersal by bats in the Neotropics. (The Bronx, New York: New York Botanical Garden Press).
Lu, S., Zhao, Y., Yu, W., Yang, Y., Gao, J., Wang, J., Kuang, D., Yang, M., Yang, J., Ma, C.*, et al.* (2020). Comparison of nonhuman primates identified the suitable model for COVID-19. Signal Transduct Target Ther *5*, 157.
Luan, J., Jin, X., Lu, Y., and Zhang, L. (2020). SARS-CoV-2 spike protein favors ACE2 from Bovidae and Cricetidae. J Med Virol.
Luby, S.P., Rahman, M., Hossain, M.J., Blum, L.S., Husain, M.M., Gurley, E., Khan, R., Ahmed, B.N., Rahman, S., Nahar, N.*, et al.* (2006). Foodborne transmission of Nipah virus, Bangladesh. Emerg Infect Dis *12*, 1888-1894.
Machain-Williams, C., López-Uribe, M., Talavera-Aguilar, L., Carrillo-Navarrete, J., Vera-Escalante, L., Puerto-Manzano, F., Ulloa, A., Farfán-Ale, J.A., Garcia-Rejon, J., Blitvich, B.J.*, et*

al. (2013). Serologic evidence of flavivirus infection in bats in the Yucatan Peninsula of Mexico. J Wildl Dis *49*, 684-689.
Madera, S., Kistler, A., Ranaivoson, H.C., Ahyong, V., Andrianiaina, A., Andry, S., Raharinosy, V., Randriambolamanantsoa, T.H., Ravelomanantsoa, N.A.F., Tato, C.M.*, et al.* (2022). Discovery and Genomic Characterization of a Novel Henipavirus, Angavokely Virus, from Fruit Bats in Madagascar. J Virol, e0092122.
Magazine, N., Zhang, T., Wu, Y., McGee, M.C., Veggiani, G., and Huang, W. (2022). Mutations and Evolution of the SARS-CoV-2 Spike Protein. Viruses *14*.
Marsh, G.A., de Jong, C., Barr, J.A., Tachedjian, M., Smith, C., Middleton, D., Yu, M., Todd, S., Foord, A.J., Haring, V.*, et al.* (2012a). Cedar virus: a novel Henipavirus isolated from Australian bats. PLoS pathogens *8*, e1002836-e1002836.
Marsh, G.A., de Jong, C., Barr, J.A., Tachedjian, M., Smith, C., Middleton, D., Yu, M., Todd, S., Foord, A.J., Haring, V.*, et al.* (2012b). Cedar virus: a novel Henipavirus isolated from Australian bats. PLoS Pathog *8*, e1002836.
Martines, R.B., Ritter, J.M., Matkovic, E., Gary, J., Bollweg, B.C., Bullock, H., Goldsmith, C.S., Silva-Flannery, L., Seixas, J.N., Reagan-Steiner, S.*, et al.* (2020). Pathology and Pathogenesis of SARS-CoV-2 Associated with Fatal Coronavirus Disease, United States. Emerg Infect Dis *26*, 2005-2015.
Maru, M., and Sato, K. (1982). Characterization of a coronavirus isolated from rats with sialoadenitis. Arch Virol *73*, 33-43.
Memish, Z.A., Mishra, N., Olival, K.J., Fagbo, S.F., Kapoor, V., Epstein, J.H., Alhakeem, R., Durosinloun, A., Al Asmari, M., Islam, A.*, et al.* (2013). Middle East respiratory syndrome coronavirus in bats, Saudi Arabia. Emerg Infect Dis *19*, 1819-1823.
Miao, E.A., Rajan, J.V., and Aderem, A. (2011). Caspase-1-induced pyroptotic cell death. Immunol Rev *243*, 206-214.
Middleton, D.J., Morrissy, C.J., van der Heide, B.M., Russell, G.M., Braun, M.A., Westbury, H.A., Halpin, K., and Daniels, P.W. (2007). Experimental Nipah virus infection in pteropid bats (Pteropus poliocephalus). J Comp Pathol *136*, 266-272.
Middleton, D.J., Westbury, H.A., Morrissy, C.J., van der Heide, B.M., Russell, G.M., Braun, M.A., and Hyatt, A.D. (2002). Experimental Nipah virus infection in pigs and cats. J Comp Pathol *126*, 124-136.
Milne-Price, S., Miazgowicz, K.L., and Munster, V.J. (2014). The emergence of the Middle East respiratory syndrome coronavirus. Pathog Dis *71*, 121-136.
Miot, E.F., Worthington, B.M., Ng, K.H., de Lataillade, L.G., Pierce, M.P., Liao, Y., Ko, R., Shum, M.H., Cheung, W.Y., Holmes, E.C.*, et al.* (2022). Surveillance of Rodent Pests for SARS-CoV-2 and Other Coronaviruses, Hong Kong. Emerg Infect Dis *28*, 467-470.
Montecino-Latorre, D., Goldstein, T., Gilardi, K., Wolking, D., Van Wormer, E., Kazwala, R., Ssebide, B., Nziza, J., Sijali, Z., Cranfield, M.*, et al.* (2020). Reproduction of East-African bats may guide risk mitigation for coronavirus spillover. One Health Outlook *2*, 2.
Mortlock, M., Dietrich, M., Weyer, J., Paweska, J.T., and Markotter, W. (2019). Co-Circulation and Excretion Dynamics of Diverse Rubula- and Related Viruses in Egyptian Rousette Bats from South Africa. Viruses *11*.
Munster, V.J., Feldmann, F., Williamson, B.N., van Doremalen, N., Pérez-Pérez, L., Schulz, J., Meade-White, K., Okumura, A., Callison, J., Brumbaugh, B.*, et al.* (2020). Respiratory disease and virus shedding in rhesus macaques inoculated with SARS-CoV-2. bioRxiv.
Murray, K., Selleck, P., Hooper, P., Hyatt, A., Gould, A., Gleeson, L., Westbury, H., Hiley, L., Selvey, L., Rodwell, B.*, et al.* (1995). A Morbillivirus that Caused Fatal Fisease in Horses and Humans. Science *268*, 94-97.
Mushtaq, K., Khan, M.U., Iqbal, F., Alsoub, D.H., Chaudhry, H.S., Ata, F., Iqbal, P., Elfert, K., Balaraju, G., Almaslamani, M.*, et al.* (2021). NAFLD is a predictor of liver injury in COVID-19

hospitalized patients but not of mortality, disease severity on the presentation or progression – The debate continues. Journal of Hepatology *74*, 482-484.
Negrete, O.A., Wolf, M.C., Aguilar, H.C., Enterlein, S., Wang, W., Mühlberger, E., Su, S.V., Bertolotti-Ciarlet, A., Flick, R., and Lee, B. (2006). Two key residues in ephrinB3 are critical for its use as an alternative receptor for Nipah virus. PLoS Pathog *2*, e7.
Nelson, J.B. (1952). Acute hepatitis associated with mouse leukemia. II. Etiology and host range of the causal agent in mice. J Exp Med *95*, 303-312.
Nikolay, B., Salje, H., Hossain, M.J., Khan, A., Sazzad, H.M.S., Rahman, M., Daszak, P., Ströher, U., Pulliam, J.R.C., Kilpatrick, A.M.*, et al.* (2019). Transmission of Nipah Virus - 14 Years of Investigations in Bangladesh. N Engl J Med *380*, 1804-1814.
Omatsu, T., Bak, E.J., Ishii, Y., Kyuwa, S., Tohya, Y., Akashi, H., and Yoshikawa, Y. (2008). Induction and sequencing of Rousette bat interferon alpha and beta genes. Vet Immunol Immunopathol *124*, 169-176.
Oreshkova, N., Molenaar, R.J., Vreman, S., Harders, F., Oude Munnink, B.B., Hakze-van der Honing, R.W., Gerhards, N., Tolsma, P., Bouwstra, R., Sikkema, R.S.*, et al.* (2020). SARS-CoV-2 infection in farmed minks, the Netherlands, April and May 2020. Euro Surveill *25*.
Oude Munnink, B.B., Sikkema, R.S., Nieuwenhuijse, D.F., Molenaar, R.J., Munger, E., Molenkamp, R., van der Spek, A., Tolsma, P., Rietveld, A., Brouwer, M.*, et al.* (2021). Transmission of SARS-CoV-2 on mink farms between humans and mink and back to humans. Science *371*, 172-177.
Pacheco, P.M., K.; Dudley, N.; Shapiro, A.; Aguilar-Amuchastegui, N.; Ling, P.Y.; Anderson, C; and Marx, A. (2021). Deforestation fronts: Drivers and responses in a changing world. WWF.
Pallister, J., Middleton, D., Crameri, G., Yamada, M., Klein, R., Hancock, T.J., Foord, A., Shiell, B., Michalski, W., Broder, C.C.*, et al.* (2009). Chloroquine administration does not prevent Nipah virus infection and disease in ferrets. J Virol *83*, 11979-11982.
Pallister, J., Middleton, D., Wang, L.F., Klein, R., Haining, J., Robinson, R., Yamada, M., White, J., Payne, J., Feng, Y.R.*, et al.* (2011). A recombinant Hendra virus G glycoprotein-based subunit vaccine protects ferrets from lethal Hendra virus challenge. Vaccine *29*, 5623-5630.
Palosaari, H., Parisien, J.P., Rodriguez, J.J., Ulane, C.M., and Horvath, C.M. (2003). STAT protein interference and suppression of cytokine signal transduction by measles virus V protein. J Virol *77*, 7635-7644.
Parisien, J.P., Lau, J.F., Rodriguez, J.J., Sullivan, B.M., Moscona, A., Parks, G.D., Lamb, R.A., and Horvath, C.M. (2001). The V protein of human parainfluenza virus 2 antagonizes type I interferon responses by destabilizing signal transducer and activator of transcription 2. Virology *283*, 230-239.
Pavlovich, S.S., Lovett, S.P., Koroleva, G., Guito, J.C., Arnold, C.E., Nagle, E.R., Kulcsar, K., Lee, A., Thibaud-Nissen, F., Hume, A.J.*, et al.* (2018). The Egyptian Rousette Genome Reveals Unexpected Features of Bat Antiviral Immunity. Cell *173*, 1098-1110.e1018.
Peavey, C.A., and Lane, R.S. (1995). Transmission of Borrelia burgdorferi by Ixodes pacificus nymphs and reservoir competence of deer mice (Peromyscus maniculatus) infected by tick-bite. J Parasitol *81*, 175-178.
Pernet, O., Schneider, B.S., Beaty, S.M., LeBreton, M., Yun, T.E., Park, A., Zachariah, T.T., Bowden, T.A., Hitchens, P., Ramirez, C.M.*, et al.* (2014). Evidence for henipavirus spillover into human populations in Africa. Nat Commun *5*, 5342.
Pierson, T.C., and Diamond, M.S. (2020). The continued threat of emerging flaviviruses. Nature Microbiology *5*, 796-812.
Plowright, R.K., Field, H.E., Smith, C., Divljan, A., Palmer, C., Tabor, G., Daszak, P., and Foley, J.E. (2008). Reproduction and nutritional stress are risk factors for Hendra virus infection in little red flying foxes (Pteropus scapulatus). Proc Biol Sci *275*, 861-869.

Premkumar, L., Segovia-Chumbez, B., Jadi, R., Martinez, D.R., Raut, R., Markmann, A.J., Cornaby, C., Bartelt, L., Weiss, S., Park, Y.*, et al.* (2020). The receptor-binding domain of the viral spike protein is an immunodominant and highly specific target of antibodies in SARS-CoV-2 patients. Science Immunology *5*, eabc8413.
Qiu, X., Fu, Q., Meng, C., Yu, S., Zhan, Y., Dong, L., Song, C., Sun, Y., Tan, L., Hu, S.*, et al.* (2016). Newcastle Disease Virus V Protein Targets Phosphorylated STAT1 to Block IFN-I Signaling. PLOS ONE *11*, e0148560.
Quick, J., Grubaugh, N.D., Pullan, S.T., Claro, I.M., Smith, A.D., Gangavarapu, K., Oliveira, G., Robles-Sikisaka, R., Rogers, T.F., Beutler, N.A.*, et al.* (2017). Multiplex PCR method for MinION and Illumina sequencing of Zika and other virus genomes directly from clinical samples. Nature Protocols *12*, 1261-1276.
Reed, L.J., and Muench, H. (1938). A SIMPLE METHOD OF ESTIMATING FIFTY PER CENT ENDPOINTS12. American Journal of Epidemiology *27*, 493-497.
Rockx, B., Bossart, K.N., Feldmann, F., Geisbert, J.B., Hickey, A.C., Brining, D., Callison, J., Safronetz, D., Marzi, A., Kercher, L.*, et al.* (2010). A novel model of lethal Hendra virus infection in African green monkeys and the effectiveness of ribavirin treatment. J Virol *84*, 9831-9839.
Rockx, B., Brining, D., Kramer, J., Callison, J., Ebihara, H., Mansfield, K., and Feldmann, H. (2011). Clinical outcome of henipavirus infection in hamsters is determined by the route and dose of infection. J Virol *85*, 7658-7671.
Rockx, B., Kuiken, T., Herfst, S., Bestebroer, T., Lamers, M.M., Oude Munnink, B.B., de Meulder, D., van Amerongen, G., van den Brand, J., Okba, N.M.A.*, et al.* (2020). Comparative pathogenesis of COVID-19, MERS, and SARS in a nonhuman primate model. Science *368*, 1012-1015.
Rodero, M.P., Decalf, J., Bondet, V., Hunt, D., Rice, G.I., Werneke, S., McGlasson, S.L., Alyanakian, M.A., Bader-Meunier, B., Barnerias, C.*, et al.* (2017). Detection of interferon alpha protein reveals differential levels and cellular sources in disease. J Exp Med *214*, 1547-1555.
Rodriguez, J.J., Cruz, C.D., and Horvath, C.M. (2004). Identification of the nuclear export signal and STAT-binding domains of the Nipah virus V protein reveals mechanisms underlying interferon evasion. J Virol *78*, 5358-5367.
Rodriguez, J.J., Parisien, J.P., and Horvath, C.M. (2002). Nipah virus V protein evades alpha and gamma interferons by preventing STAT1 and STAT2 activation and nuclear accumulation. J Virol *76*, 11476-11483.
Rosa, R.B., Dantas, W.M., do Nascimento, J.C.F., da Silva, M.V., de Oliveira, R.N., and Pena, L.J. (2021). In Vitro and In Vivo Models for Studying SARS-CoV-2, the Etiological Agent Responsible for COVID-19 Pandemic. Viruses *13*.
Sacher, G.A., and Hart, R.W. (1978). Longevity, aging, and comparative cellular and molecular biology of the house mouse, Mus musculus, and the white-footed mouse, Peromyscus leucopus. Birth Defects, Orig Artic Ser;(United States) *14*.
Satterfield, B.A., Cross, R.W., Fenton, K.A., Agans, K.N., Basler, C.F., Geisbert, T.W., and Mire, C.E. (2015). The immunomodulating V and W proteins of Nipah virus determine disease course. Nature Communications *6*, 7483.
Satterfield, B.A., Cross, R.W., Fenton, K.A., Borisevich, V., Agans, K.N., Deer, D.J., Graber, J., Basler, C.F., Geisbert, T.W., and Mire, C.E. (2016). Nipah Virus C and W Proteins Contribute to Respiratory Disease in Ferrets. Journal of virology *90*, 6326-6343.
Schlottau, K., Rissmann, M., Graaf, A., Schon, J., Sehl, J., Wylezich, C., Hoper, D., Mettenleiter, T., Balkema-Buschmann, A., Harder, T.*, et al.* (2020a). SARS-CoV-2 in fruit bats, ferrets, pigs, and chickens: an experimental transmission study. The Lancet Microbe, 1-6.
Schlottau, K., Rissmann, M., Graaf, A., Schön, J., Sehl, J., Wylezich, C., Höper, D., Mettenleiter, T.C., Balkema-Buschmann, A., Harder, T.*, et al.* (2020b). SARS-CoV-2 in fruit bats, ferrets, pigs, and chickens: an experimental transmission study. Lancet Microbe *1*, e218-e225.

Schmaljohn, C., and Hjelle, B. (1997). Hantaviruses: a global disease problem. Emerg Infect Dis *3*, 95-104.
Schountz, T., Campbell, C., Wagner, K., Rovnak, J., Martellaro, C., DeBuysscher, B.L., Feldmann, H., and Prescott, J. (2019). Differential Innate Immune Responses Elicited by Nipah Virus and Cedar Virus Correlate with Disparate In Vivo Pathogenesis in Hamsters. Viruses *11*.
Schountz, T., Green, R., Davenport, B., Buniger, A., Richens, T., Root, J.J., Davidson, F., Calisher, C.H., and Beaty, B.J. (2004). Cloning and characterization of deer mouse (Peromyscus maniculatus) cytokine and chemokine cDNAs. BMC Immunol *5*, 1.
Schountz, T., Prescott, J., Cogswell, A.C., Oko, L., Mirowsky-Garcia, K., Galvez, A.P., and Hjelle, B. (2007). Regulatory T cell-like responses in deer mice persistently infected with Sin Nombre virus. Proc Natl Acad Sci U S A *104*, 15496-15501.
Schountz, T., Quackenbush, S., Rovnak, J., Haddock, E., Black, W.C.t., Feldmann, H., and Prescott, J. (2014). Differential lymphocyte and antibody responses in deer mice infected with Sin Nombre hantavirus or Andes hantavirus. J Virol *88*, 8319-8331.
Schuh, A.J., Amman, B.R., Sealy, T.K., Kainulainen, M.H., Chakrabarti, A.K., Guerrero, L.W., Nichol, S.T., Albarino, C.G., and Towner, J.S. (2019). Antibody-Mediated Virus Neutralization Is Not a Universal Mechanism of Marburg, Ebola, or Sosuga Virus Clearance in Egyptian Rousette Bats. J Infect Dis *219*, 1716-1721.
Schuh, A.J., Amman, B.R., Sealy, T.K., Spengler, J.R., Nichol, S.T., and Towner, J.S. (2017a). Egyptian rousette bats maintain long-term protective immunity against Marburg virus infection despite diminished antibody levels. Sci Rep *7*, 8763.
Schuh, A.J., Amman, B.R., and Towner, J.S. (2017b). Filoviruses and bats. Microbiol Aust *38*, 12-16.
Schulz, J.E., Seifert, S.N., Thompson, J.T., Avanzato, V., Sterling, S.L., Yan, L., Letko, M.C., Matson, M.J., Fischer, R.J., Tremeau-Bravard, A.*, et al.* (2020a). Serological Evidence for Henipa-like and Filo-like Viruses in Trinidad Bats. J Infect Dis *221*, S375-s382.
Schulz, J.E., Seifert, S.N., Thompson, J.T., Avanzato, V., Sterling, S.L., Yan, L., Letko, M.C., Matson, M.J., Fischer, R.J., Tremeau-Bravard, A.*, et al.* (2020b). Serological Evidence for Henipa-like and Filo-like Viruses in Trinidad Bats. J Infect Dis *221*, S375-s382.
Seetahal, J.F.R., Greenberg, L., Satheshkumar, P.S., Sanchez-Vazquez, M.J., Legall, G., Singh, S., Ramkissoon, V., Schountz, T., Munster, V., Oura, C.A.L.*, et al.* (2020). The Serological Prevalence of Rabies Virus-Neutralizing Antibodies in the Bat Population on the Caribbean Island of Trinidad. Viruses *12*.
Seifert, S.N., Letko, M.C., Bushmaker, T., Laing, E.D., Saturday, G., Meade-White, K., van Doremalen, N., Broder, C.C., and Munster, V.J. (2020). Rousettus aegyptiacus Bats Do Not Support Productive Nipah Virus Replication. J Infect Dis *221*, S407-s413.
Selvey, L.A., Wells, R.M., McCormack, J.G., Ansford, A.J., Murray, K., Rogers, R.J., Lavercombe, P.S., Selleck, P., and Sheridan, J.W. (1995). Infection of humans and horses by a newly described morbillivirus. Med J Aust *162*, 642-645.
Shang, J., Ye, G., Shi, K., Wan, Y., Luo, C., Aihara, H., Geng, Q., Auerbach, A., and Li, F. (2020). Structural basis of receptor recognition by SARS-CoV-2. Nature *581*, 221-224.
Shaw, M.L., García-Sastre, A., Palese, P., and Basler, C.F. (2004a). Nipah virus V and W proteins have a common STAT1-binding domain yet inhibit STAT1 activation from the cytoplasmic and nuclear compartments, respectively. J Virol *78*, 5633-5641.
Shaw, M.L., García-Sastre, A., Palese, P., and Basler, C.F. (2004b). Nipah Virus V and W Proteins Have a Common STAT1-Binding Domain yet Inhibit STAT1 Activation from the Cytoplasmic and Nuclear Compartments, Respectively. Journal of Virology *78*, 5633-5641.
Shi, J., Wen, Z., Zhong, G., Yang, H., Wang, C., Huang, B., Liu, R., He, X., Shuai, L., Sun, Z.*, et al.* (2020a). Susceptibility of ferrets, cats, dogs, and other domesticated animals to SARS-coronavirus 2. Science *368*, 1016-1020.

Shi, J., Wen, Z., Zhong, G., Yang, H., Wang, C., Huang, B., Liu, R., He, X., Shuai, L., Sun, Z.*, et al.* (2020b). Susceptibility of ferrets, cats, dogs, and other domesticated animals to SARS–coronavirus 2. Science *368*, 1016-1020.
Shriner, S.A., Ellis, J.W., Root, J.J., Roug, A., Stopak, S.R., Wiscomb, G.W., Zierenberg, J.R., Ip, H.S., Torchetti, M.K., and DeLiberto, T.J. (2021). SARS-CoV-2 Exposure in Escaped Mink, Utah, USA. Emerg Infect Dis *27*, 988-990.
Shulla, A., Heald-Sargent, T., Subramanya, G., Zhao, J., Perlman, S., and Gallagher, T. (2011). A transmembrane serine protease is linked to the severe acute respiratory syndrome coronavirus receptor and activates virus entry. J Virol *85*, 873-882.
Sia, S.F., Yan, L.-M., Chin, A.W.H., Fung, K., Choy, K.-T., Wong, A.Y.L., Kaewpreedee, P., Perera, R.A.P.M., Poon, L.L.M., Nicholls, J.M.*, et al.* (2020a). Pathogenesis and transmission of SARS-CoV-2 in golden hamsters. Nature *583*, 834-838.
Sia, S.F., Yan, L.M., Chin, A.W.H., Fung, K., Choy, K.T., Wong, A.Y.L., Kaewpreedee, P., Perera, R., Poon, L.L.M., Nicholls, J.M.*, et al.* (2020b). Pathogenesis and transmission of SARS-CoV-2 in golden hamsters. Nature.
Stephan, H.A., Gay, G.M., and Ramírez, T.C. (1988). Encephalomyelitis, reproductive failure and corneal opacity (blue eye) in pigs, associated with a paramyxovirus infection. Vet Rec *122*, 6-10.
Steppan, S.J., and Schenk, J.J. (2017). Muroid rodent phylogenetics: 900-species tree reveals increasing diversification rates. PLoS One *12*, e0183070.
Subudhi, S., Rapin, N., Dorville, N., Hill, J.E., Town, J., Willis, C.K.R., Bollinger, T.K., and Misra, V. (2018). Isolation, characterization and prevalence of a novel Gammaherpesvirus in Eptesicus fuscus, the North American big brown bat. Virology *516*, 227-238.
Sun, Y., Lin, W., Dong, W., and Xu, J. (2022). Origin and evolutionary analysis of the SARS-CoV-2 Omicron variant. J Biosaf Biosecur *4*, 33-37.
Sutherland, A.P., Joller, N., Michaud, M., Liu, S.M., Kuchroo, V.K., and Grusby, M.J. (2013). IL-21 promotes CD8+ CTL activity via the transcription factor T-bet. J Immunol *190*, 3977-3984.
Tahsili-Fahadan, P., and Geocadin, R.G. (2017). Heart-Brain Axis: Effects of Neurologic Injury on Cardiovascular Function. Circ Res *120*, 559-572.
Takeuchi, K., Kadota, S.-i., Takeda, M., Miyajima, N., and Nagata, K. (2003). Measles virus V protein blocks interferon (IFN)-α/β but not IFN-γ signaling by inhibiting STAT1 and STAT2 phosphorylation. FEBS Letters *545*, 177-182.
Terry, J.S., Anderson, L.B., Scherman, M.S., McAlister, C.E., Perera, R., Schountz, T., and Geiss, B.J. (2020). Development of SARS-CoV-2 Nucleocapsid Specific Monoclonal Antibodies. bioRxiv.
Tong, S., Chern, S.-W.W., Li, Y., Pallansch, M.A., and Anderson, L.J. (2008). Sensitive and Broadly Reactive Reverse Transcription-PCR Assays To Detect Novel Paramyxoviruses. Journal of Clinical Microbiology *46*, 2652-2658.
Tong, S., Zhu, X., Li, Y., Shi, M., Zhang, J., Bourgeois, M., Yang, H., Chen, X., Recuenco, S., Gomez, J.*, et al.* (2013). New world bats harbor diverse influenza A viruses. PLoS Pathog *9*, e1003657.
Torres-Castro, M., Noh-Pech, H., Hernández-Betancourt, S., Peláez-Sánchez, R., Lugo-Caballero, C., and Puerto, F.I. (2021a). West Nile and Zika viruses in bats from a suburban area of Merida, Yucatan, Mexico. Zoonoses and Public Health *68*, 834-841.
Torres-Castro, M., Noh-Pech, H., Hernández-Betancourt, S., Peláez-Sánchez, R., Lugo-Caballero, C., and Puerto, F.I. (2021b). West Nile and Zika viruses in bats from a suburban area of Merida, Yucatan, Mexico. Zoonoses Public Health *68*, 834-841.
Towner, J.S., Amman, B.R., Sealy, T.K., Carroll, S.A., Comer, J.A., Kemp, A., Swanepoel, R., Paddock, C.D., Balinandi, S., Khristova, M.L.*, et al.* (2009). Isolation of genetically diverse Marburg viruses from Egyptian fruit bats. PLoS Pathog *5*, e1000536.

Towner, J.S., Pourrut, X., Albariño, C.G., Nkogue, C.N., Bird, B.H., Grard, G., Ksiazek, T.G., Gonzalez, J.P., Nichol, S.T., and Leroy, E.M. (2007). Marburg virus infection detected in a common African bat. PLoS One *2*, e764.
Tsoleridis, T., Chappell, J.G., Onianwa, O., Marston, D.A., Fooks, A.R., Monchatre-Leroy, E., Umhang, G., Muller, M.A., Drexler, J.F., Drosten, C.*, et al.* (2019). Shared Common Ancestry of Rodent Alphacoronaviruses Sampled Globally. Viruses *11*.
Tsoleridis, T., Onianwa, O., Horncastle, E., Dayman, E., Zhu, M., Danjittrong, T., Wachtl, M., Behnke, J.M., Chapman, S., Strong, V.*, et al.* (2016). Discovery of Novel Alphacoronaviruses in European Rodents and Shrews. Viruses *8*, 84.
Turgay, C., Emine, T., Ozlem, K., Muhammet, S.P., and Haydar, A.T. (2015). A rare cause of acute flaccid paralysis: Human coronaviruses. J Pediatr Neurosci *10*, 280-281.
Turmelle, A.S., Jackson, F.R., Green, D., McCracken, G.F., and Rupprecht, C.E. (2010). Host immunity to repeated rabies virus infection in big brown bats. J Gen Virol *91*, 2360-2366.
Valmas, C., Grosch, M.N., Schümann, M., Olejnik, J., Martinez, O., Best, S.M., Krähling, V., Basler, C.F., and Mühlberger, E. (2010). Marburg virus evades interferon responses by a mechanism distinct from ebola virus. PLoS Pathog *6*, e1000721.
Van de Vuurst, P., Díaz, M.M., Rodríguez-San Pedro, A., Allendes, J.L., Brown, N., Gutiérrez, J.D., Zarza, H., de Oliveira, S.V., Cárdenas-Canales, E., Barquez, R.M.*, et al.* (2022). A database of common vampire bat reports. Scientific Data *9*, 57.
Vanmechelen, B., Meurs, S., Horemans, M., Loosen, A., Joly Maes, T., Laenen, L., Vergote, V., Koundouno, F.R., Magassouba, N.F., Konde, M.K.*, et al.* (2022). The characterization of multiple novel paramyxoviruses highlights the diverse nature of the subfamily Orthoparamyxovirinae. Virus Evolution *8*.
Veronesi, M.C., Alhamami, M., Miedema, S.B., Yun, Y., Ruiz-Cardozo, M., and Vannier, M.W. (2020). Imaging of intranasal drug delivery to the brain. Am J Nucl Med Mol Imaging *10*, 1-31.
Virtue, E.R., Marsh, G.A., Baker, M.L., and Wang, L.F. (2011). Interferon production and signaling pathways are antagonized during henipavirus infection of fruit bat cell lines. PLoS One *6*, e22488.
Walls, A.C., Park, Y.J., Tortorici, M.A., Wall, A., McGuire, A.T., and Veesler, D. (2020). Structure, Function, and Antigenicity of the SARS-CoV-2 Spike Glycoprotein. Cell *181*, 281-292 e286.
Wan, S., Yi, Q., Fan, S., Lv, J., Zhang, X., Guo, L., Lang, C., Xiao, Q., Xiao, K., Yi, Z.*, et al.* (2020). Relationships among lymphocyte subsets, cytokines, and the pulmonary inflammation index in coronavirus (COVID-19) infected patients. Br J Haematol *189*, 428-437.
Wang, W., Lin, X.-D., Zhang, H.-L., Wang, M.-R., Guan, X.-Q., Holmes, E.C., and Zhang, Y.-Z. (2020). Extensive genetic diversity and host range of rodent-borne coronaviruses. Virus Evolution *6*.
Wang, W., Lin, X.D., Guo, W.P., Zhou, R.H., Wang, M.R., Wang, C.Q., Ge, S., Mei, S.H., Li, M.H., Shi, M.*, et al.* (2015). Discovery, diversity and evolution of novel coronaviruses sampled from rodents in China. Virology *474*, 19-27.
Wei, C., Shan, K.-J., Wang, W., Zhang, S., Huan, Q., and Qian, W. (2021). Evidence for a mouse origin of the SARS-CoV-2 Omicron variant. J Genet Genomics, S1673-8527(1621)00373-00378.
WHO. Middle East respiratory syndrome coronavirus (MERS- CoV).
WHO (2021). Rabies.
Willgert, K., Didelot, X., Surendran-Nair, M., Kuchipudi, S.V., Ruden, R.M., Yon, M., Nissly, R.H., Vandegrift, K.J., Nelli, R.K., Li, L.*, et al.* (2022). Transmission history of SARS-CoV-2 in humans and white-tailed deer. Sci Rep *12*, 12094.
Williams-Guillén, K., and Perfecto, I. (2010). Effects of Agricultural Intensification on the Assemblage of Leaf-Nosed Bats (Phyllostomidae) in a Coffee Landscape in Chiapas, Mexico. Biotropica *42*, 605-613.

Williamson, M.M., Hooper, P.T., Selleck, P.W., Gleeson, L.J., Daniels, P.W., Westbury, H.A., and Murray, P.K. (1998). Transmission studies of Hendra virus (equine morbillivirus) in fruit bats, horses and cats. Aust Vet J *76*, 813-818.
Williamson, M.M., Hooper, P.T., Selleck, P.W., Westbury, H.A., and Slocombe, R.F. (2000). Experimental Hendra Virus Infectionin Pregnant Guinea-pigs and Fruit Bats(Pteropus poliocephalus). Journal of Comparative Pathology *122*, 201-207.
WOAH (2022). Cases of SARS-Cov-2 infection in animals reported to WOAH since March 2020 (World Organisation for Animal Health).
Wong, K.T., Grosjean, I., Brisson, C., Blanquier, B., Fevre-Montange, M., Bernard, A., Loth, P., Georges-Courbot, M.C., Chevallier, M., Akaoka, H.*, et al.* (2003). A golden hamster model for human acute Nipah virus infection. Am J Pathol *163*, 2127-2137.
Woon, A.P., Boyd, V., Todd, S., Smith, I., Klein, R., Woodhouse, I.B., Riddell, S., Crameri, G., Bingham, J., Wang, L.F.*, et al.* (2020). Acute experimental infection of bats and ferrets with Hendra virus: Insights into the early host response of the reservoir host and susceptible model species. PLoS Pathog *16*, e1008412.
Wu, C., Chen, X., Cai, Y., Xia, J., Zhou, X., Xu, S., Huang, H., Zhang, L., Zhou, X., Du, C.*, et al.* (2020a). Risk Factors Associated With Acute Respiratory Distress Syndrome and Death in Patients With Coronavirus Disease 2019 Pneumonia in Wuhan, China. JAMA Intern Med.
Wu, P., Duan, F., Luo, C., Liu, Q., Qu, X., Liang, L., and Wu, K. (2020b). Characteristics of Ocular Findings of Patients With Coronavirus Disease 2019 (COVID-19) in Hubei Province, China. JAMA Ophthalmol.
Wu, Z., Han, Y., Liu, B., Li, H., Zhu, G., Latinne, A., Dong, J., Sun, L., Su, H., Liu, L.*, et al.* (2021). Decoding the RNA viromes in rodent lungs provides new insight into the origin and evolutionary patterns of rodent-borne pathogens in Mainland Southeast Asia. Microbiome *9*, 18.
Wu, Z., Lu, L., Du, J., Yang, L., Ren, X., Liu, B., Jiang, J., Yang, J., Dong, J., Sun, L.*, et al.* (2018). Comparative analysis of rodent and small mammal viromes to better understand the wildlife origin of emerging infectious diseases. Microbiome *6*, 178.
Wu, Z., Yang, L., Yang, F., Ren, X., Jiang, J., Dong, J., Sun, L., Zhu, Y., Zhou, H., and Jin, Q. (2014). Novel Henipa-like virus, Mojiang Paramyxovirus, in rats, China, 2012. Emerg Infect Dis *20*, 1064-1066.
Xiao, X., Newman, C., Buesching, C.D., Macdonald, D.W., and Zhou, Z.-M. (2021). Animal sales from Wuhan wet markets immediately prior to the COVID-19 pandemic. Scientific Reports *11*, 11898.
Yen, H.L., Sit, T.H.C., Brackman, C.J., Chuk, S.S.Y., Gu, H., Tam, K.W.S., Law, P.Y.T., Leung, G.M., Peiris, M., and Poon, L.L.M. (2022). Transmission of SARS-CoV-2 delta variant (AY.127) from pet hamsters to humans, leading to onward human-to-human transmission: a case study. Lancet *399*, 1070-1078.
Yokosawa, N., Yokota, S.-I., Kubota, T., and Fujii, N. (2002). C-terminal region of STAT-1alpha is not necessary for its ubiquitination and degradation caused by mumps virus V protein. Journal of virology *76*, 12683-12690.
Yoneda, M., Guillaume, V., Sato, H., Fujita, K., Georges-Courbot, M.-C., Ikeda, F., Omi, M., Muto-Terao, Y., Wild, T.F., and Kai, C. (2010). The Nonstructural Proteins of Nipah Virus Play a Key Role in Pathogenicity in Experimentally Infected Animals. PLOS ONE *5*, e12709.
Young, D.F., Didcock, L., Goodbourn, S., and Randall, R.E. (2000). Paramyxoviridae use distinct virus-specific mechanisms to circumvent the interferon response. Virology *269*, 383-390.
Yu, F., Le, M.Q., Inoue, S., Thai, H.T., Hasebe, F., Del Carmen Parquet, M., and Morita, K. (2005). Evaluation of inapparent nosocomial severe acute respiratory syndrome coronavirus infection in Vietnam by use of highly specific recombinant truncated nucleocapsid protein-based enzyme-linked immunosorbent assay. Clin Diagn Lab Immunol *12*, 848-854.

Zaki, A.M., van Boheemen, S., Bestebroer, T.M., Osterhaus, A.D., and Fouchier, R.A. (2012). Isolation of a novel coronavirus from a man with pneumonia in Saudi Arabia. N Engl J Med *367*, 1814-1820.
Zeller, H.G., Karabatsos, N., Calisher, C.H., Digoutte, J.P., Murphy, F.A., and Shope, R.E. (1989). Electron microscopy and antigenic studies of uncharacterized viruses. I. Evidence suggesting the placement of viruses in families Arenaviridae, Paramyxoviridae, or Poxviridae. Arch Virol *108*, 191-209.
Zhang, A.P., Bornholdt, Z.A., Liu, T., Abelson, D.M., Lee, D.E., Li, S., Woods, V.L., Jr., and Saphire, E.O. (2012). The ebola virus interferon antagonist VP24 directly binds STAT1 and has a novel, pyramidal fold. PLoS Pathog *8*, e1002550.
Zhang, X.-A., Li, H., Jiang, F.-C., Zhu, F., Zhang, Y.-F., Chen, J.-J., Tan, C.-W., Anderson, D.E., Fan, H., Dong, L.-Y.*, et al.* (2022). A Zoonotic Henipavirus in Febrile Patients in China. New England Journal of Medicine *387*, 470-472.
Zhao, Y., Wang, J., Kuang, D., Xu, J., Yang, M., Ma, C., Zhao, S., Li, J., Long, H., Ding, K.*, et al.* (2020). Susceptibility of tree shrew to SARS-CoV-2 infection. Scientific Reports *10*, 16007.
Zhou, P., Tachedjian, M., Wynne, J.W., Boyd, V., Cui, J., Smith, I., Cowled, C., Ng, J.H., Mok, L., Michalski, W.P.*, et al.* (2016). Contraction of the type I IFN locus and unusual constitutive expression of IFN-alpha in bats. Proc Natl Acad Sci U S A *113*, 2696-2701.
Zhou, P., Yang, X.-L., Wang, X.-G., Hu, B., Zhang, L., Zhang, W., Si, H.-R., Zhu, Y., Li, B., Huang, C.-L.*, et al.* (2020a). A pneumonia outbreak associated with a new coronavirus of probable bat origin. Nature *579*, 270-273.
Zhou, P., Yang, X.L., Wang, X.G., Hu, B., Zhang, L., Zhang, W., Si, H.R., Zhu, Y., Li, B., Huang, C.L.*, et al.* (2020b). A pneumonia outbreak associated with a new coronavirus of probable bat origin. Nature *579*, 270-273.
Zhu, N., Zhang, D., Wang, W., Li, X., Yang, B., Song, J., Zhao, X., Huang, B., Shi, W., Lu, R.*, et al.* (2020a). A Novel Coronavirus from Patients with Pneumonia in China, 2019. New England Journal of Medicine *382*, 727-733.
Zhu, N., Zhang, D., Wang, W., Li, X., Yang, B., Song, J., Zhao, X., Huang, B., Shi, W., Lu, R.*, et al.* (2020b). A Novel Coronavirus from Patients with Pneumonia in China, 2019. N Engl J Med *382*, 727-733.
Zieger, U., Cheetham, S., Santana, S.E., Leiser-Miller, L., Matthew-Belmar, V., Goharriz, H., and Fooks, A.R. (2017). Natural exposure of bats in Grenada to rabies virus. Infect Ecol Epidemiol *7*, 1332935.